MINEO

IST–1999-10337

Assessing and monitoring the environmental impact of mining activities in Europe using advanced Earth Observation techniques

MINEO Southern Europe environment test site

Contamination /impact mapping and modelling – Final report

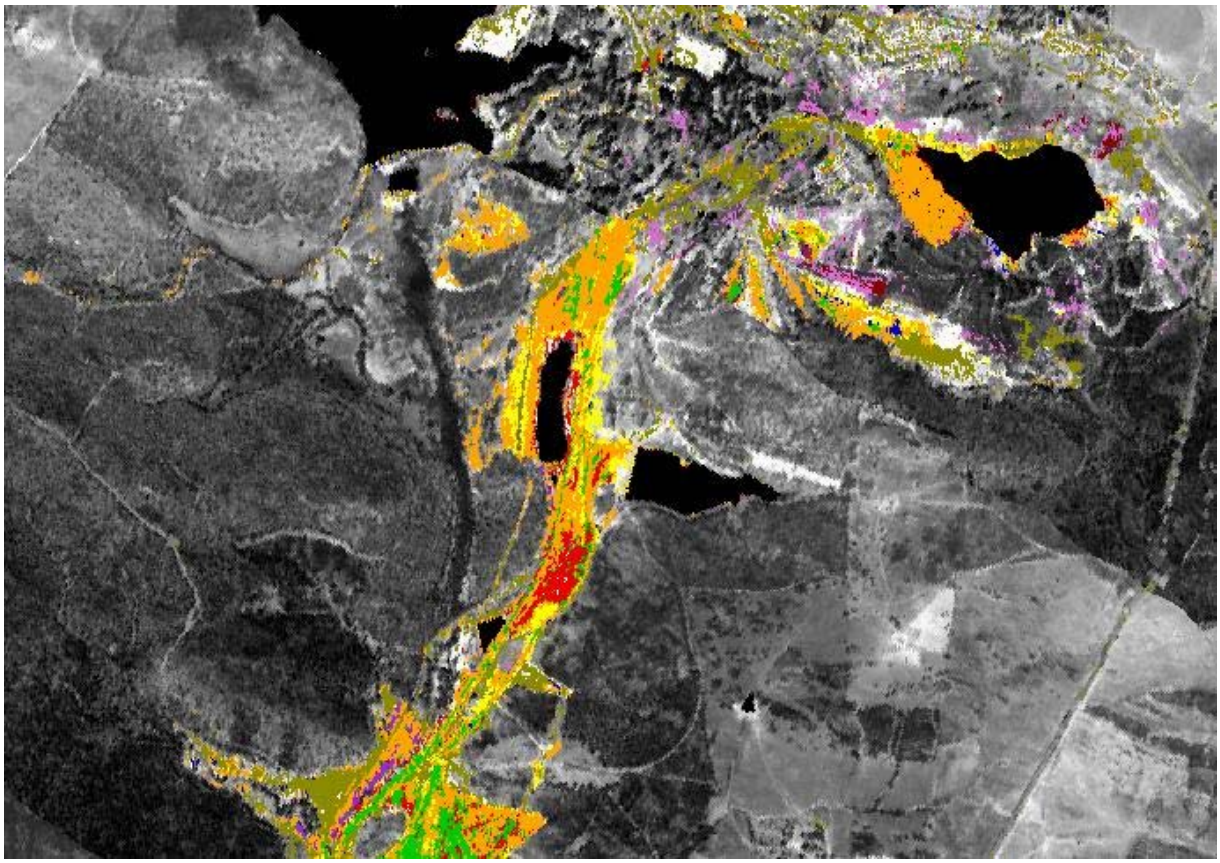

Project funded by the European Community under the "Information Society Technology" Programme (1998-2002)

Primary authors of this report:

Lidia Quental[1], Anne Bourguignon[2], António Jorge Sousa[3], Maria João Batista[1], Maria Graça Brito[4], Teresa Tavares[3], Maria Manuela Abreu[5], Margarida Vairinho[1] & Francis Cottard[2]

[1]Instituto Geológico e Mineiro
Est.Portela, Zambujal, Ap.7586
2721-866 Alfragide - Portugal

[2]Bureau de Reserche Geologique et Miniére
DR/LGT
BP 6009
45060 ORLEANS Cedex 2 - France

[3]Instituto Superior Técnico
Av. Rovisco Pais,1
1049-001 Lisboa - Portugal

[4]Faculdade de Ciências da Universidade Nova de Lisboa
Quinta da Torre
2829-516 Caparica - Portugal

[5]Instituto Superior de Agronomia
Tapada da Ajuda,
1349-017 Lisboa - Portugal

Front cover: Waste mining material hyperspectral classification (HyMap^{TM}2000). Shows materials dispersion near S.Domingos open pit (upper right corner) and mining infrastructures to west and south.

Abstract

Under the framework of the MINEO project, the abandoned S.Domingos mining area as been selected as representative of Southern Europe Environment to test methods and tools for assessing and monitoring the environmental impact of mining activities using hyperspectral data and other relevant data sets.

The S.Domingos mining area, is characterised by a long-term mining activity, since pre-roman times till the 1960's, and is included in the group of Volcanogenic Massive Sulphide deposits of the Iberian Pyrite Belt. The orebody contained Cu, and also Zn and Pb. Several facilities were developed for mining works and ore transportation, covering an area of 50km^2, facilitating dispersion of related pollutants. The main environmental problems can be summarised as related to waste material and their pollutant content (Zn, Pb, Sb, Cu, As, Hg and Cd), acid waters (minimum pH value of 1.7) and associated dispersion, as well as landscape disruption.

Hyperspectral images were able to identify mineralogical/chemical dispersion of waste material related to Acid Mine Drainage (AMD) following two approaches: one related to AMD waste material field spectra and the other based on AMD minerals, using standard spectral libraries. The processing techniques used were mainly based on the Spectral Angle Mapper classifier and Mixture Tunned Matched Filtering. Globally, both mapping results obtained, either in AMD waste material either in AMD minerals, were able to detect mineralogical/chemical characteristics of imaged ground data, which were validated by field data.

The GIS geochemical modelling allowed the determination of effective AMD area of influence, based in water pH values, using geostatistical methods. The Indicator "Collocate-Cokriging" of the water pH using the distance to the highest correlated AMD waste material (*mixed sulphur materials* from hyperspectral classification) predicts the AMD dispersion in the area related to that material. This methodology achieved good results and could be applied in new areas using waste material hyperspectral image classification for AMD delimitation area.

Content

List of Appendices

List of Figures

List of Tables

1. INTRODUCTION

The project *Assessing and monitoring the environmental impact of mining in Europe using Advanced Earth Observation Techniques* (MINEO) is a shared cost action under the program of Information Society Technologies of the European Commission. The MINEO project aims at developing methods and tools for assessing and monitoring the environmental impact of mining activities using advanced Earth Observation (EO) techniques and other relevant data sets.

EO data, when integrated into Geographic Information Systems and combined with other data relevant to environmental concerns, have been proven valuable in the environmental impact assessment of mining, both on local and regional scales. In particular, they can be used in the production of pollution-risk maps around mining areas. It is therefore proposed to develop the contribution of various EO techniques further.

To undertake the envisaged developments, six mining areas, five within Europe and one in Greenland, have been selected for investigation, to reflect European climatic, geographic and socio-economic diversity. The now abandoned S.Domingos Mine, located in southeastern Portugal, corresponds to one of these test sites and represents the Southern European Environment.

The S.Domingos Mine previously exploiting Volcanogenic Massive Sulphide deposits for more than a century mainly for Cu, Fe and S (secondary Pb, Zn and Au) until 1966, produced in excess of 25Mt of ore. Related to the mining and processing of the ore the Acid Mine Drainage (AMD) was intensive, according to the volume of ore exploited, with effects that endure until today. Nowadays, the mine waste materials such as tailings, slags and heap dumps are estimated at several hundred thousand tons, including pre-roman and roman times. These materials and the remaining superficial ore, when leached by waters can have a high acid generating potential, are the present source of AMD and consequently facilitate the dispersion of the enclosed pollutants.

Hyperspectral sensors, with very high spectral resolution, have the ability to identify mineralogical and/or chemical characteristics of the imaged ground, based on distinct spectral features of the materials. This property can allow the detection of some traces related to superficial AMD. Therefore, the objective of the present study is to evaluate the possibility of using advanced EO data set, i.e. hyperspectral, to environmentally assess S.Domingos mining area. According to the characteristics of this test site, the study is focused on waste materials dispersion and their characteristics related to AMD.

2. DESCRIPTION OF THE SITE

2.1. General characteristics

Located in SE Portugal (Figure 1), within the Baixo Alentejo Province, some 60 km SE of the city of Beja, near the Spanish border (Figure 1), the now abandoned S.Domingos mining area has a Mediterranean climate with Atlantic or Continental influences, characterised by long dry summers and short winters.

The annual average air temperature is 17.6ºC, reaching its maximum value in August and July, 37.8ºC and 33.7ºC respectively. Annual precipitation is 558.5 mm with the highest rate in November and the lowest in July. Average wind velocity is below 10 km/h. Evapotranspiration reaches 206,9 mm in July

and 187.9 mm in August with an annual evapotranspiration of 1270.5 mm. Water holding capacity is zero from May to October and water excess is reported only in January and February when the rainfall

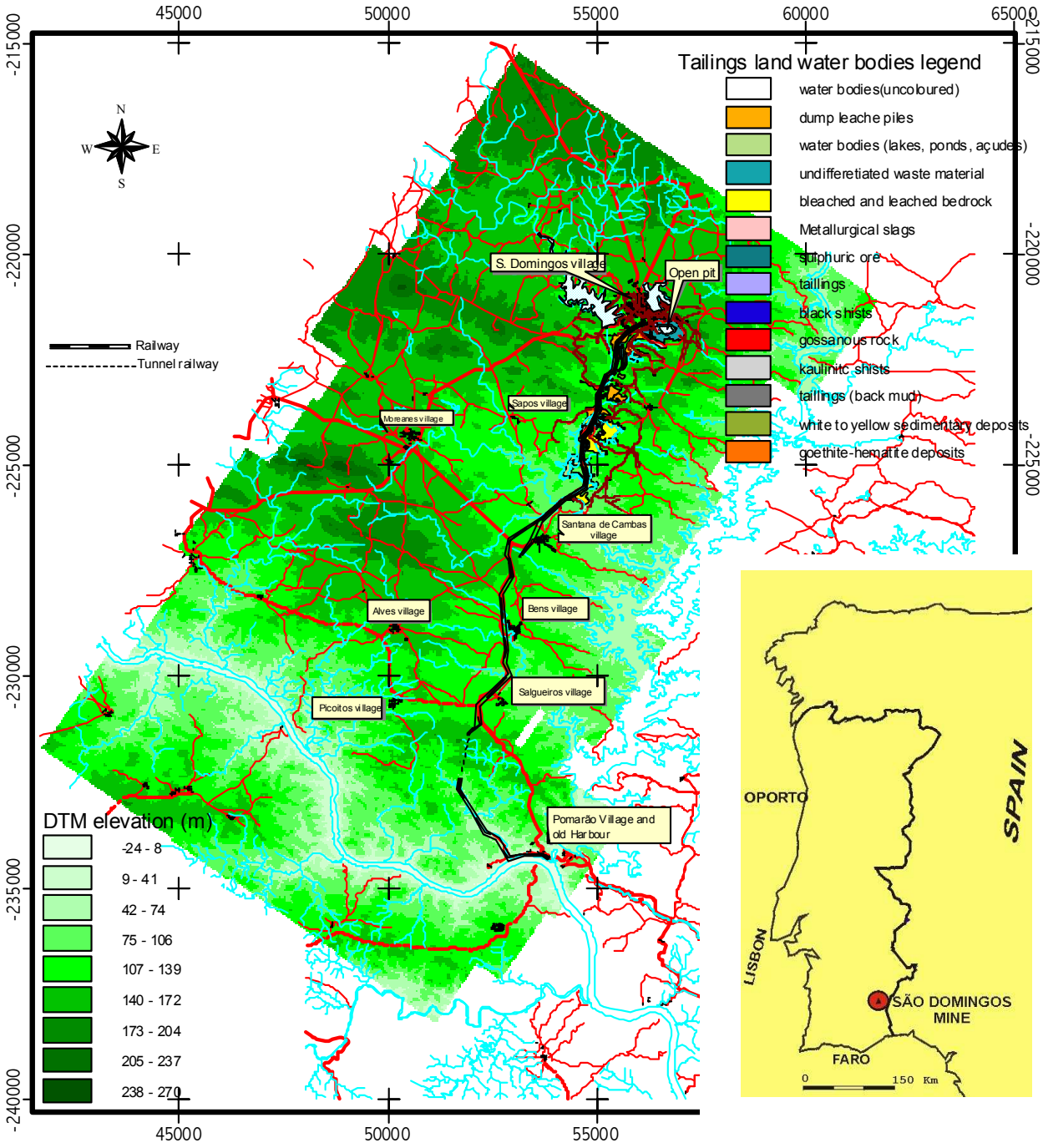

Figure 1. S. Domingos Mine location and main characteristics.

declines and temperature rises until October. Annual average humidity is about 75% and water deficit is reported from May to October.

The population density is currently low nowadays although it has reached nearly 5000 persons whose main activity was related with the extraction of massive sulphides.

Most of the area is covered by thin soils, and natural rock outcrops are abundant.

In the S. Domingos Mine, pre-roman and roman works are known to have exploited Ag, Cu and, Au, mainly in the gossan resulting from the oxidation sulphide mass. The modern exploitation started in the XIX century, both in the gossan and massive sulphide orebody that besides Cu also contained some Zn and Pb, and ended in 1966 due to exhaustion of the ore. Associated with the mining works several facilities were developed, including a village (S.Domingos, Figure 1), water reservoirs, cementation tanks, sulphur factory, network channels for acid water evaporation, and a railway and harbour (Pomarão) for ore transportation. From the beginning of pre-roman times until 1968 the Mine produced 25 Mt, and mine waste material in the area is estimated at several hundred thousand tons. In this context, important environmental problems are associated, which are visible within an area around 50km^2. Although correlated, these problems can be summarised as related to waste material and their pollutant content, acid waters and associated dispersion, as well as landscape disruption.

2.2. Geology

2.2.1. Regional Geology

The Iberian Pyrite Belt (IPB) extends from Spain along southern Portugal. It constitutes one of the most important metallogenic provinces for Volcanogenic Massive Sulphide deposits, and within which occurs the S. Domingos Mine.

The general geology of the Mine area consists of the outcropping Volcanic Sedimentary Complex (VSC) that consists of acid and basic rocks of Tournaisian age (App. 1).
Webb (1958) described the area as being underlain by Paleozoic sediments, “comprised mainly of clay-slates with interbedded grits, quartzites and occasional tuffaceous horizons”. Recent studies identified these Paleozoic sediments as: in the northern part, older formations from the Pulo do Lobo Antiform [Gafo Formation (schists, silts, greywackes, acid and basic volcanism) and Represa Formation (schists, silts, greywackes and quartzwackes)] of Upper Devonian age, while to the south, in the mine area outcrops the Phylito-Quartzitica Formation (phyllites, silts, quartzites and quartzwackes) and Barrranco do Homem Formation (phyllites, silts and greywackes) of the same age (Oliveira & Silva, 1990). With the Hercynian compression the sedimentary assemblage was intensely folded and the more incompetent beds marked with a strong flow cleavage, dipping at steep angles to the NNE. The strike direction of both cleavage and bedding is 110-125º. Locally, quartzites can occur in large extents. At intervals along regional strike, sediments are intruded by dykes ranging from acid (porphyries) to basic (diabases) in composition, which recently were interpreted as belonging to the VSC of Tournaisian age (Oliveira & Silva, 1990). To the south, a large area is covered by the Mértola Formation (Lower Carboniferous) that consists of a turbiditic sequence of pelites and greywackes. The VSC, host to polymetallic massive sulphides of IPB, orientated WNW-ESE, is represented by two structures, the alignment of the S. Domingos and Pomarão anticline. In the flanks of these structures representative outcrops are marked by three episodes of acid volcanism, separated by sedimentary cycles. Within the Pomarão anticline outcrops the Eira do Garcia Member [(silts and pelites and greywackes (PQ)] and the Upper Devonian Nascedios Member (grey pelites with thin interbedded limestones); the Pomarão Harbour being located in its inverse flank.

Above the VSC, there is a turbiditic sequence that can reach four thousand meters in thicnkness and is composed of alternating schists and greywackes (Baixo Alentejo Flysch).

Mapping (App.1) showed the rock to be intensivly faulted. The faults are mostly along vertical NW shear-planes and along bedding strike, and some clearly post-date the igneous rocks. Although jasper, hematite, manganese oxides and minor sulphide disseminations occur at several points, the known orebody is the only evidence of significant metal concentration (Webb, 1958).

2.2.2. Mine Geology

An irregular tract of superficial iron-staining and gossan extends southeast from the orebody and lies in part on the slopes of a shallow to moderately incised valley which drains southeast from a point about 500m from the mine.

The volcanic sequence in the mine is not well exposed and the structure is complicated. The upper volcanic levels are covered by a thick turbiditic sequence (Flysch Group) and the allochthonous Phylite Quartzite (PQ) group caps the volcanic pile. The outcropping area was formed by a unique vertical mass of cupriferous pyrite associated with zinc and lead sulphides, elongated in an E-W direction. This orebody was exploited to a depth of 120m below the topographic surface as an open pit mine and from this depth down to 420m. Mining accesses consisted of wells and galleries. The mapping of level 240m and geological section of the massive sulphide are shown in Figure 2.

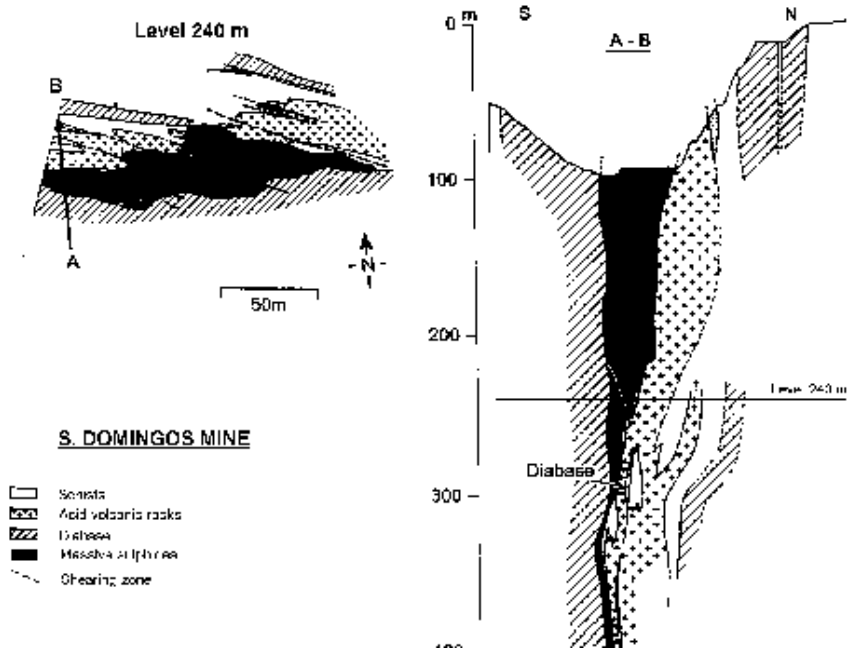

Figure 2. The massive sulphide orebody: mapping and geological section of level 240m (adapted after Webb, 1958).

The intense wall-rock alteration surrounding the orebody is typically hydrotermal, and comprises argilitisation (kaolin and allunite), sericitisation, chloritisation and silicification.
The reddish-brown gossan extending southeast from the orebody is probably an erosional relict of transported iron oxides and hydroxides that accumulated during the original weathering of the ore, which is almost completely eroded. The deep residual gossan results from a weathering process of the exposed orebody, due to eventual uplift and peneplanation.
Figure 3 illustrates the northern side of the open pit mining walls where relict ancient roman galleries exploited gold, silver and copper in the gossan, can still be seen today.

From W to E, along the open pit wall levels, the white coloured alteration zones of the black shales are clearly identified, the extremely silicified felsic tuffs, host rocks of the stockwork feeders, and the basic lithotype, represented by green coloured rocks possibly due to hydrothermal alteration below the stockwork, chloritisation (Silva *et al*., 1997). Anastomosing veinlets, vein networks (feeder channels) and disseminations of sulphides that grade into massive sulphide lenses make up the stockwork mineralisation by coalescence of veins and replacements (Figure 4).

Figure 3. Composite photograph of northern sector of the S. Domingos Mine open pit.

Figure 4. Oxidised mineralisation. Example of stockwork local feeders, composed of felsic rocks and weathered pyrite veinlets.

Generally stockworks occur in highly silicified and chloritised footwall volcanic rocks (Barriga & Carvalho, 1983, in Silva *et al*., 1997).

2.3. History of exploitation

The exploitation at the S. Domingos test site, ranging from pre-roman activity to the 1960´s, can be summarised as follows (based on Batista, 2000):

2.3.1. Pre-roman period

Almost every archaeological study in Volcanogenic Massive Sulphide mines in the Iberian Pyrite Belt (IPB) show evidence of pre-roman exploitations of precious metals and copper in superficial ores, as a result of their concentration by supergene alteration. Despite there being no specific studies in S. Domingos, the evidence of works nearby, and the arguments supported by Allan (1965), related to the huge amount and nature of waste material found, and also the presence of megalithic structures, suggests that mining and metallurgy took place (Gaspar, 1998).

2.3.2. Roman period

The existent literature shows that at S. Domingos during this period, the underground works went below the hydrostatic level. The Romans exploited gold from the gossan, and small contemporaneous galleries are still recognisable (Figure 3). These ancient mining activities were largely confined to the oxidised ore near the surface (Webb, 1958).
Based on the volumes of ancient waste piles and the respective chemical composition phases, several authors have estimated the volume of Roman works in more than 150 000 m^3, which corresponds to 300 000t of slags, considering both mines of S. Domingos and Aljustrel (Sequeira, 1884 in Gaspar, 1998).

2.3.3. Post- roman period

After the roman expulsion by the Visigoths, around 405 A.D., a period of almost no mining activity followed in Iberian Pyrite Belt except maybe at Aljustrel and one or two mines in Spain until 1492 during the Islamic occupation of the Iberian Peninsula. Irrelevant activity probably occurred after that, but only in the XVIII century, and more intensively in the XIX century, were the exploitation works again economically significant.

2.3.4. XIX Century

The interests of French industrialists, in particular Ernest Deligny, technical director of a few mines in Spain who sent people to do exploration in Portugal, started the process that led to the concession of the S. Domingos Mine. Nicolau Biava was recognised as legal discoverer of this mine and obtained a temporary concession that was transferred in 1855 to Ernest Déligny, Luis Decazes and Eugène Duclerc, who had formed the company La Sabina in 1855.

A permanent licence was given in 1859 when Diogo Mason took charge. Mason & Barry, Ltd., was constituted later, to whom La Sabina rented the exploitation concession. The mining exploiters carried out the construction of a typical mining village, whose typology characterises the classical industrial period. They created rigorous urban planning and the village was almost autonomous with farms, orchards and even with its own police force (Alves, 1997).

The mining plan began in 1859 but the underground and surface mining only began in 1863. Due to the fluctuation of copper grades, only the richest ones were sent to England where incineration processes were used to extract sulphuric acid. This extraction process was experimental in closed ovens, in order to avoid environmental problems that occurred in an open environment, nearby in Rio

Tinto, which produced gases rich in SO_2, As, Sb and Tl, provoking disastrous effects locally in fauna and flora that have remained until today.

In S. Domingos, the first products extracted by incineration processes were separated and the richest nodules were submitted to a fusion process. The leaching of the poor products was carried out in cementation tanks but this process was abandoned in 1868 due to technical difficulties and high costs. When copper prices dropped, the material was leached in a raw state making the recovery more efficient.

The method utilised in the treatment of the ore can be summarised as follows:

1) separation of Cu>2% from Cu <2% into four piles, fines and poor material;
2) crushing of the richest and coarse grained material into pieces of more or less 5 cm;
3) accumulation of Cu<2% in piles with interior channels made of gravel material for easy circulation of the air, sandstone chimneys to control the temperature of the process as this process was strongly exothermic;
4) the leaching of the piles with water controlling the temperature to avoid spontaneous combustion of the mined material and excessive formation of sulphuric acid that could make a poor cement and raise the iron consumption (Gaspar, 1998).

The ore was exported for sulphuric acid production; the leaching products had 14% of Cu and were lidded to the tanks to decant particles and sent to cementation tanks. The iron used in the process was about 20 000t a year. From the 4 Mt of copper mineralization extracted from 1870 until 1887, 334 575 t were transported to the treatment facilities in Achada do Gamo and 378 320 t of washed product and 85 046t of copper concentrate were exported.

A railway was built in 1858, linking S. Domingos Mine to the Pomarão Harbour, in the Guadiana River, from where the ore was transported to the Atlantic Ocean. In Swansea, UK, part of the material was to obtain copper and part was to obtain gold and silver (Gaspar, 1998).

The first exploitation plan dates from 1858 and plans for the underground exploitation of the orebody in all it's extension following old works with longitudinal galleries (parallel to the orebody axis) and cross cuts, distributed over several levels with connecting wells and supporting rock piles in the exploitation areas. In 1863-65 27 vertical holes had already been built for mining circulation and sewage waste (Rego, 1996) and in the same period the sulphur smelting facilities were built in Achada do Gamo.

In 1866-67, during a copper price downturn scenario, the second exploitation plan was made in that predicted open pit exploitation with lower costs, and continuing the extraction method of underground in the untouched ore.

The first exploitation of the open pit started in 1868, causing a progressively strong impact in the landscape 122 m depth when the open pit extraction was abandoned, continuing only the underground works.

Dikes were constructed to support the mining works and the water supply of populations in 1871-73.
Acid effluents from mining, estimated at 2hm/year were diverted to a network of channels and reservoirs to improve the quality of effluent by increasing settling, to reduce its quantity by natural evaporation and infiltration. It was also a process to control its discharge into the main river, Chança, during flood periods (Pereira *et al.*, 1995). The total area of evaporation surfaces created in this system was 97ha (Mason & Barry, 1878).

2.3.5. XX Century

In the early XX Century the worldwide evolution of the sulphuric acid industry favoured its extraction from pyrite, which resulted in an increase in exploitation of S. Domingos Mine. From 1913 until 1932 S. Domingos produced 3 445 533 t of copper ore and from 1923 to 1932, 3616 t of Cu cement with average values of 72,33%. At the end of 1960, a new crisis caused by native sulphur market competition extracted from sulphur ores of low degree in deep ores (by hot water pressure) and the external market gave place to internal consumption of sulphides by the sulphur acid factories. As an example, as much as 430 000 t of acid was produced in factories like QUIMIGAL and SAPEC, being most of it used to produce fertilisers. The global ore produced in XX century in S. Domingos is estimated at 9 882 722 t (Gaspar, 1998).

Mined raw material was crushed in a mill located near the open cast pit. Three kilometres south of the mining area (at Achada do Gamo, Figure 1) the crushed material was smelted to obtain high level grades of copper ore and sulphur products, which were widely used in the chemical industry until the 50's.

Average grades of the exploited material range from 1,25% Cu (10% Cu maximum), 2-3% Zn and Pb (14% Zn and Pb, maximum). Massive pyrite grades average in the range from 45-48% in sulphur, and in addition to pyrite there are subordinate amounts of chalcopyrite, sphalerite, galena and other rare sulphides (Webb, 1958).

The Mine was closed in 1966 presumably due to exhaustion of the ore although some authors think that the ore continues deeper (Gaspar, 1998, Oliveira, V. pers. com., 1999). The open pit was flooded.

From the beginning of pre-roman times until 1968, the Mine produced 25 Mt of ore (Carvalho, 1979 in Gaspar, 1998).

On 30th July 1972, the company La Sabina, took possession of mining facilities of the S. Domingos mining concession, after the complex process of bankruptcy of Mason & Barry Limited. In 1984 La Sabina, financed by German capitals, lost the historical concession maintaining however the rights acquired in the lands and buildings covered by the mining concession.
This area has not been submitted so far to any remediation process. Removal of materials is constant for several purposes.

2.4. Related environmental problems

The type of ore, treatment, processing and transportation, as described in Section 2.3, caused important environmental problems, some of which already reported in the XIX century, and with direct economic consequences for the exploitation company.
The specific problems associated to the S. Domingos test site, can be summarised as follows:

2.4.1. Waste mining material and associated contamination

Waste mining material such as slags, heap dumps and tailings, either concentrated or dispersed in the area, are still enriched in hazardous elements such as Zn, Pb, Sb, Cu, As, Hg and Cd. These waste materials leached by rainwater and stream waters can have highly acid generating potential, due to sulphide oxidation and Fe-hydrolisis, which increases dissolution and mobility of elements. They constitute hot spots for waters, soils and plants contamination (Figure 5).

Figure 5. Acid generating materials enrich waters in sulphur and metals. Precipitation of sulphates and of Fe oxihydroxides.

Chemical analyses after leaching of these materials are given in Section 4.2.1.

2.4.2. Acid waters and dispersion of elements

The Acid Drainage *s.l.* (AD), mainly from Acid Mine Drainage but also from Acid Rock Drainage, is the main vehicle for the dispersion of elements in waters, soils and sediments, which covers significant areas in this test site. Water pH in the S. Domingos River can reach very low values (App.7).

The network system of channels developed for evaporation of acid waters from mining works strongly affected soil constitution in some areas (Figure 9).

2.4.3. Landscape disruption

The open pit with an area of 0,25km^2, ponds, water dams and waste mining material (slags and dumps), concentrated or spread out, have a striking imprint in the area. The presence of unvegetated slopes due to leaching by acid waters still remains (Figure 9).

Slags and dumps are still today being moved by human action moved, which alters topography and the existing chemical equilibrium conditions whithin the dumps. This disequilibrium favours acid drainage.

The remnants of mining infrastructures distributed in the area present several degrees of degradation and consequent hazard (Figure 6).

Figure 6. Achada do Gamo: remnants of mining infrastructures and dispersed or concentrated waste mining material.

2.4.4. Waste material mapping

The main objective of the field work carried out between the 28th of January and the 1st of February 2002 was to identify and map the **remaining surficial ore material** and the **waste materials** generated during almost a century from the different mining operations (extraction, processing of the ore and smelting) in the S. Domingos area. Specifically, the mapping aimed to:

- characterize the different waste materials found on surface;
- locate acidic minerals exposed at the surface and evaluating the potential for acidic drainage at the surface;
- locate and characterise instantaneous sources of acid and metals mainly through the identification of a complex array of soluble secondary salts (soluble sulfates, hydrous sulfates such as melanterite, copiapite, jarosite, chalcanthite, brochantite etc..) which are a common result of sulphide oxydation in the superficial environment. It is worth noting that those salts are of environmental concern because they store acid and metals during dry seasons and release these contaminants into the ground and surface waters during the wet season.

App. 2 shows the map of the remaining superficial ore material and waste materials on the São Domingos test site. A summary description of the map is presented below.

Brief description of the different facies mapped

As with many massive sulphide deposits, the S. Domingos deposit is characterized by silicifeid host rocks (volcanic and sedimentary rocks) which are deeply weathered due to the natural oxidation of massive accumulations of sulphides (mainly pyrite with lesser amounts of base-metal sulphide minerals such as chalcopyrite, galena and sphalerite). This weathering process superimposed on the

hydrothermal wallrock alteration (phyllic and argillic alterations) gives rise, through extraction, to a large amount of coloured **waste rocks** (gossan rocks, kaolonitic schists, black schists etc), generally dumped around the pit over large areas. A large part of the village is built on such waste rocks.

The different facies of materials identified in the S. Domingos mining area are the following:

Waste rocks mainly extracted from the open pit:
They are composed of gossanous schists and gossan (iron oxyhydroxides-bearing rocks), kaolinitic schists, undifferentiated black schists, dumped around the pit and the village in heaps generally poorly vegetated and sources of physical erosion.

Low grade spent ore disposed in large dump leach piles (Figure 7):
These heaps are located in different areas on either side of the railway track. They are mainly composed of low grade schists with disseminated sulphide mineralization still active in acid drainage production (accumulation at the surface of retention water with very low pH during the rainy season). The heaps can exhibit different colours (from reddish to brownish-yellow) corresponding to oxidised materials with various concentrations of iron oxyhydroxydes.

Figure 7. View of dump leach piles partly covered with sulphidic ore (North of Moitinhos).

Sulphidic ore (Figure 7) corresponding to massive pyrite and base metal sulphides disposed of heaps, which are currently being oxidised.
Three small size different heaps of massive ore have been mapped in Achada do Gamo and in the North of Moitinhos. Those heaps are an important source of secondary salts deposited extensively around the mining area (jarosite), and locally efflorescent crust of blue mixed complex hydrated sulphates of Pb, Cu, Zn, K, Al, As, Fe, Ca (Figure 8).

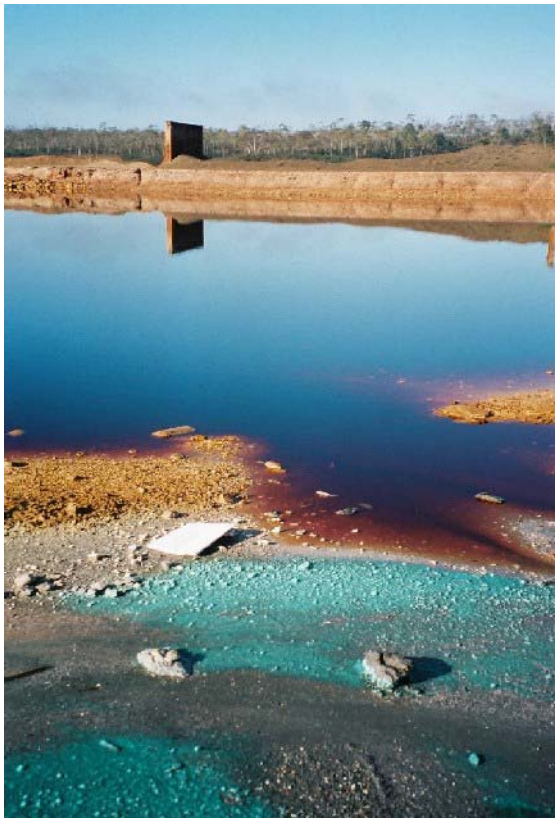

Figure 8. Complex hydrated sulphates precipitated in the vicinity of acidic water pond (Achada do Gamo).

Tailings and black muds:
Two different types of tailings (fine-grained waste remaining after beneficiation of ore through a milling process) have been identified in the area.
The most important one is composed of black mud enriched with sulphides, which is disposed at two different areas in Achada do Gamo. The enrichment process at the origin of this material is unknown.
A second type of tailings probably corresponding to crushing waste enriched with debris of schists and quartz has been dumped in the western part of the pit slope.

Metallurgical slags:
A number of slag piles, resulting from the smelting of ore, have been mapped in different places of the mining area (pit slope, Moitinhos and Achada do Gamo). In Achada do Gamo, the heap is presently partially exploited for road construction. This type of waste slags, is generally enriched in many of the same metals that were present in the ore being smelted. Furthermore, most of them exhibit secondary salts (sulphates) deposition and efflorescent crusts and are still very active in acid drainage production.

Supergene goethite-hematite deposit (ferricrete):
Ferricrete corresponds to Fe-hydroxides that precipitate directly on pre-existing surfaces and/or cement rock fragments. In Achada do Gamo and Telheiro, ferricrete occurs around the stream channel or within talus the deposits.

Leached bedrocks:
Corresponds to Volcano-Sedimentary and Flysch Formations affected by the channels and ditches with acidic seepage:

Large surfaces of barren landscape can be in around Achada do Gamo and in the south of Achada do Gamo (Figure 9). These outcropping VS and Flysch Formations (composed of reactive aluminosilicate minerals) have been exposed during decades to the effects of acidic water seepage downstream of the network of ditches and canal drainages. Those rock types that afford little or none acid-neutralizing capacity might have generated secondary minerals such as alunite (hydroxysulfates of Fe, Al, K, Na) and clays.

Figure 9. View of the leached bedrocks (Flysch Formation) in the south of Achada do Gamo.

Stream / pond sediment deposits:
Several water bodies exist in the study area (lakes and ponds are generally filled with coloured or uncoloured acidic water). Sediment deposition, mainly composed of secondary minerals, precipitated from the surface waters, has been mapped along the riverbeds as well as in the bottom of the dry ponds.

2.5. Expected contribution of hyperspectral data and GIS modelling

The most important contribution expected from hyperspectral data at the S.Domingos test site will be to detect evidence of superficial Acid Mine Drainage (AMD) (Section 2.4.2). This can be done using two different approaches concerning the imaged ground, one based on waste mining materials and other based on AMD minerals:

I) Waste mining materials

Some waste mining materials when leached by rainwater and stream waters can have high acid generating potential due to sulphide oxidation and Fe hydrolysis, which increases dissolution and mobility of polluting elements (Zn, S, Pb, Sb, Cu, As, Hg and Cd) that are enclosed (Section 2.4.1.). They constitute hot spots for waters, soils and plants contamination, being the present source of AMD. As described in Section 2.4.4., waste mining materials are easily identified in the S. Domingos test site and reflect complex chemical systems that can be seen far away from the main source. Mapping these materials using hyperspectral data can highlight the spread/dispersion of potential pollutants related to AMD according to their acid generating potential.

II) AMD Minerals

Traces of AMD can be detected through mineralogical data, where specific mineral assemblages define different degrees of acidity, as already highlighted by previous studies with hyperspectral data (Swayze *et al*.1999). Minerals such as copiapite, jarosite, hematite and goethite reflect haloes with different degrees of AMD. Some clay minerals also indicate AMD under certain conditions. Mapping these specific minerals will be indicative of the contamination potential related to AMD.

Most of the S.Domingos mining area is covered with incipient soils. The response of vegetation to assess vegetation stress, in small areas where significant data are present, involves assemblages of different species, with distinct spectral signatures, which makes the retrieval of this information very complex and time consuming.

Buffering minerals such as carbonates and silicates, with large surface areas and permanent charges such as smectites, have a very small expression on this test site.

The two potential contributions from hyperspectral data in this test site for AD detection will only be able to give the dispersion of the superficial AMD. However, for a reliable environmental assessment, it is required the interface with other relevant data in a GIS, thus allowing a global understanding of the problem. After superficial contamination mapping based on hyperspectral image processing, GIS tools can highlight the pollutant dissemination pathways, inducing soils and water contamination, and define their direction and extension. This can be achieved based on data such as drainage system and topography.

3. HYPERSPECTRAL DATA SET

3.1. Data acquisition survey

The HyMap^{TM} hyperspectral imaging spectrometer operated by *Hyvista Corporation* (HVC) covered the area using an aircraft *Dornier* 228, on 21August, 2000.
The *Deutsches Zentrum für Luft und Raumfahrt* (DLR) were responsible for the aircraft operations as well as acquisition of aerial photography with a Zeiss-RMK A 15/23 camera. Average altitude was 2500m and average velocity was 277 km/h, giving a ground resolution of 5x5m.
The area covered 726 km^2 corresponding to 11 strips (Figure 10), from which 8 have been partially selected (11, 10, 9, 8, 7, 6, 5, and 4) for detailed study as shown by the red rectangle encompassing the S.Domingos abandoned mining area.
397 aerial photos were acquired for generation of a Digital Terrain Model.

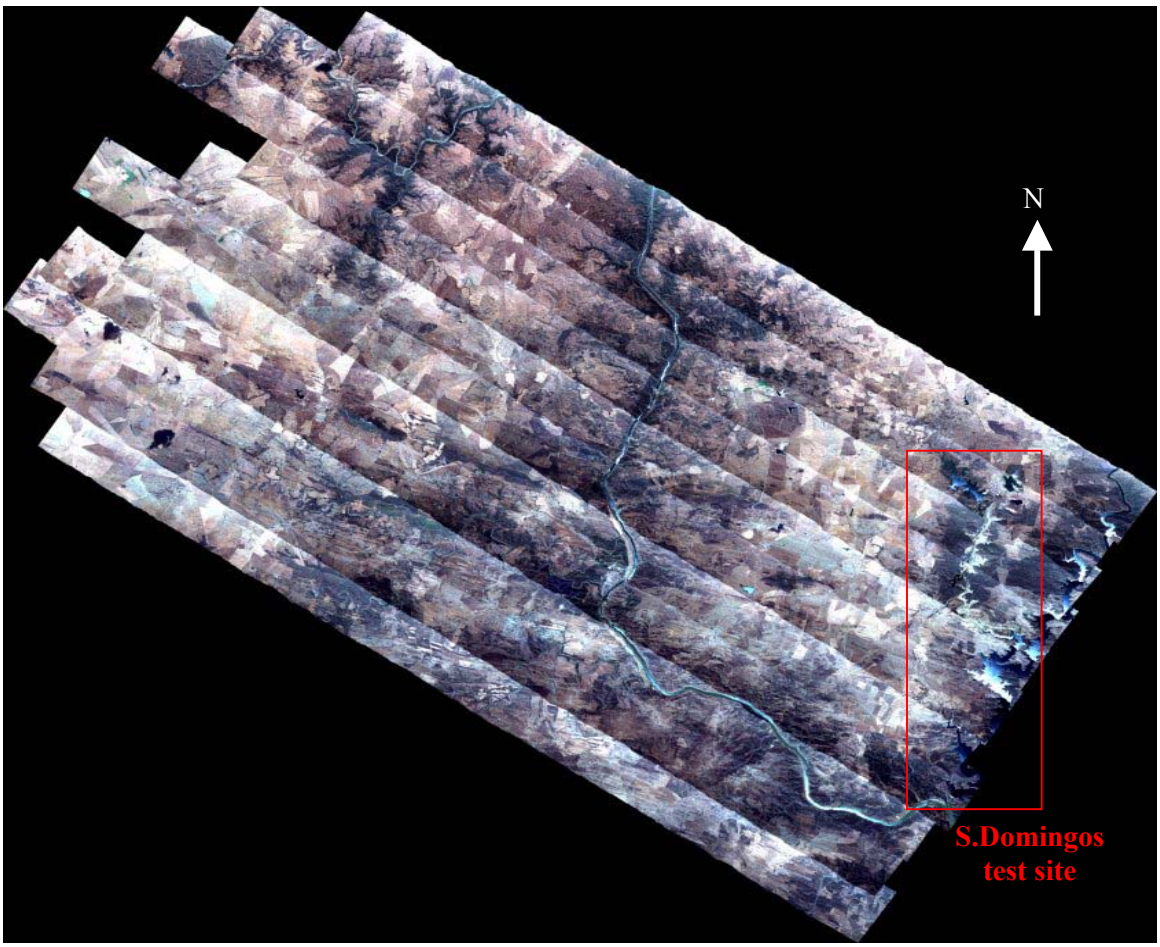

Figure 10. Georeferenced and mosaicked strips from HyMap sensor (After Hyvista Corporation).

3.2. Data quality checking, problems encountered

HyVista Corporation (HVC) delivered the HyMap data, acquired over the MINEO test site in Portugal, to the IGM at the end of January 2001. Due to anomalies verified in the data, further re-processing was carried out by HVC at the IGM´s request. The reprocessed data was delivered at the end of June 2001, with additional reflectance data and geocorrection files. An explanatory report was delivered in October 2001 (App. 3.1). The IGM´s data quality checking is presented in App.3.2, and shows slight differences compared to HVC since it excludes laboratory data calibration.

To analyse the quality of the Hymap images, negative and saturated pixels where identified and respective distribution graphs obtained for each image (strips 1 to 11), for the total 126 spectral bands. On average, these pixels represent only 1% of each image data, except for strip 6, where negative pixels total 1,55% of total pixels. Generally, anomalous data (negative and saturated pixels) occur mainly in spectral atmospheric image bands (i.e. near strong water vapour absorption bands). However, images from strips 7, 9 and 11 also show negative and saturated pixels along the visible (VIS) spectral region and in part of the near infrared (NIR) region. It was observed that the occurrence of anomalous pixels is more relevant along water bodies, probably due to specular reflectance, and on the top of the buildings. To reduce the effect of anomalous pixels, spectral atmospheric bands where removed from each image and spatial masks for water bodies where applied to the whole image datasets.

4. OTHER AVAILABLE RELEVANT ENVIRONMENTAL DATA

4.1. Selection of subareas

The area under study in the MINEO project comprises approximately 70 km^2 (Figure 10). Within this area, six subareas have been selected for data collection (soils, sediments, waste materials, waters and vegetation), for correlation and validation of hyperspectral data (spectroradiometric measurements, geochemical analysis, and parameters of environmental interest).

Previous knowledge based on the lithologic variability (App.1) and aspects related to mining and vegetation, helped in the definition of these sub areas expecting to assess different levels of contamination (Table 1). Sampling points were defined in a multiple distance of 5m, according to variability expressed in the field of the types of materials to be collected, to facilitate geostatistical analysis (Section 9.4.2). The projection system utilized was the national Hayford-Gauss *datum* Lisboa, with high precision GPS equipment.

Table 1. Definition of subareas for validation.

Items **Subareas**	**Environmen_ tal targets for validation**	**Sampling points**	**Geological Formations represented (App.1)** **Pyrite Belt (PB)** **Flysch Group of Baixo Alentejo (FGBA)**	**Dominant Vegetation**	**Mining Structures or absence**
Tapada	*Non Contaminated* (Reference)	34	Volcanic Sedimentary Complex (PB) Phylitic Quartzitic Formation (PB) Represa Formation (Chança Group)	*Lavandula sampaiana* Herbs	Proximity of clean water reservoirs developed for mining works
S. Domingos	Contaminated	23	Slags, dumps Volcanic Sedimentary Complex (PB)	*Erica australis or andevalensis/ Cystus ladanifer /Lavandula sampaiana*	Exploitation area, open pit
Achada do Gamo	Contaminated	35	Slags piles, heap dumps Mértola Formation (FGBA) Volcanic Sedimentary Complex (PB) Phylitic Quartzitic Formation (PB)	*Cystus ladanifer, Erica australis and/or andevalensis* Herbs	Sulphur factory rejects of processing
Telheiro	Contaminated	39	Mértola Formation (FGBA)	*Eucaliptus camaldulensis/ Genista polyanthus/ Erica australis and/*or *andevalensis* Herbs	Confluence of mining effluents/ uncontaminated waters, barren slopes due to AD
PomarãoN	*Non Contaminated* (Reference)	30	Mértola Formation (FGBA) Volcanic Sedimentary Complex (PB) Phylitic Quartzitic Formation (PB)	*Cystus ladanifer* Herbs	E of railway for ore transportation
PomarãoS	Contaminated	18	Volcanic Sedimentary Complex (PB) Mértola Formation (FGBA)	*Rosmarinus officinallis* Herbs	Harbor, shipment of the ore

Additional information out of these subareas was provided by a COBA Company study (COBA, 2000) unrelated to the MINEO project, except for local information concerning waters collected by IGM.

4.2. Potential and effective contamination

The potential and effective contamination has been assessed through different types of analyses, carried out on slags, sediments, soils and waters.

4.2.1. Slags

The solution collected after leaching waste material samples with water during 24 hours, were analysed for the elements Ba, Ca, Mg, Na, K, Al, Fe, Mn, Sb, As, Bi, Cd, Pb, Co, Cu, Cr, Hg, Ni, Ag, Au, Se, Zn, total N (Nkjeld) and for the anions Cl^-, SO_4^{2-}, S^{2-}, NO_2^-,NO_3^- and for total organic carbon (TOC).

Figure 11 shows sample location overlain on the waste material mapping (App. 2, Section 2.4.4).

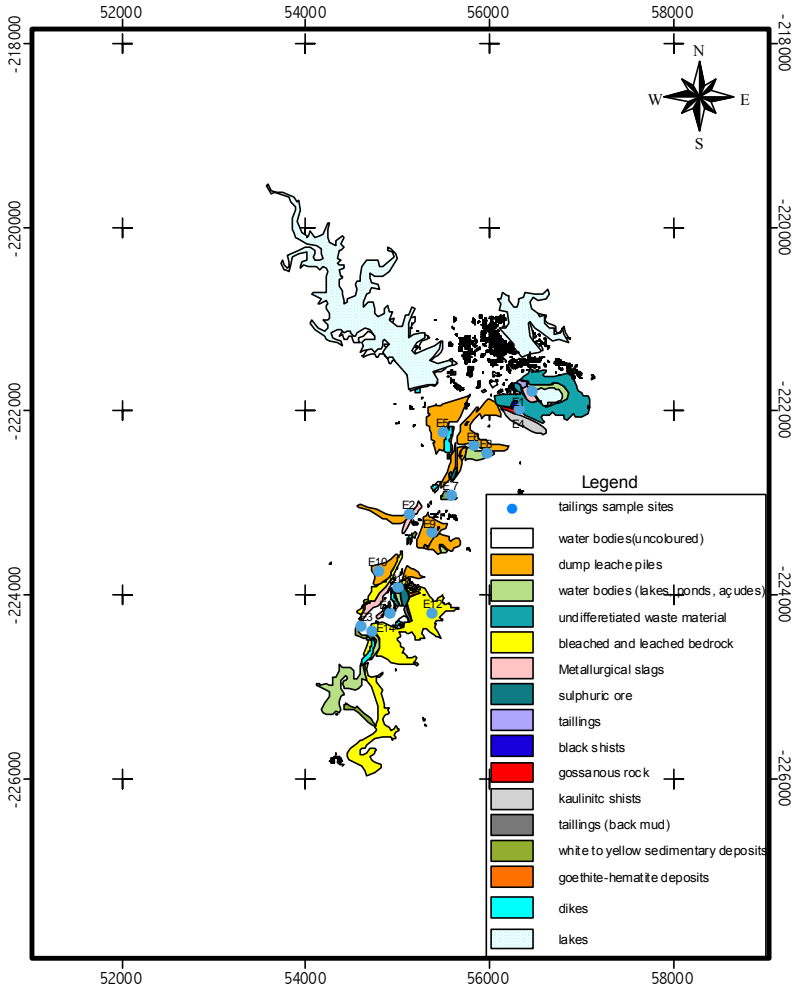

Figure 11. Sampling location of leached tailings waste material overlain on waste material mapping.

The leached solutions contain high levels in Al, Fe and SO_4^{2-}, with maximum values of 39400, 70205 and 116000 mg/kg respectively occurring in the area between the open pit and Achada do Gamo. Trace metals such as Zn, Cr, Pb and Cu also register the maximum values for the same area, respectively 15052, 4180, 1355 and 10780 mg/kg. The anions, with the exception of Cl^-, present negligible values. Table 2 represents several statistics of Al, Fe, Pb, Cu, Cr SO_4^{2-} and As.

Table 2. Statistics of leached tailing concentration results.

Statistics	Al	Fe	Pb	Cu	Cr	SO_4^{2-}	As
Average	14831.07	42087.29	295.05	1031.07	469.93	76907.14	62.06
Median	9650.00	34450.00	66.50	164.50	117.50	70850.00	9.15
Geom. M.	7971.82	39896.73	94.75	216.51	156.75	74720.31	18.53
Minimum	476.00	29548.00	11.70	15.00	28.00	56000.00	2.70
Maximum	39400.00	70205.00	1355.00	10780.00	4180.00	116000.00	298.00

4.2.2. Soils and sediments

Soil samples were collected in the 6 defined subareas (Figure 12) according to Table 1.

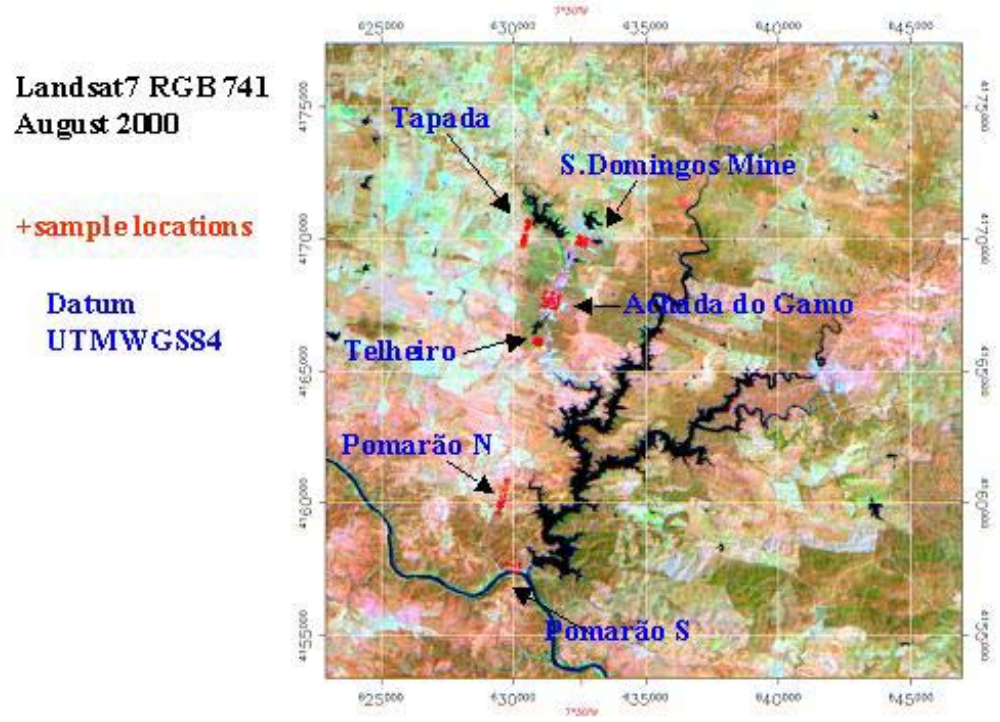

Figure 12. Environmental targets: subareas selection.

With respect to soil characteristics shown in App. 4.1 the potentially non contaminated subareas present pH>5, whereas the other pH values are mostly <5, except where soils were developed on silicate rock materials either *in situ* or either allocthonous (ranging from 5.5 to 8.0). Free iron (non silicate iron), organic carbon and particle size distribution present high variability in all the subareas, according to the bedrock weathering conditions and land use. The high content of the organic carbon in the contaminated subareas, are mainly related to ore processing conditions and transportation

Basic statistics for some elements, considered environmentally more relevant, are shown in App. 4.2. Potentially contaminated areas present high values of Pb, As, S, Cu, Zn, Cd and Hg. For instance, the maximum values determined for Achada do Gamo, Telheiro, Pomarão S and S. Domingos are 9300, 420, 24 and 11mg/kg for Hg and 80.01, 22.78, 0.90 and 14.17 mg/kg for Cd, respectively. These values are higher than the European maximum acceptable values for soils (1.5 mg/kg for Hg and 3.0 mg/kg for Cd).

The geochemical data and some soil characteristics were assessed via Principal Components Analysis (PCA), in order to improve the identification and interpretation of geochemical patterns and meaningful anomalies related to environmental problems or lithological background. This step reduces the volume of data creating 6 main composite variables (components), instead of the original 34. The components more clearly correlated with meaningful geochemical dispersion (App.4.3) were selected for geochemical mapping using geostatistic interpolation (ordinary Kriging).

Maps estimated for Tapada and Pomarão N, validate these two subareas as environmental background reference targets**.** In fact, soils from these areas present geochemical values related to the normal background lithology (App. 4.4).

The maps presented on the next figures are overlayed on the Digital Terrain Model and stream waters for better visualisation.

Maps estimated for S. Domingos reflect the chemical composition of the materials from which soils were developed, i.e. mining related materials (slags and dumps) or outcrop rocks. The 1st component (Figure 13) reflects the strong association between Hg, Pb, As, Sb, Au, Ag and Fe (gossanous materials). In opposition the association K, Mg, Na and U (lithological material).

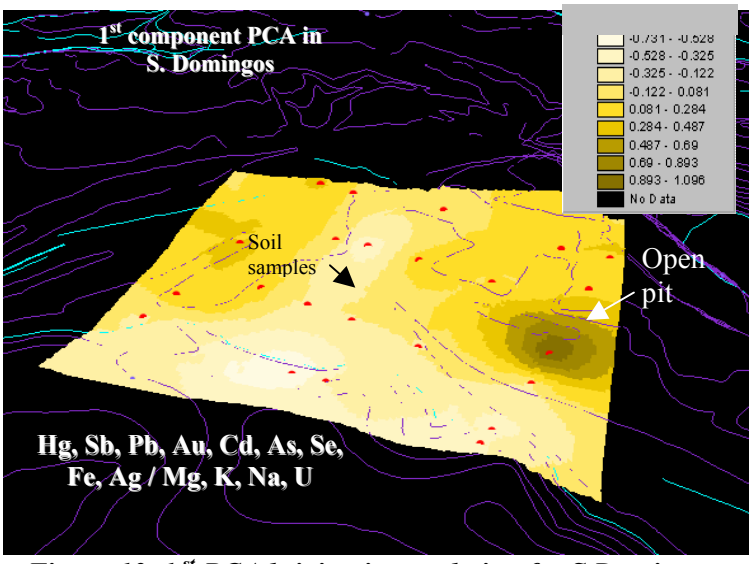

Figure 13. 1 st PCA kriging interpolation for S.Domingos.

In Achada do Gamo 1st PCA mapping (Figure 14) shows the strong association of Ag, As, Pb, S, Sb and Se, linked to waste material near the sulphur factory and sediments related to acid mine drainage (AMD).

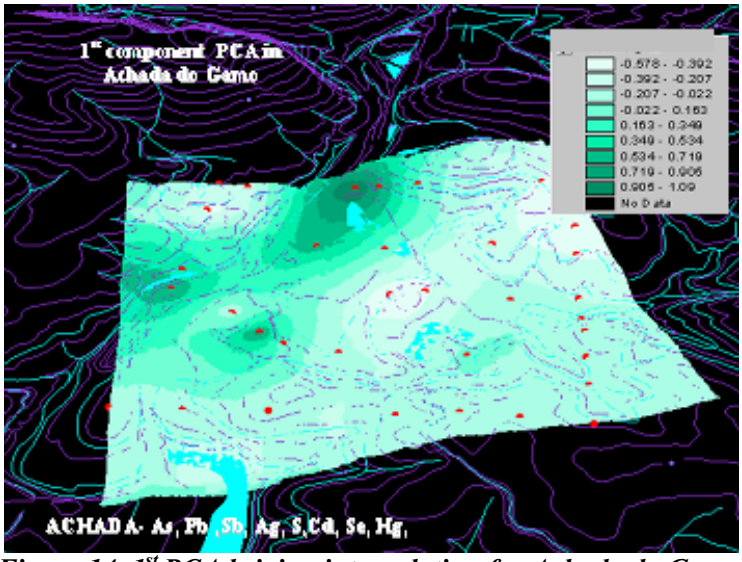

Figure 14. 1st PCA kriging interpolation for Achada do Gamo.

The Telheiro 1st PCA reflects the AMD pattern (Figure 15). In fact strong correlation between S, As, Pb, Sb, Cd, Ag, Au and Hg follow acid waters flow. Contamination is associated to mobilization of elements from Achada do Gamo (particulate material or dissolved) and acid waters/channels on the slope.

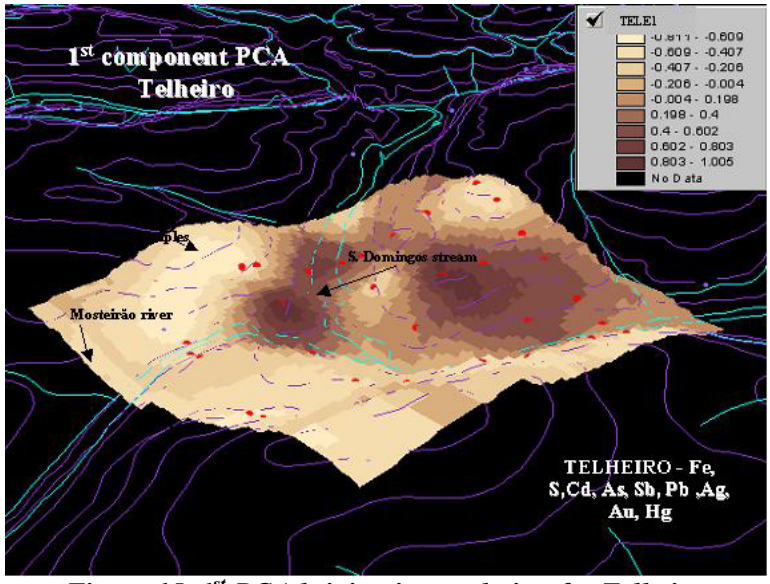

Figure 15. 1st PCA kriging interpolation for Telheiro.

In Pomarão S, the PCA analysis and spatial distribution of samples shows that contamination is strongly concentrated in the Harbour area with Pb, S, Sb, Zn, As and Cu near the shipping site. The contaminated samples located at high altitudes can only be explained by local wind conditions.

4.2.3. Mineralogical data

The soil mineralogy analysis for the non-contaminated areas of Tapada and Pomarão N shows that the soils are mainly composed of mica, kaolinite, quartz, interstratified mica-vermiculite, berthierine, halloysite, haematite and vermiculite. In the contaminated areas of S.Domingos, Achada do Gamo, the clay soil composition is made of mica, kaolinite, hydroxy-interlayer Al/Fe vermiculite, quartz,

goethite, haematite, and halloysite. Salts identified in the soils of S. Domingos, Telheiro and Achada are jarosite, natrojarosite, anglesite and plumbogummite. Salt efflorescence, only recognised in Achada do Gamo and S. Domingos, show a mixture of complex hydrated sulphates of Pb, Cu, Zn, K, Al, As, Fe and Ca. A mixture of copiapite and rumerite have only be recognised in Achada do Gamo. Alunite was also identified in S.Domingos.

Jarosite only occurs in soil samples with pH < 4.2 whereas hydroxy-interlayer Al/Fe vermiculite occurs in soil samples where pH lies between 3.5-6. This clay mineral does not occur in soils developed on dumps, which were not leached by acid waters (S. Domingos) even if pH lies in the same range.

4.2.4. Waters

The water data used in this review corresponds to superficial waters from artificial lakes in the S. Domingos stream and open pit, stream water, seepage waters and groundwater from wells and drillholes. Redox potential (*Eh)* was related to pH in order to determine the stability field of natural environmental waters and is represented in Figure 16. Groundwater, superficial water and seepage water distribution is shown in App.5.

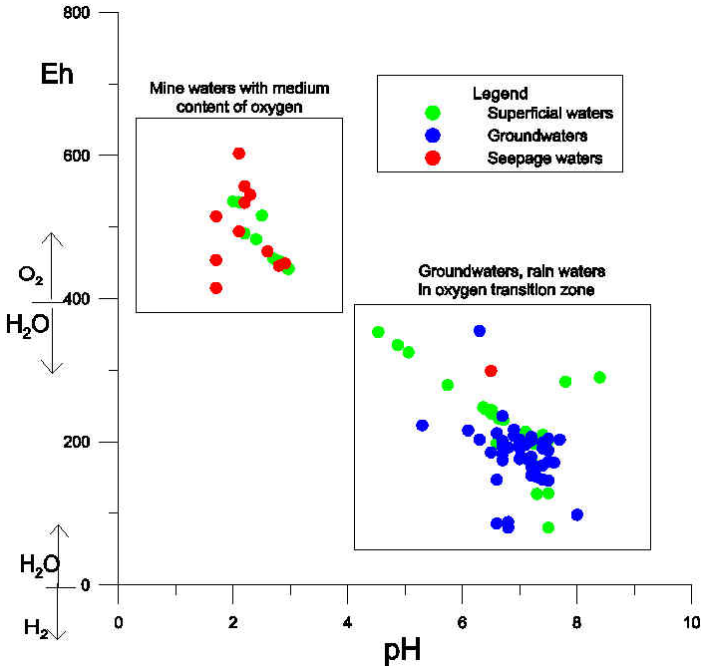

Figure 16. pH-Eh Stability diagram of the waters in the S. Domingos mining area (modified from Garrels & Christ, 1965* in *Appello & Postma, 1996).

4.2.4.1. Groundwaters

COBA (2002) analysed 10 samples from the 54 groundwater samples of drillholes and wells for several parameters, but only pH, Eh and Conductivity were determined for all the samples. The underground waters analysed are considered hard ($CaCO_3$ is above 100 mg/l); only one drillhole water located in Mertola Formation in Montes Altos has $CaCO_3$ below 100 mg/l. All the samples presented SO_4^{2-} (mg/l) content above maximum admitted values (all sites are in the surrounding area of mining influence). Iron was above maximum admitted values in all the samples except two groundwater

samples whose level was near the maximum. The most important water points were only analysed in the field and showed very high values for conductivity and normal values for pH (5-7.5).
The stability diagram pH-Eh for the 54 groundwater samples is shown in Figure 16. These waters lie in the stability field of mixed composition waters with medium content of oxygen and are represented in the diagram in blue colour.

4.2.4.2. Seepage waters

This water appears from under the tailings near the main mining stream. It results from the underflow of the infiltrated water in the waste materials in the limit between consolidated bedrock material and unconsolidated weathered material.

In Achada do Gamo and S. Domingos all kind of waste materials, varying from raw, coarse-grained materials to sulphuric acid in a liquid state, were abandoned since closure of the factory. This situation causes different chemical reactions and different surfaces for ion exchange in porous media where the water flows. These seepage waters were analysed for pH, Conductivity and *Eh*.

The lowest values of pH were measured in waters located in Achada do Gamo and in the S. Domingos infrastructures, in the waste material near cementation tanks. Leaching of waste materials by stream and rain waters lead to very low pH values which are sufficient to maintain dissolved trace elements such as Cu, As, Pb and Zn in high concentrations in solution. Generally, these waters are enriched in sulphur, iron and the above-mentioned elements as well as other elements leading to a change in their electric properties. Consequently these waters present high conductivity values. These values are highest in the Achada do Gamo area with pH 1.7 and 14800 μS/cm conductivity.

These waters were considered in mine water stability field in pH-Eh diagram (Figure 16) and are marked in red colour.

4.2.4.3. Superficial waters

Waters in natural and artificial lakes outside of the direct influence of the mining area and in stream waters and artificial lakes of the main mining stream were analysed. Physical and chemical properties of these superficial waters probably vary during the year due to climatic conditions of the region.

Waters collected outside of the direct influence of mining area presented high pH and low Eh and conductivity values. By contrast, the waters related to mining activities showed the lowest pH values and high conductivity.

The stability of these superficial waters is observed in pH-Eh diagram (green)(Figure 16). Its composition lies in the mine waters stability field for the waters from artificial lakes, in the main mining stream and open pit, while the rest of superficial waters, not directly located in mining area, appears to be in the rainwaters and intermediate stability field.

The most important spots in this scenario are located to the south of Achada do Gamo where pH values range from 1.4 to 2.5 (App.7).

A campaign for MINEO water sampling was conducted at the end of July 2000. The objective of this campaign was the use of physical and chemical characteristics of the superficial water in the interpretation of hyperspectral information. Due to some pixel saturation in water locations, that information was not considered and therefore results are not presented in this report.

4.3. Plants

Samples of *Erica andevalensis* and *Erica australis* were collected, in the same areas as that of the soil sampling, based on previous work that associate these plants with contaminated environments and taking into account their spatial distribution. The plants were analysed by INAA and ICP and correlated with the chemical composition of the soil, water presence in soils and sediments. The following conclusions are important:

- *Erica andevalensis* generally appears in soils with low pH (4.1>pH>3) and with relatively high concentrations in some chemical elements (e. g. Pb, Hg, Cu, As, Sb).
- *Erica australis* installed nearby the first species, grow in soils with relatively higher pH (3.5<pH<5).
- Both species seem to occupy distinct territories and seem to be tolerant to high contents of heavy metals and eventually develop accumulation mechanisms in the aerial parts.
- *E. australis* plants growing in soils with a medium heavy metal content, seems to concentrate chemical elements being its content higher in the plant than in the soils. This capacity for element accumulation is specially observed for Pb, As, Mn, Cu, Cd and Ni.
- *E. andevalensis* always appears in soils and sediments close to acidic waters and seems to be less tolerant to dryness than *E. australis*.

5. FIELD SPECTRORADIOMETRY CAMPAIGN

5.1. Sample selection, description of the material, relevance in environmental perspective

The spectroradiometric measurements have been carried out on soils, vegetation and rocks, as well as waste mining materials. Some spectroradiometric measurements were collected on the sampling points defined in the subareas presented in Section 4.1. for the S.Domingos test site. The reason for this is that these sampling points have ancillary data as the chemical or X-Ray diffraction analysis, which can aid on to better assess the contamination pattern that can be highlighted on spectral signatures.

The variability expressed in the S. Domingos test site has been translated through several spectral measurements, either collecting spectra on areas affected by contamination either without (Section 4.1.).

The spectra collected in contaminated areas have high relevance in an environmental perspective, once they can work directly as endmembers when mapping hyperspectral data.

The field spectroradiometry campaign is summarised in Table 3.

Table 3. Field spectroradiometric measurements.

Year (August)	**Spectroradiometers**	**Number Of spectra**	**Targets** **S**-soils, **V**-vegetation, **R**-rock, **W**-mining waste, **C**-calibration	**Areas** (Figure 12): **SD**-Sdomingos, **TA**-Tapada, **AG**-Achada do Gamo, **TE**-Telheiro, **PN**-Pomarão N, **PS**-Pomarão S, **O**-other
2000	GER MARK V	60	S, V, R, W, C	SD, TA, AG, O
2000	PIMA II	300	S, R	SD, TA, AG, TE, PN, PS
2001	ASD FieldSpec	200	S, V, R, W	SD, AG, TE, PN, PS, O

The spectra collected corresponds both to radiance and reflectance measurements, except for PIMA II that collects reflectance data.

5.2. Brief description of the spectroradiometer used

Three spectroradiometers were utilised in the field campaigns 2000/2001, as follows:

- PIMA II

Is a compact (shoe-box size) field-portable infrared spectrometer. The PIMA uses the short wavelength infrared (SWIR), from 1300-2500nm, and measures the reflected radiation from the surface of a sample using an internal light source. Each measurement requires no sample preparation and takes 30-60 seconds, allowing the rapid collection of a large number of analysis. The PIMA II has a spectral sample interval of 2 or 4nm and a spectral resolution of 7-10nm.

- GER MARK V

Is a self-contained optical system, rugged and portable, that works in the spectral range 300-3000nm. Spectral resolution is selectable in 2, 4 or 6 nm bandwithds. Scan time varies from 10 seconds to several minutes.

- ASD FIELDSPEC

A portable system that works in the spectral range 350-2500 nm, with three detectors, VNIR 350-1050 nm, SWIR1 1000-1800 nm and SWIR2 1800-2500 nm. It acquires reflectance, radiance or irradiance spectra in 100 milliseconds, with less than 10 nm spectral resolution.

5.3. Feeding MSL, spectra categories included in MSL

The spectra measured were introduced in the MSL in national geographic coordinates (national Hayford-Gauss *datum* Lisboa). The spectra have the same number of the nearest sampling point of the related subtest areas as described in Section 4.1 or additional numbers if distinct, maintaining however the subareas name if nearby.

Main categories of materials (site classification) comprise alluvial deposits, dump and mixed materials, rock outcrop, vegetation, vegetation and rocky surfaces, and a more generic waste.

Concerning the vegetation, with Mediterranean characteristics, signatures of the following species have been registered:
Eucaliptus camaldulensis, Genista polyanthu,Cystus ladanifer, Erica andevalensis and Erica australis. Generic grass and mixed vegetation are also included.

The Acid Mine Drainage (AMD) is the main contamination pattern found in the area. Signatures of waste material related to AMD have been extracted from HyMap^{TM} hyperspectral data, particularly where similar field signatures exist for comparison.

The definition of contaminated samples was based solely on their chemical analysis, irrespective of the obtained spectra.

5.4. Description of main spectral features representative of the materials to be mapped

SWIR spectra of all samples were measured with a PIMA-II infrared spectrometer. The samples were taken in the different subtest areas (Section 4.1.).
Qualitative examination of the data set obtained by PIMA indicates that most spectra are dominated by clay minerals: illite/muscovite and kaolinite/halloysite. Some samples contain sulphates: jarosite, gypsum.

In Figure 17 the PIMA II spectra are compared with USGS standard libraries available at ENVI Software (ENVI, 1999).

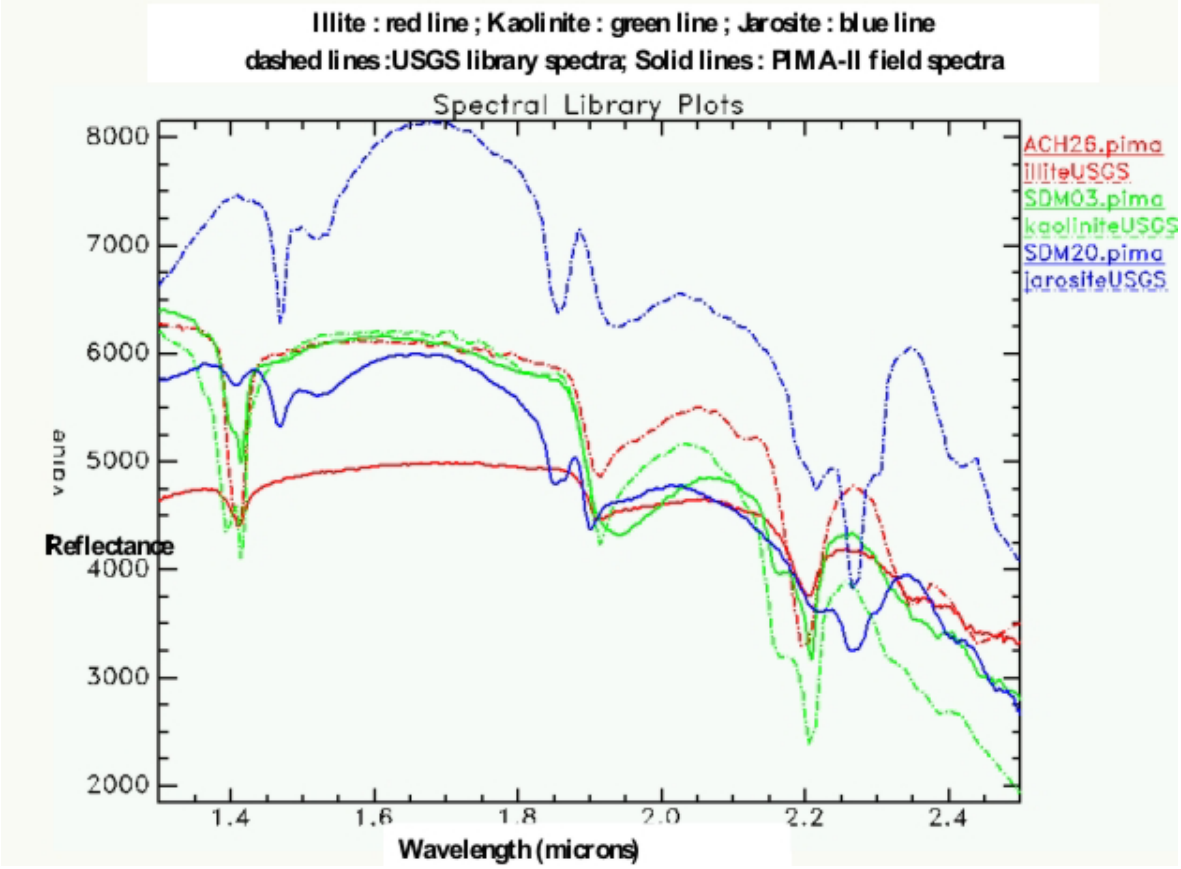

Figure 17. Comparative plot of PIMA-II field reflectance and reference library (U.S.G.S.) spectra of different types of field minerals.

Waste mining material has distinct signatures, varying from very low and homogeneous spectra, which is the case of dark metallurgical slag, to higher definition on the VNIR, depending of the weathering ratio.
In Figure 18 are presented some examples of dark metallurgical slag and mixed sulphur materials.

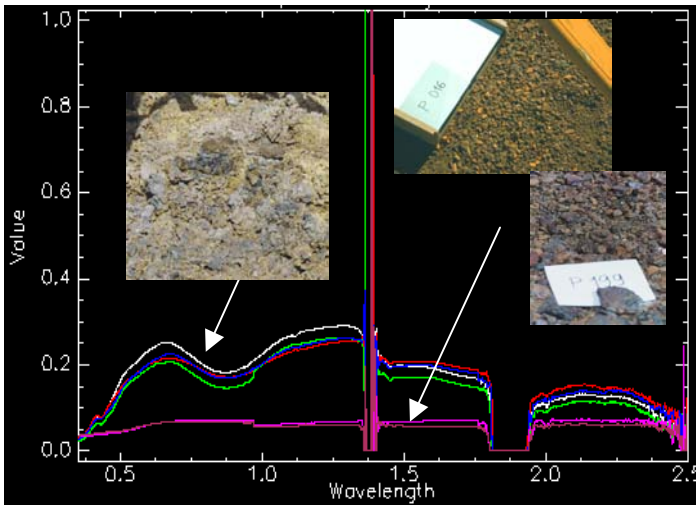

Figure 18. Spectra of waste mining materials using a GER Mark V spectrometer.

Other waste mining materials signatures show some dependency of others parameters such as water content and grain particle size.

The most interesting signatures utilised for hyperspectral processing are shown in Figure 23.

6. DATA PRE-PROCESSING

6.1. Atmospheric corrections

The objective of an atmospheric correction on Earth Observation data is the elimination of atmospheric effects, which influence the signal registered by the sensor and therefore mask the surface properties. An atmospheric correction can be performed using statistical or physical models to convert radiance to reflectance. The statistical methods are based on image data and/or ancillary ground data, while physical models utilise atmospheric data.

Concerning the Portuguese hyperspectral data, the contractor, HyVista Corporation (HVC), on its second delivery (Section 3.2) calibrated the radiance data to relative reflectance using the HyCorr algorithm. This is a modified version of the ATmospheric REMoval algorithm (ATREM) (GAO *et al*. 1999). The ATREM algorithm is an operational code for retrieving "scaled surface reflectance" from spectral imaging data collected by hyperspectral sensors, using image data.

These two software, HyCorr and ATREM, seem to produce similar results, according to the work performed by GBA MINEO partner (Groesel *et al*. 2002), who applied both to the Alpine Europe environment test site.

Afterwards, HVC executed an Empirical Flat Field Optimal Reflectance Transformation TM (EFFORT) program. This program determines and applies mild adjustments to ATREM (in this case to HyCorr) apparent reflectance data so the spectra appear more like spectra of real materials, and improving the accuracy of the apparent reflectance without field measurements (ENVI, 1999).

However, the correction performed assumes that the surface is horizontal and has a Lambertian reflectance, i.e. a perfectly diffusing surface where the brigthness of a point is independent of the

viewer direction, therefore leaving the effects of topography and illumination. In fact, the reflectance of real surfaces is represented in function of illumination geometry and viewing angle (through Bidirectional Reflectance Distribution Function, BRDF).

As illumination variations remain evident across the strips of reflectance data (Figure 10), additional corrections have been performed. These corrections were applied to strips 10, 9, 8, 7, 5, and 4 using a program developed by the BRGM for MINEO, requiring the use of MATLAB and ENVI software. The user empirically selects homogeneous training areas. After correcting the illumination effects in each strip, images are normalised to homogenise the whole data set. However, correction results do not seem to be completely satisfactory as they still present illumination variations. This method was subsequently abandoned and new corrections were performed.

To all the strips concerning the data selected for the MINEO project, a Cross-Track Illumination Correction, available in the ENVI software, was performed to remove these variations. Along-track mean values are calculated and a polynomial function, in this case of order 1, is fitted to the means (Figure 19).

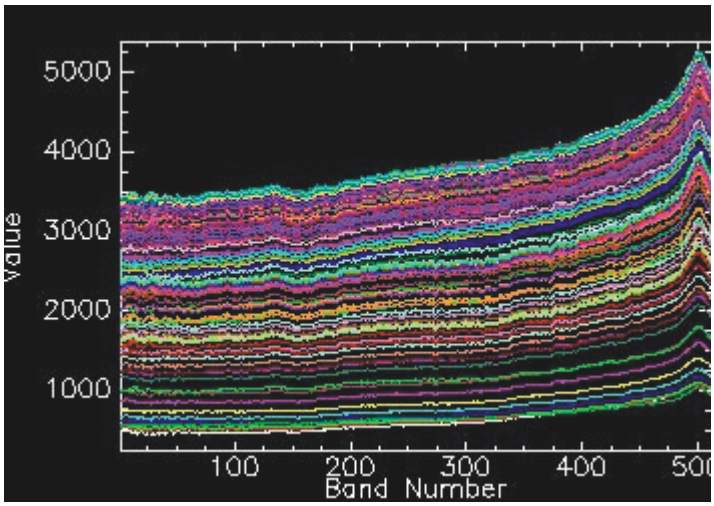

Figure 19. Example of fitted polynomial on Cross-Track illumination Correction.

The reflectance data is divided by the fitted polynomial, removing the most striking illumination variations. An example can be seen in Figure 20, where on the left side image there is no illumination correction, while on the right image the reflectance data has been divided by a fitted polynomial similar to Figure 19, homogenising the strip. The Figure 20 also shows the geometric correction (Section 6.2).

6.2. Geometric corrections, mosaicking

The contractor HyVista Corporation (HVC) provided additional data that reconstructs the scanning geometry of each image pixel using information from the sensor geometry and aircraft attitude (Differential GPS data flight). These data are *Input Geometry Map* file (IGM) and *Geographic Look Up Table* file (GLT) generated on ENVI software.

The IGM file contains map information stored in two bands, one for X coordinates (e.g., latitude or easting) and one for Y coordinates (e.g., longitude or northing). This file itself is not geocorrected, but does contain the geolocation information for each original raw pixel. The IGM file is used to create a G*eographic Look-up Table* (GLT) file that contains the information about which original pixel occupies which output pixel in the final product and can geocorrect any band or derived product through a simple lookup table procedure.

Each strip of hyperspectral reflectance data set has been geocoded, using GLT files, into rotated UTM system, *datum* WGS84, Zone 29N, reducing or eliminating significant distortions related to flight disturbances (Figure 20). Geocoded strips from 04 to 11 (Figure 10) were mosaicked (Figure 21, left image), resulting in a pixel size of 4.1m.

The reflectance data set corrected by the BRGM program (strips 10, 9, 8 and 7) have been also geocoded and mosaicked (Figure 21, rigth image) resulting in a pixel size of 4.2m. This data set was used for mineralogical mapping.

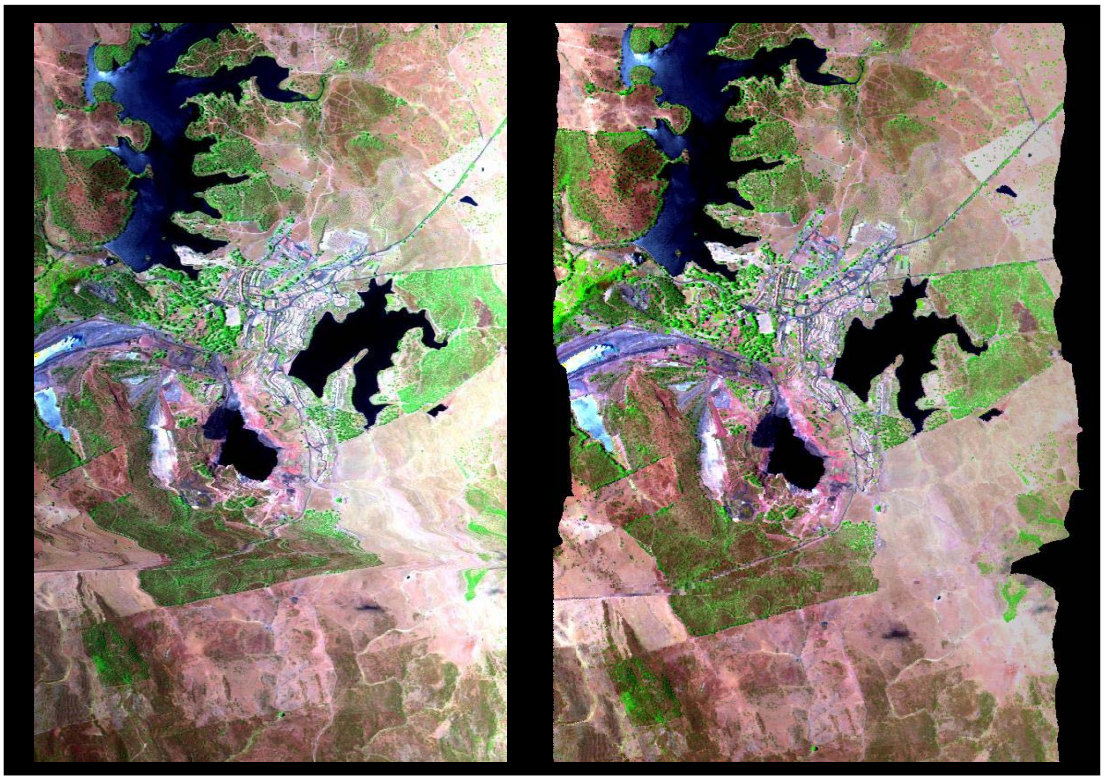

Figure 20. Example of geometric correction on a strip with strong flight distortion effects, after illumination correction (RGB: 1.634, 0.875, 0.678 nm).

The final mosaic data sets still present slight accuracy offsets due to lack of topographic information and absolute map position.

7. DESCRIPTION OF IMAGE PROCESSING PROCEDURES AND ALGORITHMS USED IN CONTAMINATION/IMPACT MAPPING

7.1. Objective

According to what is expected from hyperspectral image processing (Section 2.5.), the objective of surface contamination/impact mapping will be focus on the waste mining material signatures related to Acid Mine Drainage (AMD). To achieve this objective, the data has been worked separately under two targets, one related to waste material field signatures, and the other one related to mineralogical signatures. These two targets for mapping purposes are worked separately, within two distinct areas and also with different data sets (Figure 21). The mineralogical approach (performed by BRGM) is focused in S.Domingos, Achada do Gamo and Telheiro subtest areas, which are the most contaminated (right side of Figure 21), while waste material encompasses all the study area to assess the dispersion of acid generating materials globally (excluding strip6 as recommended by Hyvista Corporation, App.3.1). Mineralogical mapping has been performed on a data set that has a previous illumination correction using a program developed by BRGM (Section 6.1, 6.2).

Figure 21. Relative scale of both mosaics.

7.2. Procedures and/or algorithms

For mapping Acid Mine Drainage (AMD) generating materials the procedures and algorithms are described below.

7.2.1. Acid Mine Drainage waste material

According to the preliminary data set analysis, statistical, spatial and spectrally, a few steps were performed, before proceed with contamination mapping itself:

- Exclusion of some bands related to noisy signatures e.g. 1, 126, and to strong water vapour absorption bands, others that still have a high number of negative pixels and effects that still seem related to water vapour bands. Therefore, the data set selected for subsequent treatment corresponds to 114 bands (2-61, 67-91 and 97-125)
- Masks on water bodies have been applied due to some anomalies observed (Section 3.2)
- A vegetation index, where the image data set is transformed into a single band that shows the vegetation distribution, has been applied. The standard algorithm *Normalised Difference Vegetation Index (*NDVI, ENVI, 1999) was the one used, and very clear and fresh vegetation areas have been masked applying a threshold to the vegetation image

The decision to use both VNIR and SWIR bands is due to the fact that the waste mining materials show spectral signatures of interest that cover all this range or they are excessively flat to select a specific range.

Spectral analysis and mapping

The HyMap™ data set has been analysed using algorithms standardised in ENVI 3.5. Software (Boardman and Kruse, 1994, Green *et al.* 1988, ENVI, 1999):

- Minimum Noise Fraction (MNF) – applied to determine the inherent dimensionality of image data, to segregate noise in the data, and to reduce the computational requirements for subsequent processing
- Pixel Purity Index (PPI) - to find the most "spectrally pure" (extreme) pixels which typically correspond to mixing endmembers. The PPI image is computed on selected MNF bands by repeatedly projecting n-dimensional scatterplots onto a random unit vector. This image allows to retrieve endmembers when shown in n-Dimensional Visualizer
- Spectral Angle Mapper (SAM, see Section 7.2.2 description) – Classification method that match image spectra to reference spectra in n-dimensions using a physically-based spectral classification method

The procedures developed for AMD waste material contamination mapping are summarised as follows:

I) Analysis based solely on image information using spectral algorithms
II) Selection of target area based on expert information
III) Using field data for classification
IV) Enhancement of classified image

These procedures and their relationship are specified in flow diagram of Figure 22.

The part I) of the procedure analyses the image taking into account information solely based on image data, using automatic standard procedures (MNF, PPI). The endmembers retrieved on this analysis corresponds to n=48 and are considered as reference spectra for the next step, using the SAM classifier to match the spectra in the image.

On part II), the analysis of SAM results shows that several classified areas are known to be non-contaminated or even affected by mining works. To facilitate the next processing steps, minimise the data set size and concentrate in the area of interest, the *HyMap data set 1* has been masked (subset) of these classified areas, leading to *HyMap data set 2*.

Although not mentioned in Figure 22, another mapping algorithm as been tested: Matched Tunned Matched Filtering (MTMF, see Section 7.2.2 description). However, this classification method gives obscure results.

On part III) is involved a careful observation and analysis of spectroradiometric field signatures. Based on this observation, some spectra were selected (Figure 23) which take into account ancillary data (geochemical or mineralogical) when it exists. Even if some signatures are similar they have been also included, due to their importance and for eventual merging at the end. Others are not shown, once they are clipped at the final classification.

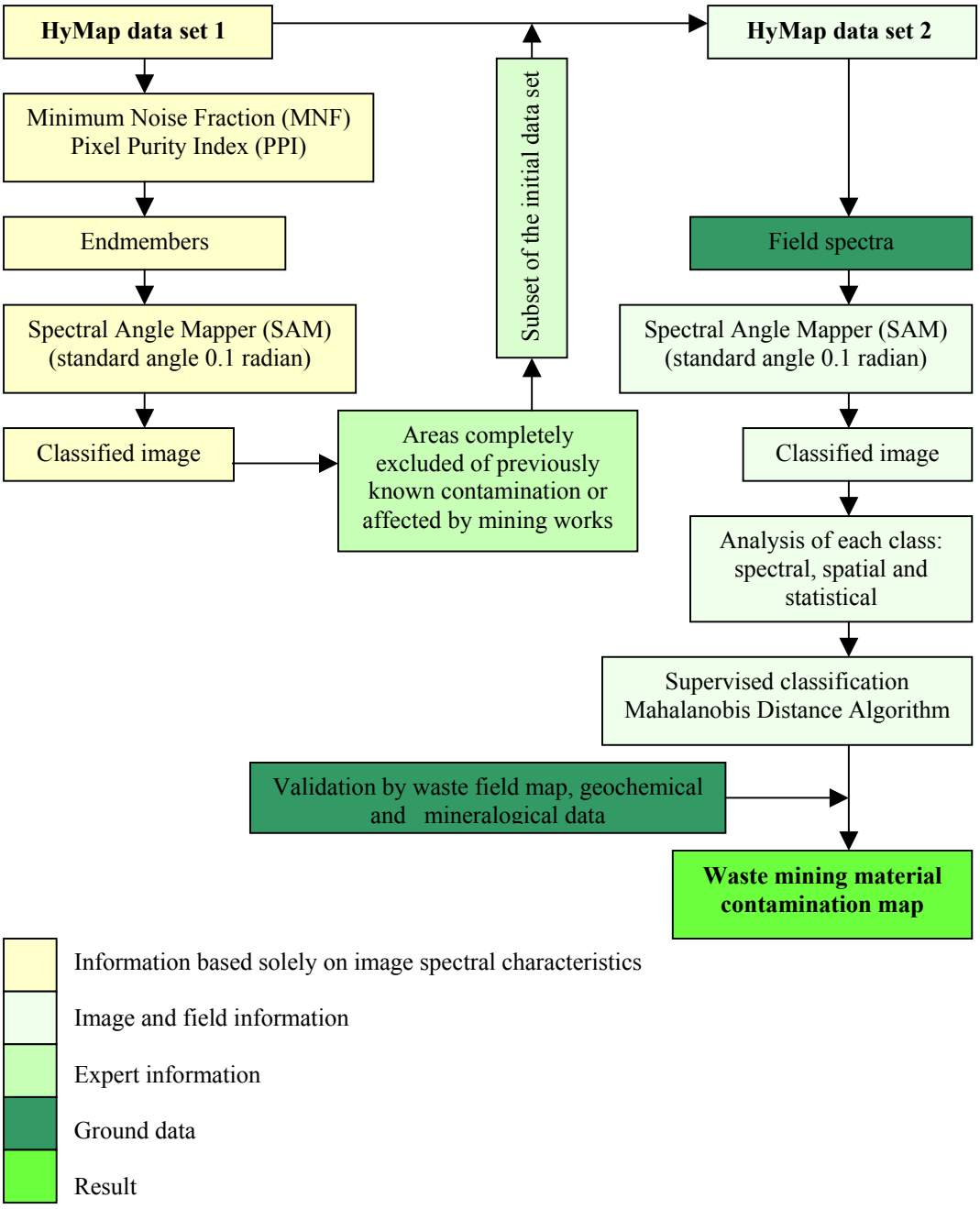

Figure 22. Flow diagram of procedures for the AMD waste mining material mapping.

In fact, the SAM algorithm has the advantage of being insensitive to remnant illumination effects, but all the endmembers must be known. The technique to achieve good results is to introduce several endmembers that would translate the reality of the image, therefore including spectra that are not of specific interest for detection of surface contamination.

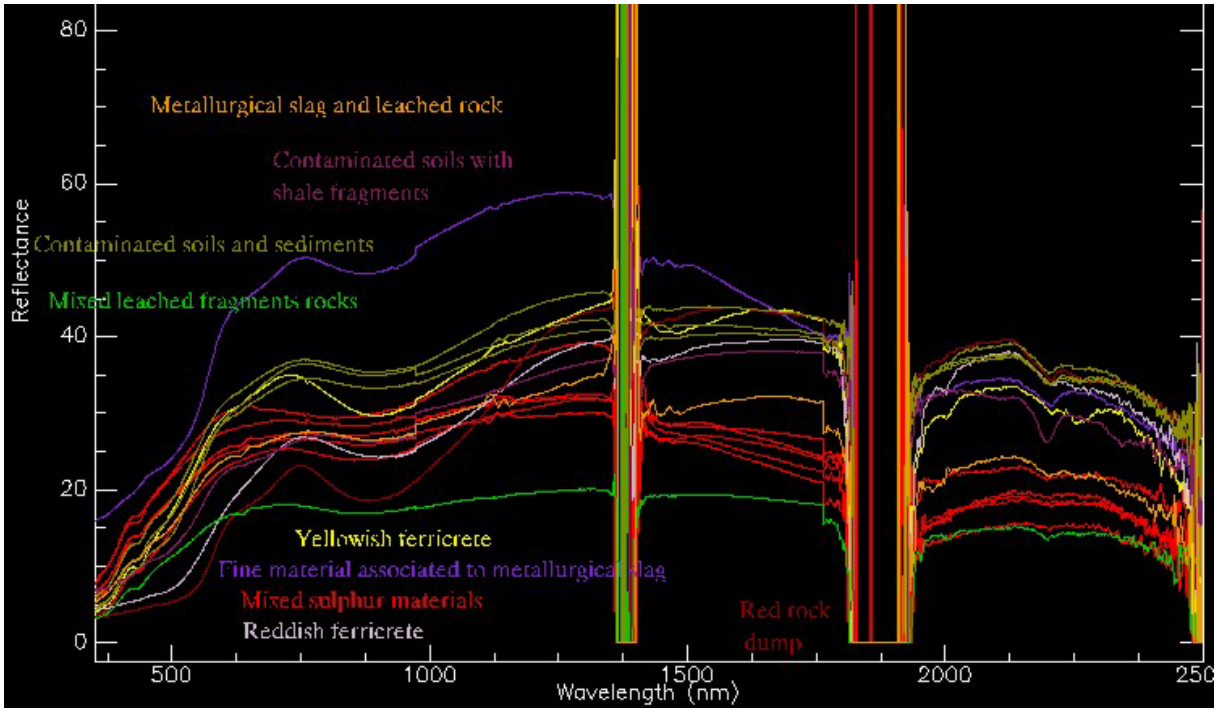

Figure 23. Field spectra used in the SAM classifier.

These spectra were used to map the hyperspectral data using the SAM algorithm with a maximum angle of 0.10 radian, a default number that gives good classification results. Again, the MTMF algorithm shows obscure results, as already highlighted previously.

On part IV) the SAM results are analysed (spectral, spatial and statistically). Some classes are grouped based on similar spectral signatures (similar field signatures) and spatially contiguous results. Other classes show some clusters of the medium spectra classified. In fact, differences in spectra may not be separated by the same angle, remaining in distinct clusters (Figure 24).

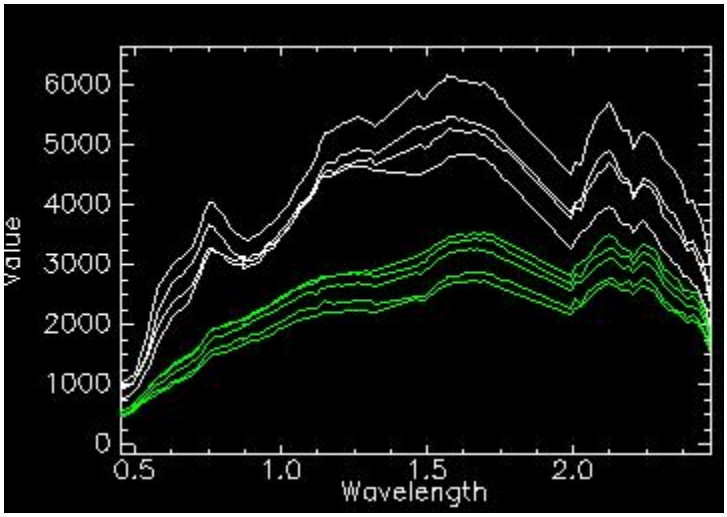

Figure 24. Example of distinct clusters for the same class from SAM results.

A supervised classification using the Mahalanobis algorithm, a direction-sensitive distance classifier that uses statistics for each class, has been successfully applied to some of the more critical classes, taking into account that different spectra correspond to distinct field areas. This led to an image that

separates different spectral signatures, clearing some classification mismatches. A final adjustment has been done to the class's nomenclature as a way to be more understandable for a user not familiar with the test site, and taking into account ancillary field data and observations.

7.2.2. Acid Mine Drainage mineral mapping

The analyses of the HyMap data have, until now, resulted in maps of Fe-bearing minerals indicators of acidic mine waste. For this investigation, attention focused on the pyrite weathering minerals: jarosite, goethite and hematite. Pyrite oxidation is the primary source of mining-related acidic runoff because sulfuric acid (H_2SO_4) is a product of this weathering reaction. Pyrite itself is difficult to detect directly using HyMap because of its extremely low reflectance; however its oxidation products are spectrally bright and have strong 1-µm absorption due to Fe^{3+} in the matrix. Infrared spectra of the pyrite weathering sequence minerals show a broad Fe^{3+} absorption band centered near 0.8 µm. The exact center of this band and its shape are different for jarosite, hematite, and goethite, allowing them to be mapped by the algorithms. Jarosite can be further differentiated by a strong absorption near 2.3 µm.

Methods

Two different mapping methods have been used:

- Mixture Tuned Matched Filtering (MTMF)
- Spectral Angle Mapper (SAM)

The methods are available through the ENVI 3.5 software package and are validated extensively in the scientific literature. Further references and in-depth of the methods can be found in Kruse *et al*.(1993), Boardman *et al*. (1995) or the ENVI manual.

Mixture Tuned Matched Filtering

Mixture Tuned Matched Filtering (MTMF) is a method that estimates the relative degree of match of a given pixel to a reference spectrum and approximates the sub-pixel abundance. The images are atmospherically corrected and a Minimum Noise Fraction (MNF) is run to isolate the noise in the data in separate bands. From the Eigenvalue plot and after the visual examination of the different MNF images the first 15 MNF bands were selected for further processing. The MTMF is then done using endmembers for the requested materials. Endmembers are spectral signatures from USGS spectral library. Reference minerals were chosen from XRD (X-Ray Diffraction) results on field waste samples and are iron minerals related with AMD.

The outputs from the MTMF are two bands for each endmember, estimating the abundance of the spectrum in the pixel (MF-score) and an estimate to reduce the 'false positives' (infeasibility). Correctly classified pixels will have a high MF-score and a low infeasibility. The higher the MF-score is the higher the abundance of the material will be in the pixel. Final mapping has been done using subjective selection on a 2D-scatterplot of the MF-score and infeasibility based on the related spectra.

For the goethite only areas with infeasibility below 20 and MF-score above 0.35 were chosen. The MF-score value is different for each mineral mapped.

Spectral angle Mapper classifier

The Spectral Angle Mapper (SAM) is a supervised classification technique that measures the similarity of image spectra to reference spectra from a spectral library, or from field and laboratory spectra. SAM measures similarity by calculating the angle between the two spectra, treating them as vectors in n-dimensional space, with n being the number of bands (Kruse et al., 1993). Smaller values for the angle indicate higher similarity between pixel and reference spectra. SAM is an interesting classification tool in that sense it is independent from variation in illumination

For both classification methods, vegetation ad water areas have been masked to work only on bare-soil pixel an avoid problems related to specular reflectance in water.

7.3. Description and assessment of the map(s) produced vs. expected results

7.3.1. Acid Mine Drainage waste material

Extension of acidic waste material

A simultaneous classification for all the hyperspectral mosaic using the procedures described in Section 7.2.1, are shown in App.6, 6.1.AMD Waste Material (S.Domingos) and 6.2. AMD Waste Material (Pomarão). To be more comprehensive, the App.6.1 reports to the same area that is covered by mineral mapping (Section 7.3.2), and also because it concerns the areas of greater interest, i.e. S. Domingos, Achada do Gamo, Telheiro, and also Tapada. In App.6.2, the results report to the Pomarão Harbour, 7 km to the south of Telheiro from the area covered in App.6.1, including also some sectors in Spain divided by the Chança dam.

It is very clear how the spectral signatures map the dispersion of materials, on a regional scale, i.e. until the Pomarão Harbour, some 15 km from the village, highlighting the railway track from Telheiro with contamination materials (App.6.1 and 6.2) as well as other others areas.

A remark should be done that the better mapping was obtained using some local signatures in the Pomarão, S.Domingos and Telheiro areas, while signatures obtained directly in Achada were not relevant. An explanation could be that the complex chemical system that is present in Achada do Gamo, due to intense interaction of materials, while in Pomarão they correspond to less mixed materials.

In fact, only the processed ore was transported here, while at Achada it corresponds to its production. Also, similar signatures obtained from ASD Fieldspec and GER spectroradiometers were predominantly mapped by the former.

To reliably check the extension of contamination signatures, further local chemical and mineralogical analysis should be made, in places where there is no data available.

The equivalent of some HyMap classes and field signatures are shown in Figure 25.

Globally, the results obtained, using the combined steps mentioned, are quite interesting, and highlight the extension of distinct types of waste materials. Table 4 shows the main characteristics of the classification results and the importance related to AMD.

Generally, the classification matches well with field mapping, geochemical data and also mineralogical mapping, when available. Table 5 shows the classified image results when intersected by ancillary field data results and analysis. Concerning waste field map, must be take into account that classification results show much higher discrimination then the units defined, and the scale is not as accurate as the classification image. Geochemical results of soils and leached tailings give an extensive intersection table of elements, (not shown) and confirm the pollutant content of the classes.

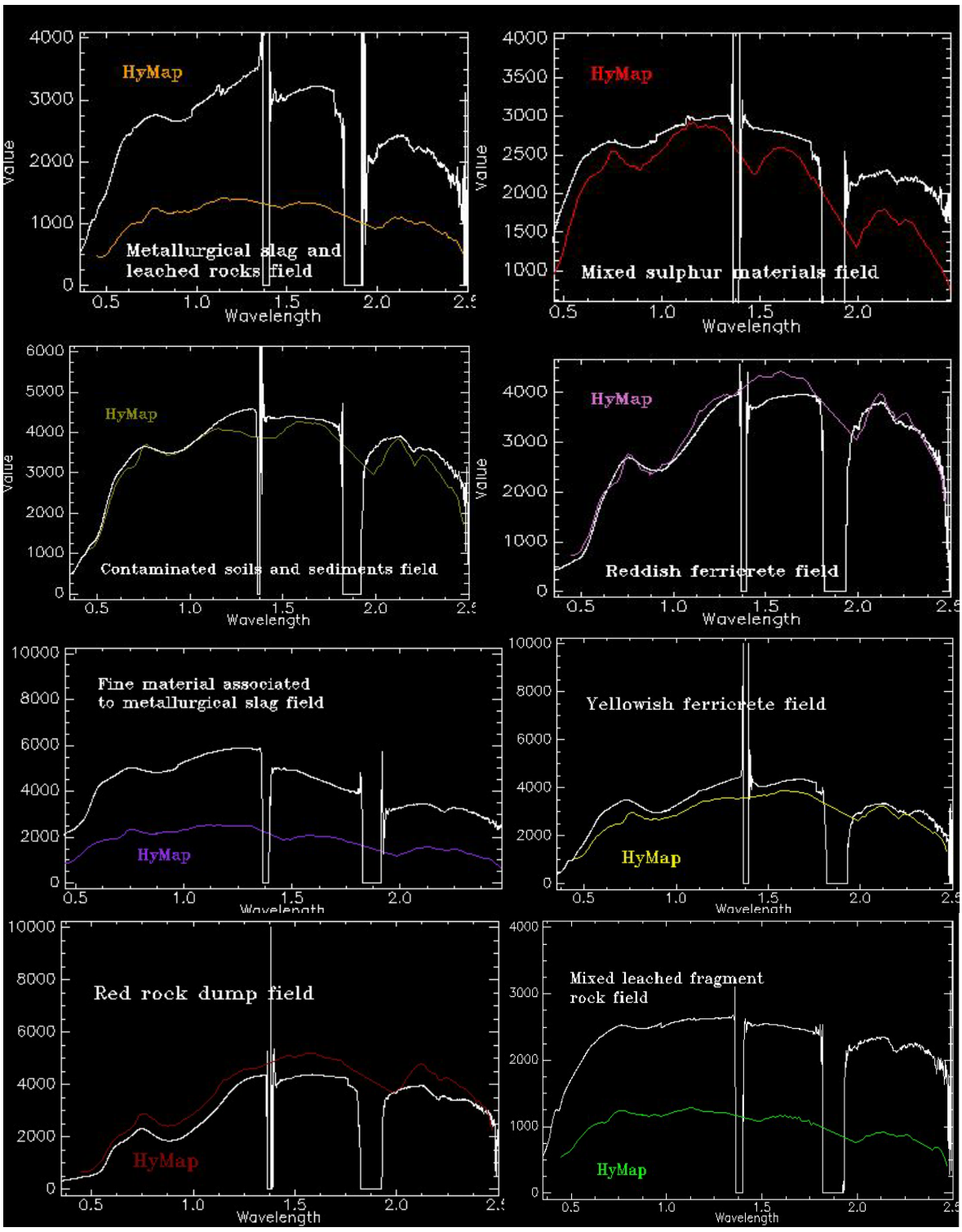

Figure 25. Examples of most important spectra of the HyMap classification image (colour) and respective field spectra (white).

Table 4. Main characteristics of the classification results.

CLASSIFICATION RESULTS	CLASSIFIED AREAS (2,172,776.444 m² of 7,446,191.220m²)	MAIN CHARACTERISTICS *validated by partial field checking
Mixed sulphur materials	83,243.116 m² (3.83%)	High acidic potential, systematically map surrounding tailings ponds and dams, highligths other unknown areas
Metallurgical slag and leached rock	570,027.072 m²(26.23%)	Metallurgical slags (high acidic potential) and leached rocks, the 2nd most important cover *Mahalanobis algorithm not yet included for separation
Fine material associated to metallurgical slag	19,818.989 m²(0.91%)	Essentially related to metallurgical slag, surrounding or overlaying some piles of these materials
Yellowish ferricrete	246,955.698 m² (11.37%)	Significant spread in the area, particularly associated to areas affected by AMD
Reddish ferricrete	44,176.678 m²(2.03%)	Gossaneous materials around open pit and other areas
Mixed leached fragment rocks	159,459.652 m²(6.76%)	Heterogeneous materials of several grain sizes and colours
Whitish leached rock	146,784.913 m²(0.23%)	Variation from previous, mostly located at higher altitude.
Red rock dump	5,059.810 m²	Particularly distributed around open pit area
Contaminated soils and sediments	876,322.067 m²(40.33%)	Spread over the area, including the village and part of dump leach piles, correspond to contaminated field spectra signature
Contaminated soils with shale fragments	20,928.449 m²(0.96%)	A variation from the previous, with a more heterogeneous grain size and less dispersed

Table 5. Field waste validation map and mineralogical data intersection of classified results.

CLASSIFICATION RESULTS	MAIN FIELD WASTE MAP UNITS	X-Ray diffraction results (soil clay fraction and salts)
Mixed sulphur materials	Sulphidic ore, tailings (including black mud), dump leach piles, metalurgical slag	Jarosite, goethite Mixture of complex hydrated sulphates of Pb, Cu, Zn, K, Al, As, Fe and Ca. Mixtures of copiapite and rumerite (vestigial)
Metallurgical slag and leached rock	Metallurgical slag Dump leach piles and	Complex mixtures
Fine material associated to metallurgical slag	Metallurgical slag, Bleached and leached bedrock	Complex mixtures
Yellowish ferricrete	Tailings (including black mud), dump leach piles, leached and bleached rocks	Goethite, heamatite
Reddish ferricrete	Gossaneous rock, goethite/heamatite bodies	Heamatite, goethite
Mixed leached fragment rocks	Dump leach piles, Metallurgical slag	Illite, Kaolinite, quartzo
Whitish leached rock	Bleached and leached bedrock, Dump leach piles	Illite, jarosite, interstratified vermiculite-smectite, goethite, quartz
Red rock dump	Gossaneous rock, undifferenciated waste rocks	Hematite, goethite
Contaminated soils and sediments	White to yellow sedimentary deposits, Kaolinitic schist, Dump leach piles, kolinitic schist	Kaolinite, illite, jarosite, natrojarosite, sulphur (vestigial)
Contaminated soils with shale fragments	Bleached and leached rocks, Dump leach piles	Illite, kaolinite, quartz, jarosite

This classification shows how an area exposed to long time exploration and complex chemical systems can be environmentally assessed by specific signatures related to AMD, which is the first step for the development of monitoring systems.

7.3.2. Acid Mine Drainage minerals

Extension of Fe-bearing minerals indicators of acidic mine waste

Using MTMF it was possible to delimitate the extension of Fe-bearing minerals. To facilitate comparison with the map of mining residues drawn from field observations and with features on the ground, waste map was transformed to vectors and overlaid on HYMAP image together with mineral map issued from image classification (App.6.3).

Spectral Angle Mapping technique using USGS mineral spectral library in the 1µm (SWIR1) spectral domain has revealed excellent capabilities in mapping minerals from the pyrite weathering sequence responsible for AMD at the Sao Domingos Portuguese test site. Preliminary SAM classifications are then refined on the rules images, by shortening the angle used in the process to better discriminate between the classes. The most significant materials detected were then assembled into color-coded mineral map. Here again, to facilitate comparison with the map of mining residues drawn from field observations and with features on the ground, waste map was transformed to vectors and overlaid on HYMAP image together with mineral map issued from image classification (App.6.4).

Both mapping methods led to the identification of AMD-generating minerals. Their extension is correlated with the extension of different waste types mapped on the field.

Goethite occurs in gossan (iron-oxide bearing rocks) areas and around the open pit. Jarosite and alunite are mapped mostly in dump leach pile areas, sulphidic ore areas and tailings and black mud areas Moitinhos and Achada do Gamo). Goethite and, to a certain extent hematite correspond to supergene goethite and hematite deposits. Characterising and mapping jarosite and alunite enables thus to retrieve areas exhibiting pyrite, secondary salts (sulphates) deposition and efflorescent crusts which are still very active in acid drainage production.

Results from both classification methods are convergent, even if the mapped extension for each class is different. Indeed, SAM overestimates the extension of pyrite-weathering sequence minerals compared to MTMF. Pixels identically mapped from both methods have been reported on map App.6.5.

N-Dimensional visualizer enables the representation of pixel spectra identically mapped from both methods, for MNF bands 1, 3 and 7, together with USGS spectral library corresponding spectra. The representation of the regions in the spectral feature space forms elongated data clouds in the n-D Visualizer, showing global class separability (Figure 26).

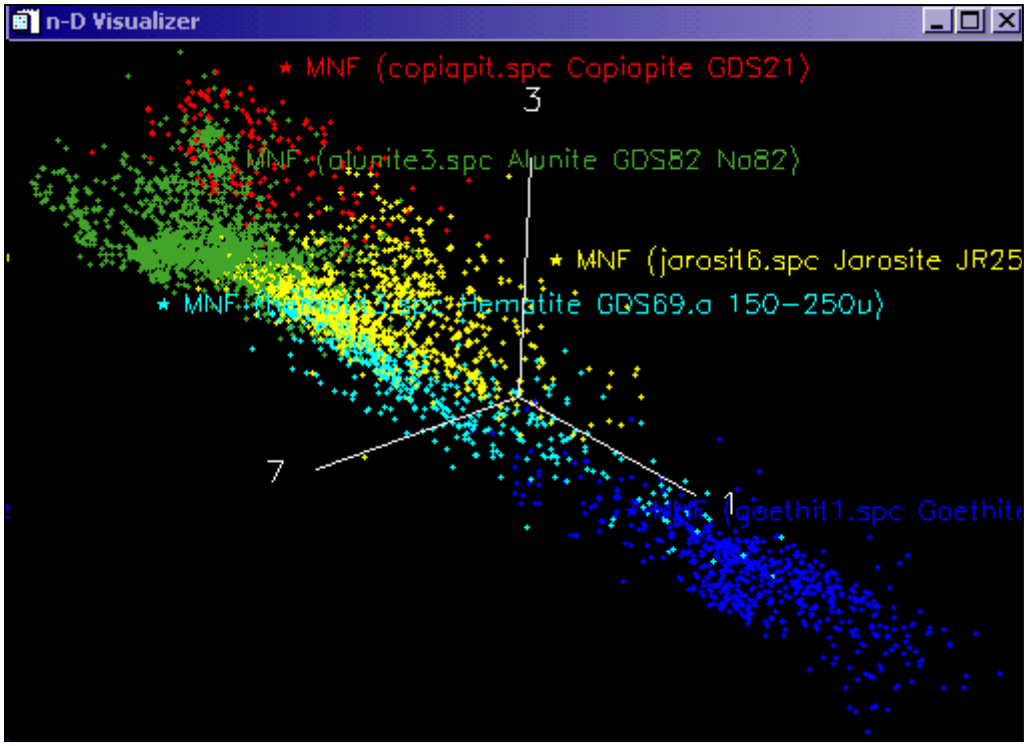

Figure 26. n-Dimensional Visualizer projections for iron-bearing minerals for 3 MNF components. USGS spectra chosen as references for SAM and MTMF treatments.

Figure 27 shows average spectra from HYMAP image for regions classified by both SAM and MTMF methods as AMD minerals and USGS library spectra used as end-members. Similarity of most of them and the spectral features of interest are obvious, in particular in the 1µm region. However, the similarity between USGS and HyMap image is low for hematite. It is worth noting that all end-member minerals present on the site have not been studied.

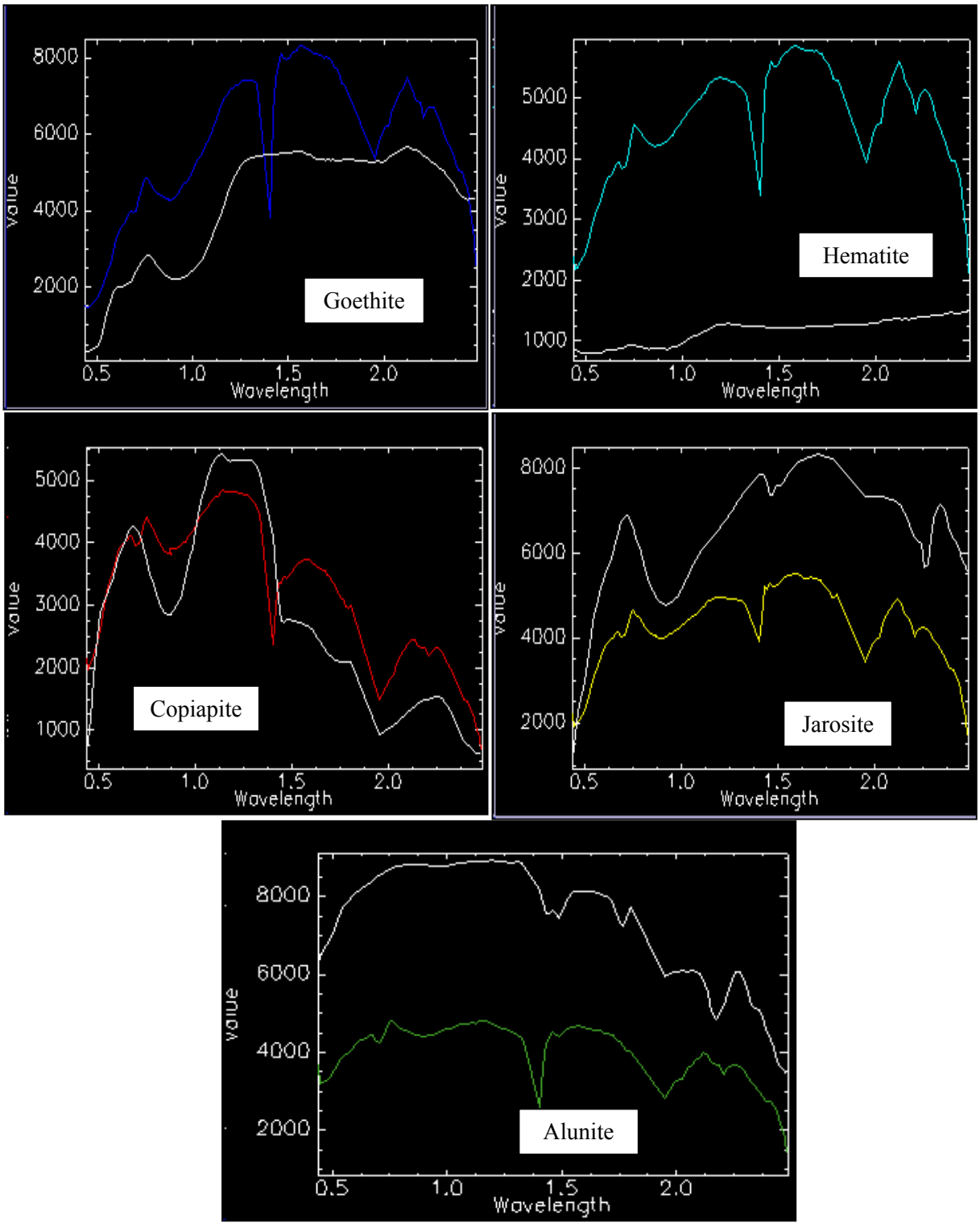

Figure 27. Mean spectra from HYMAP image for regions classified by SAM and MTMF as AMD minerals (color lines) and USGS library spectra (white lines) used as end-members.

It must be mentioned furthermore, the influence of clay minerals, systematically present on the site modify the spectral signature of the studied object compared to laboratory spectra.

7.4. Invaluable contribution of hyperspectral imagery vs. conventional sensors

Hyperspectral sensors show significant added value compared to conventional sensors, especially linked with spatial and spectral discrimination capabilities but also concerning the statistical/mathematical methods used. Hyperspectral image processing can identify minerals based on spectroscopic principles using spectral libraries, while conventional sensors are usually used to discriminate and classify natural targets.

The preliminary results of Image Processing performed on a conventional sensor, Landsat ETM+, using the same methodology as applied for hyperspectral sensors (Section 7.2.1, 7.3.1) are presented in this chapter. The results obtained with both sensors, HyMap and Landsat ETM+, are compared.

7.4.1. Landsat ETM+

Some preliminary studies in a Landsat ETM+ data imagery over S.Domingos test site, contemporaneously with hyperspectral data acquisition from (August 2000), highlights the possibility of mapping some general features linked with mining activity and related pollutants. Some algorithms were developed using Principal Component Analysis (PCA) factors and also HIS and Colour Normalised (Brovey) sharpening by merging a higher resolution greyscale image (panchromatic band 8 from Landsat ETM+).

For comparative purposes, preliminary studies proceed on the Landsat ETM+ image, using the same methodology as described for waste material hyperspectral mapping on Section 7.2.1. The first step of the procedure, based solely on image information (Figure 22) gives the SAM classification image illustrated in Figure 28, in one case without using thermal infra red (TIR) bands 6 (Figure 28a), in another case using TIR (Figure 28b) not covered by HyMap™ sensor.

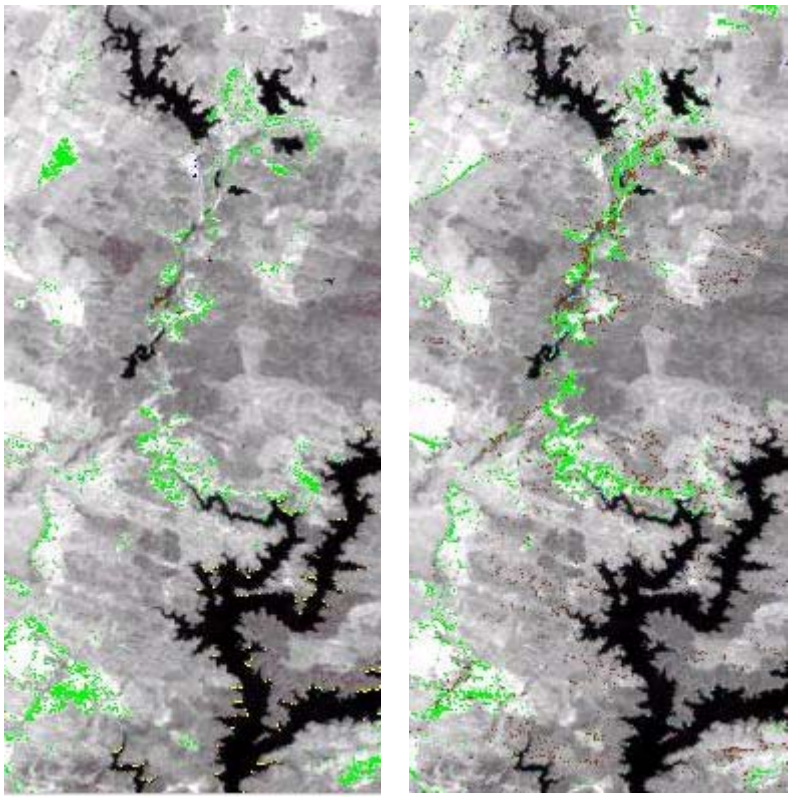

a) Without TIR bands b) With TIR bands

Figure 28. SAM Classification results of Landsat ETM+ based on image endmembers.

Both images show, in green, the influence area of the impact of mining, without discriminating the different type of materials. As can be observed, variability of materials composition is not evident probably due to low spectral resolution of TM sensors. Nevertheless, results obtained using thermal bands slightly enhance thermal contrast of waste materials especially at Achada do Gamo and S. Domingos open pit (in brown). In fact, it is expected that thermal infrared bands could improve identification of contamination in cases where local temperature is higher, which is the case of the S. Domingos metallurgical slags, associated with intense and continuous chemical changes.

The next step of the methodology, shown in the diagram of Figure 22, utilises a new image data set excluded of some classes not related to the mapping targets, i.e. waste mining material. For the classification of this new image, field spectra were utilised as endmembers. The spectral signatures resampled to Landsat ETM+ spectral bandwith, i.e. from 126 to 8 bands, Figure 29, show significant change when compared to spectral hyperspectral bandwith (Figure 23).

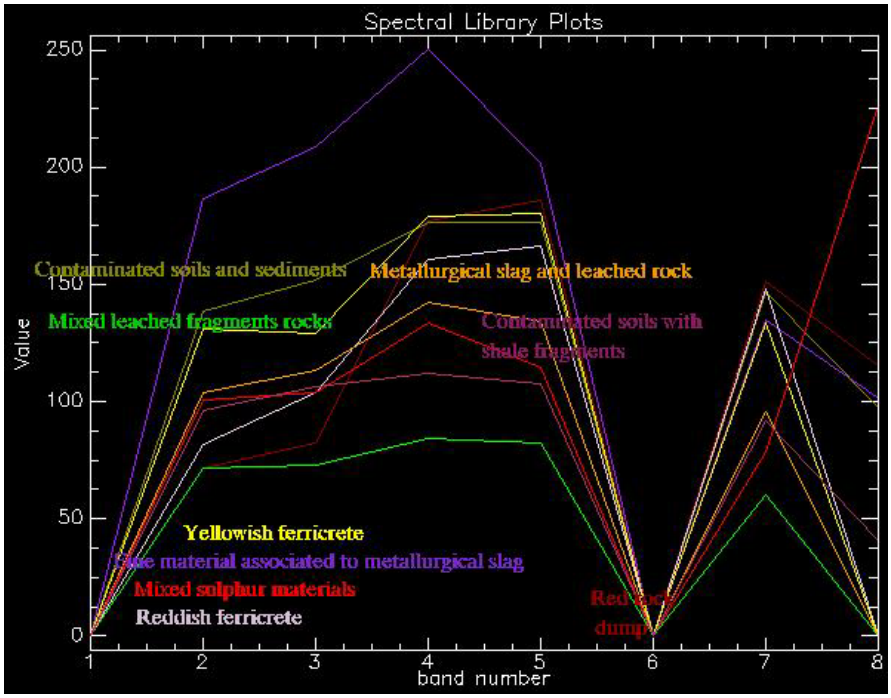

Figure 29. Field spectra (Figure 23) resampled to Landsat ETM+.

The SAM results using the spectra of Figure 29 are illustrated in Figure 30. However, to reach these results a maximum angle threshold of 0.50 radian has to be utilised, instead of the standard 0.1 radian for hyperspectral images, increasing the uncertainty about the match of the spectra.

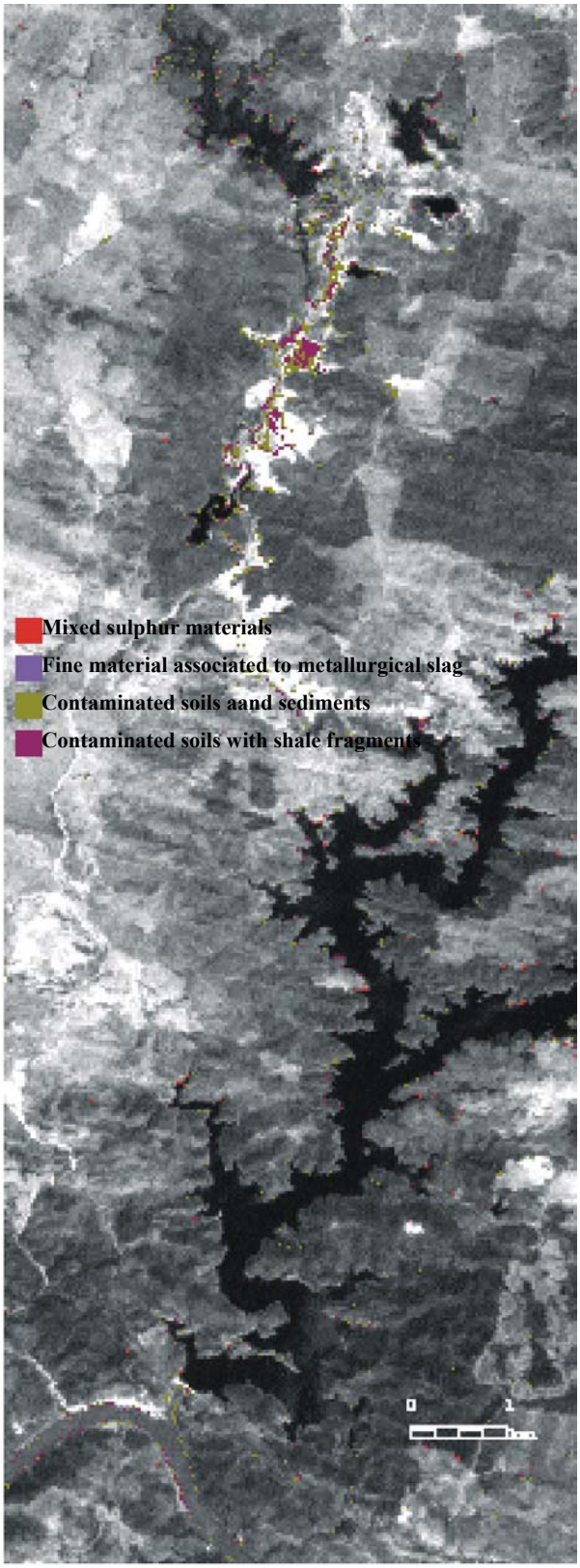

Figure 30. SAM results for Landsat ETM+.

7.4.2. HyMap™ vs Lansat ETM+

In Figure 31 is illustrated for a small area the comparison between HyMap™ (left, App.6.1) and Lansat ETM+ classification results.

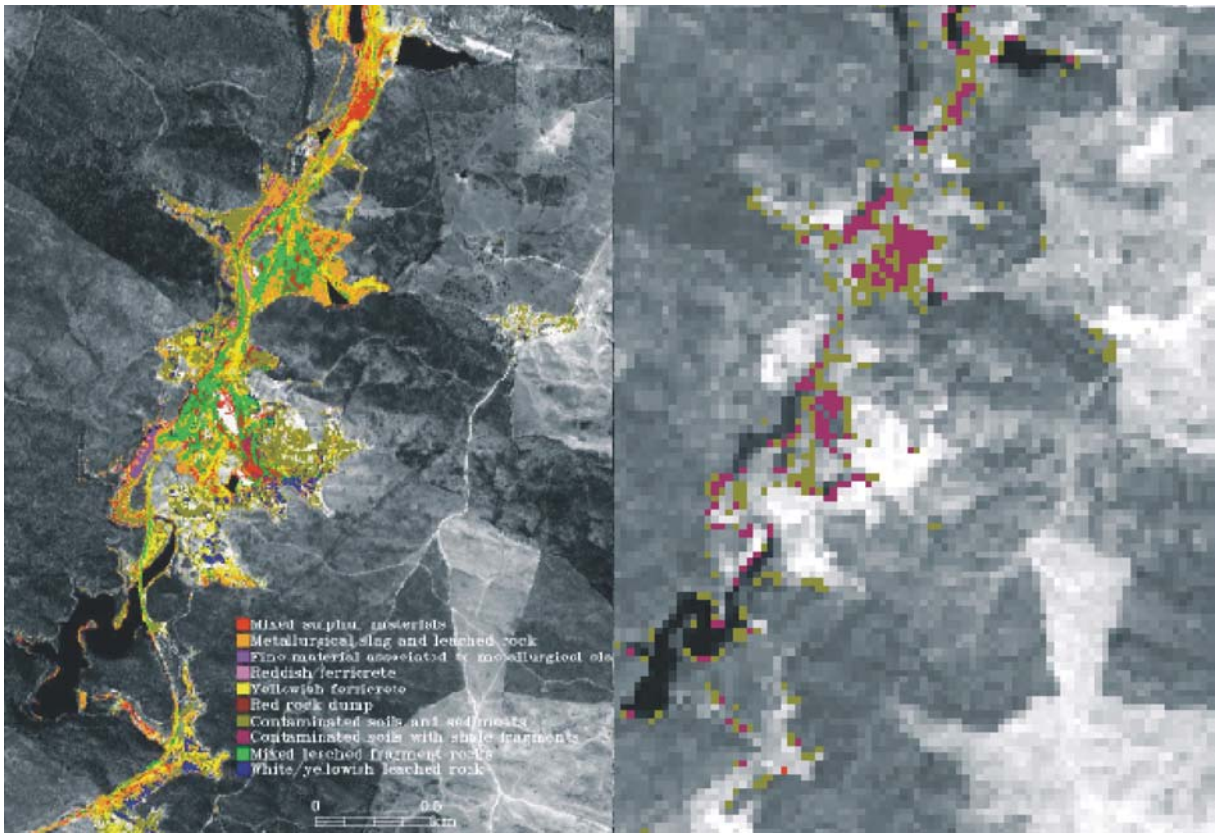

Figure 31. HyMap™ (left) and Lansat ETM+(right) classification results using the same methodology.

These preliminary results seem quite limited on Lansat ETM+, due to low spectral and spatial resolution. In fact, the variability of materials expressed on HyMap™, in particular the ones clearly related to AMD does not appear on this area.

Under these circumstances, Landsat ETM+ image does not seem suitable for such local studies concerning AMD. However, must be taken into account that this are preliminary conclusions, and it has been exclusively tested the same procedure developed for HyMap™ image on S.Domingos test site (Figure 22).

Nevertheless, this methodology with some particular changes can probably be useful at a more regional scale, as e.g. location of mining impact through Pyrite Belt probably without such a discrimination.

7.5. Generic character of the procedure/algorithm

The procedure developed for waste mining material mapping related to AMD shows some potentialities to be tested on other areas. However, waste mining material must have a significant spread on the area to be tested. Although it has been tested under Southern Europe environment test

with specific field spectra collected for the effect, it could also be tested with image spectra or using these same spectra on a similar environment, e.g. Volcanogenic Massive Sulphides deposits.

8. DESCRIPTION OF THE GIS DATABASE

8.1. Database preparation

The information modelled was selected according to its importance of the MINEO objective. The IGM has a large volume of information produced during exploration evaluation of the areas. S. Domingos was studied with other objectives in mind, e.g. ecotoxicity, exploration of tailings and slags for precious metals, etc. The information was in different formats that had to be compatible in ArcGIS 8.0 system. The following procedures were executed.

- Shapefiles of topographic maps of mine infrastructures, and regional topography;
- Shapefiles of geology in 1/25 000 scale;
- Shapefiles of hydrographic mapping in regional and local scale;
- DEM was introduced in a grid feature (generated by BGS Mineo partner);
- Country shapefiles of climatic information (precipitation, average temperature, evapotranspiration, etc.)
- Available hydrochemistry with field parameters and chemical analysis when they were available:
    - groundwater
    - superficial water from lakes, pit and streams
    - seepage waters
- Soil geochemistry and mineralogy MINEO
- Landuse mapping from CORINE image of SNIG (Governmental Information Centre);
- Waste mapping in shapefile;
- Tailings leached waste materials chemical analysis
- Hyperspectral imaging and multispectral Lansat ETM+ from MINEO acquired in 2000
- Groundwater vulnerability (DRASTIC)

The method used to evaluate the aquifer vulnerability in S. Domingos mining area was DRASTIC methodology (ALLER *et al*., 1987, Table 6).

Table 6. ***DRASTIC Vulnerability in the S. Domingos mining area.***

FEATURES (WEIGHT)	*FEATURES RANGES*	*RATING*
D – Depth to Water *(5)*	*<1.5 to 22.9m*	*10 to 3*
R – Net Recharge *(4)*	*<51 mm/yr*	*1*
A – Aquifer Media *(3)*	Weathered shales	*4*
S – Soil Media *(2)*	*Thin or absent and sandy-loam dominant*	*10 to 6*
T – Topography *(1)*	*Slope from 2 to 18% dominant*	*9 to 3*
I - Impact of the Vadose Zone Media *(5)*	Weathered shales	*4*
C – Hydraulic Conductivity of the Aquifer *(3)*	*<4.1 m/day*	*4*

From the overlapping and consideration of the seven features presented indicates an average DRASTIC index of 78 to 127 meaning low vulnerability of groundwater in weathered shales formation

8.2. Database content

The GIS project was built in a first stage with the following information in ArcGIS 8:

- Topographic maps of mine infrastructures, and regional topography;
- Geology in 1/25 000 scale;
- Hydrographic mapping in regional and local scale;
- DEM with a cell size of 10m (generated by BGS);
- Available hydrochemistry information;
- Produced soil geochemistry and mineralogy mapping from MINEO;
- Hyperspectral and multispectral imaging from MINEO;
- Waste mapping;
- Tailings leached waste materials chemical analysis
- Thematic maps obtained during database loading.

9. GIS MODELLING

9.1. Description of the conceptual environmental model

To obtain a conceptual environmental model, the local conditions described in Chapter 2 are again empathised and synthesised.

Problematic situations are located in S. Domingos open pit and the surrounding area, in the Achada do Gamo sulphur factory complex area, and less significant then the previous mencioned, Telheiro because the confluence of the Mosteirão river that carries extra water volumes with different chemical composition and mixed with acidic waters from the S.Domingos stream. The Pomarão Harbour is also a problematic area due to remnants of the ore, which was transported from the mine to the harbour for shipment.

Climatic conditions directly influence environmental conditions. Rainfall ratios are low, the sun hours/yr are considered significant. Although the wind direction favours the dispersion of piles of unconsolidated materials, the intensity is generally low so it is considered not significant.

Concerning the S. Domingos open pit, this mine structure is partially flooded with brown to orange coloured, low pH, high conductivity, and high SO_4^{2-} content water. Bellow the open pit, the underground mining galleries are completely flooded to a depth of 390 m. In S. Domingos open pit, flooding started at the end of exploitation. The process began in the underground works filling all gaps with water and at least partially, with time, in bedrock fault systems with fine grained material as well.

In the margins of the open pit and downstream from the old exploitation to Telheiro, are deposited different type of tailings. These tailings and other waste material were mapped for this project by BRGM. In the past they have been locally mapped for exploration purposes (especially for gold).

Along the stream to the confluence with the Guadiana River existed a railway (nowadays in ruins) that transported the concentrate ore material to the harbour. Knowing that exploitation occurred for more

than 100 years, the presence of dispersed material is also significant along the railway line, and this is the primary reason why the working area covers the Pomarão Harbour.

The most problematic area exposed to AMD is considered to be the Achada do Gamo site downstream from the S. Domingos open pit. At the end of exploitation, slag, ore, host rock materials and enriched (fine grained) ore concentrate as well as sulphuric acid was abandoned near the Achada do Gamo factory resulting in uncontrolled reactions that persist today.

Considering the above-mentioned conditions, the main transport of contaminants is by water, especially superficial water, because of constant renewable of chemical composition. The conceptual model presented in Figure 32 shows the most important contamination stressors.

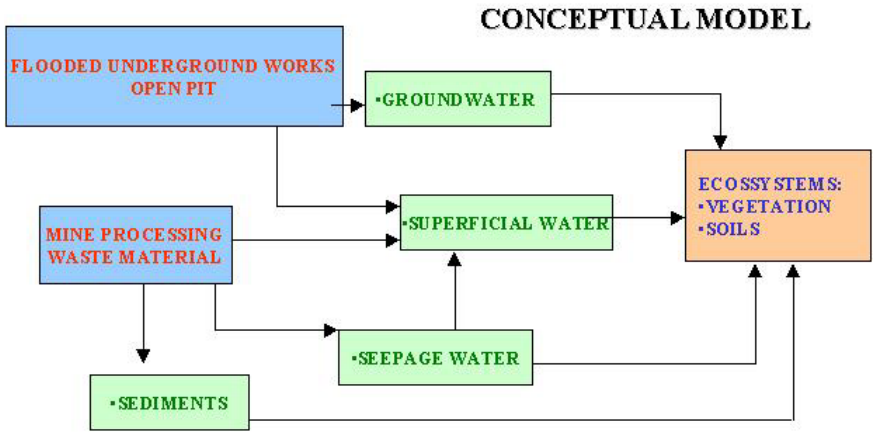

Figure 32. Conceptual model. Blue box- Major stressors; Green- Pathways; Orange- Receptors.

9.2. Objectives of GIS modelling and expected results

The objective of this task is to understand and model, using GIS tools, the contamination pathway. With GIS modelling it is envisaged to assess the Acid Mining Drainage linking all relevant terrestrial information, such as, soil geochemical multivariate interpolations, water interpolation of certain parameters such as, pH, and sulphur tailings leaching solutions.

This methodology is a guide to future development and identification of critical problematic areas.

9.3. Description of GIS derived layers

The obtained GIS derived layers based only in DTM grid and hydrographical net mapping are as follows:

- Slope map derived from DTM;
- Flow direction map derived from DTM;
- Flow accumulation map derived from flow direction mapping;

Due to insufficient climatic, groundwater, soil thickness and porosity information the following GIS derived layers (relevant for Acid Drainage modelling) were not obtained.

- Vadose Zone
- Recharge zone
- Groundwater vulnerability mapping.

GIS derived parameters:

- Distance from water pH measuring points to the nearest tailing;

9.4. Description of GIS combination and modelling

9.4.1. Geochemical modelling of water pH measurements and sulphur concentration in leached tailings material

Methodology procedures were performed in two phases:

First phase

- Kriging interpolation based on 49 superficial waters pH;
- Kriging interpolation based on 14 samples of leached tailings solutions of sulphur content;

Correlation coefficient between DTM and water pH interpolation and sulphur content in leached tailing materials

Non representative results for GIS modelling:

- Co-Kriging interpolation of pH measurements in superficial water with DTM, coefficient correlation between both variables is 0.05
- Co-Kriging interpolation of leached tailings solutions sulphur content with DTM, coefficient correlation between both variables is –0.196

Due to the low correlation with DTM the Co-kriging of water pH measurements and sulphur leached materials concentration with slope, flow direction and flow accumulation derived layers was not performed.

Second phase:

- Water pH Indicator measurements pH<5 (median value);
- Sulphur Indicator concentration SO_4^{2-} >70 mg kg^{-1} (median value);
- Correlation coefficient between water pH measurements and SO_4^{2-} leached tailings concentration and distance to the different waste material derived from hyperspectral classifcation (Table 7).

Non representative results for GIS modelling:

- Indicator *"Collocate-Cokriging"* interpolation between SO_4^{2-} tailings leached concentration and distance to the nearest waste "mixed leached fragment rock" (the highest correlation distance waste material), coefficient correlation of -0.61.

Representative results for GIS modelling:

- Indicator *"Collocate-Cokriging"* interpolation between pH measurements and distance to the nearest waste "mixed sulphur material" (the highest correlation distance waste material), coefficient correlation of -0.68.

Table 7. Correlation coefficient of SO_4^{2-} and pH with distance to waste material

Waste material	Coef. Corr. So_4^{2-}>70 vs.Dist.	Coef. Corr. pH<5 *vs.*Dist.
Mixed sulphur material	-0.27	-0.68
Fine material associated to metallurgical slag	-0.43	-0.66
Mixed leached fragment rock	-0.61	-0.59
Yellowish ferricrete materials	-0.17	-0.56
Metallurgical slags and leached rock	-0.52	-0.54
Reddish Ferricrete materials	0.04	-0.52
White/yellowish leached rock	-0.36	-0.40
Red rock dump	-0.55	-0.35

The *"Collocate-Cokriging"* interpolation between pH measurements Indicator and distance to the nearest waste material, traduce the influence of waste material types to AMD with an uncertainty area of 10%. These results are illustrated in App. 7 Map of "Effective Acid Mine Drainage". The *"Collocate-Cokriging"* interpolation between SO_4^{2-} tailings leached concentration Indicator and distance to the nearest waste material even with high correlation was not possible to map due to a very low samples number that resulted in an unrealistic map.

9.4.2. Soil analytical results geochemical modelling using hyperspectral data

The main objective of the geostatistical task was the definition of the chemical polluted areas using ground data and hyperspectral remote data. This objective can be reached through estimation of the concentrations of the chemical pollutant elements.

In order to improve the estimation of the chemical concentrations of the selected elements using the spectral signatures of the hyperspectral image, a two step methodology was developed:

- Treatment of the hyperspectral images aiming at the identification of image factors with high correlations with chemical soil composition;
- Estimation of the soil concentrations using these high-correlated factors combined with the soil chemical data.

The first step was based on multivariate data analysis, namely Principal Components Analysis (PCA), Minimum Noise Fraction (MNF) and Factorial Correspondence Analysis (FCA), applied to the spectral signatures of pixels corresponding to the sampled pixels. To avoid image 'noise', strong water absortion bands (1, 62 to 69, 93 to 96 and 126) were excluded from these analysis.

Due to spatial deviations between the ground samples locations and correspondent image pixels, for each sample location the correlation coefficients were calculated for a neighbourhood of 11x11 pixels. The objective was to take into account some spatial distortion shown by the hyperspectral images. However the results were inconclusive, so the values of the central pixel (the pixel 'corresponding' to the sample) were retained.

The factors from FCA present, in general, the highest values of correlation coefficients with the chemical variables. The factors showing high correlation coefficients were selected to improve the estimation the chemical grades in soils. However those coefficients, presented in Table 6 are not very high, probably due to problems related with the hyperspectral images. Namely, the high number of saturated pixels, the spatial calibration of the hyperspectral images and the low number and clustering of the soil samples could be responsible for these relatively low correlations.

According to the correlation coefficients obtained and to the samples spatial distribution, it was decided to divide the whole mining area into two main sub-areas:

- Area 1 – S. Domingos area
- Area 2 – includes Tapada, Achada e Telheiro areas.

The second step was based on multivariate geostatistical techniques. Several methods, which are described in the report of the geostatistical task, were tested and compared with the results of the univariate ordinary kriging using only the chemical data. In general, to map chemical soils content, the geostatistical interpolation technique named cokriging using the highest correlated factors produces good results. In the App. 8, the results of the cokriging alternative that produces the best results according to the RMSE parameter (root mean square error) were presented for the S. Domingos area.

Table 8. Correlation coefficients between soil chemical variables and CA factors (S. Domingos area)

	As	Cu	Fe	Hg	Pb	S	Sb	U	Zn	Corg	Fe*MJ*	pH
PCA1	-0.11	-0.24	-0.06	0.00	0.01	0.41	-0.10	0.30	-0.16	**-0.55**	0.06	-0.36
PCA2	-0.17	-0.29	-0.45	-0.11	-0.14	0.15	-0.18	0.04	-0.32	-0.13	-0.41	-0.14
PCA3	-0.20	0.10	0.16	-0.08	-0.36	-0.34	-0.29	0.32	-0.18	0.51	0.19	0.47
PCA4	-0.36	-0.13	-0.20	-0.49	**-0.54**	-0.10	-0.39	0.34	0.30	-0.12	-0.06	0.35
PCA5	0.39	0.52	0.48	0.16	0.13	0.34	0.15	-0.32	0.16	-0.01	0.34	-0.39
PCA6	0.05	0.14	0.21	0.30	0.31	0.28	0.19	-0.14	**-0.46**	0.02	0.26	-0.41
PCA7	-0.38	-0.12	-0.26	-0.50	-0.22	-0.11	-0.12	-0.18	0.11	-0.37	-0.54	-0.11
PCA9	0.10	0.42	0.14	-0.01	-0.05	-0.05	-0.01	**-0.47**	0.20	0.20	-0.11	0.02
MNF1	-0.35	-0.08	-0.17	-0.26	-0.42	**-0.72**	-0.31	0.17	-0.02	0.61	-0.19	0.73
MNF2	-0.20	-0.41	**-0.64**	-0.29	-0.07	0.16	-0.12	-0.17	-0.04	-0.58	-0.60	-0.35
MNF3	0.03	-0.11	-0.11	0.09	0.32	0.25	0.25	-0.32	-0.05	-0.24	-0.18	-0.46
MNF4	-0.02	0.08	0.09	-0.01	-0.24	-0.31	-0.12	0.26	0.19	0.53	0.21	**0.62**
MNF5	-0.36	-0.26	-0.17	-0.29	-0.22	0.16	-0.28	**0.47**	0.21	-0.44	-0.09	-0.05
AFC1	-0.14	-0.06	-0.28	-0.13	-0.23	-0.29	-0.15	-0.05	-0.12	0.44	-0.24	0.32
AFC2	-0.14	0.17	0.27	-0.05	-0.29	-0.42	-0.21	0.26	-0.03	0.49	0.32	**0.52**
AFC3	-0.38	-0.25	-0.33	-0.50	-0.52	-0.15	-0.37	0.34	0.20	-0.20	-0.12	0.33
AFC4	**0.53**	**0.58**	0.63	0.35	0.23	0.40	0.26	-0.23	0.03	0.11	**0.56**	-0.32
AFC5	0.40	0.17	0.24	0.23	0.04	0.05	0.06	0.04	0.22	0.17	0.25	0.11
AFC6	0.31	0.44	0.37	0.08	0.15	0.29	0.15	-0.30	0.08	-0.10	0.20	-0.45
AFC8	0.43	0.18	0.29	**0.52**	0.21	0.08	0.17	0.04	-0.06	0.43	0.56	0.17

In most cases, the cokriged maps compare favorably with the kriged maps, showing the improvement introduced by the hyperspectral information. However this improvement was not so important as we expected. The aspects related with the low correlations between hypersepctral information and chemical variables mentioned before could explain this 'not so good' performance. In general, as expected, the cokriged maps show more variability than the kriged ones. An example is the estimation of the Cu grade, shown in Figure 33.

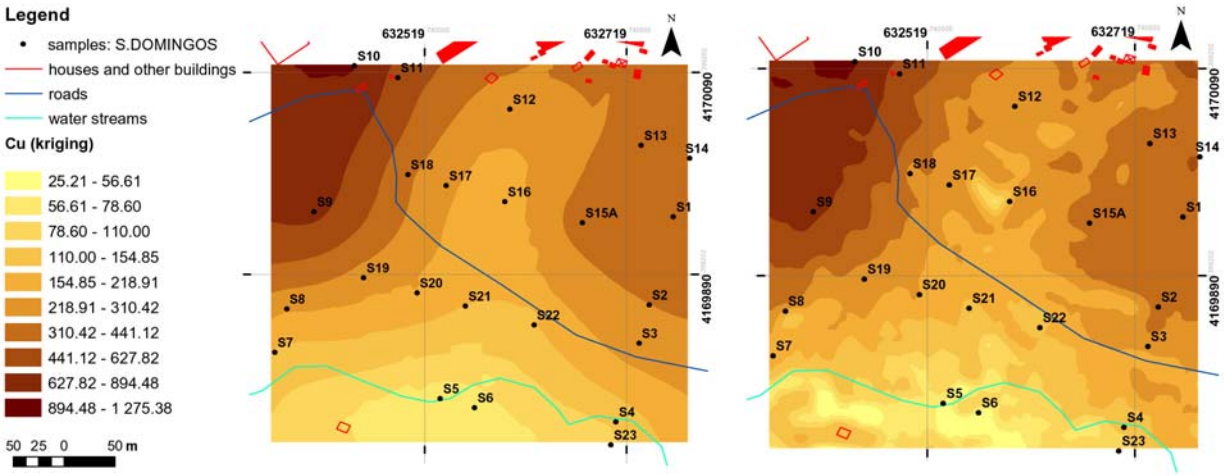

Figure 33. Cu prediction map in the S. Domingos by ordinary kriging (left) and cokriging (right).

These prediction maps identify the contaminated areas caused by the mining and metallurgical activity in S. Domingos.

The other results for the other elements and for Area 2 are presented on App. 8.

9.5. Description and assessment of the map(s) produced vs. expected results

Indicator "Collocate-Cokriging" of water pH with the nearest distance to mixed sulphur materials (App.7)

This geostatistical mapping has the advantage to obtain a reliable probability area of pH less than 5, with 10% uncertainty. Correlation of distance from water pH measurement points and the waste materials identified in hyperspectral classification (App.6.1) is much higher than correlation of the distance of water pH measurement points and tailings field mapping (App.2) and with DTM derived layers. AD prediction areas can be achieved with a continuous hyperspectral classification of the waste materials with local pH field measurements.

Prediction map in S. Domingos by ordinary kriging and cokriging

These two kinds maps (Figure 33 and App.8) represent the comparison between results of the univariate ordinary kriging using only the chemical data and the geostatistical interpolation technique named cokriging using the highest correlated factors from hyperspectral information and chemical variables. In most cases, the cokriged maps compare favourably with the kriged maps, showing the improvement introduced by the hyperspectral information. However this improvement was not so important as we expected. Although, in general the cokriged maps show more variability than the kriged ones, being more realistic.

10. CONCLUSION , ASSESSMENT OF RESULTS

10.1. Assessment of results

The results achieved until now in the Southern Environment Test Site of the MINEO Project, the São Domingos Mine, are very positive and promising, as a tool to understand and assess pollution processes related to mining areas, using hyperspectral images combined with GIS.

10.1.1. São Domingos mining area

The data collected during field surveys, and subsequent treatment and interpretation, confirmed the main focus of pollutants as the S. Domingos open pit area and Achada do Gamo (sulphur factory), where the lowest pH values are reached, while Telheiro is contaminated by Acid Mine Drainage (AMD) from the former. The Pomarão Harbour is locally contaminated in the ore shipping area. The Pomarão N and Tapada, the other two subtest areas, were validated as reference areas i.e. uncontaminated.

This work allowed the conception of an environmental model for this mining area, which was fundamental in the approach developed for Image Processing, either using field data (spectroradiometric measurements) either for validation (geochemical and mineralogical data, and waste field mapping) of the image classification results produced.

10.1.2. EO sensors contribution for environmental assessment

One of the Mineo objectives is to provide innovative and advanced EO methods for locating and monitoring environmental risks related to mining sites. The results obtained provide a potential tool for assessing environmental risk areas, which is the first step for monitoring. The added value given by hyperspectral imaging sensors is better understood when compared with results of available multispectral sensors.

Hyperspectral imaging sensors

Hyperspectral images were useful to identify mineralogical/chemical dispersion of waste material related to Acid Mine Drainage (AMD) following two approaches, one related to AMD waste material field signatures and other based on AMD minerals.

AMD waste material mapping

The extension of AMD waste material was achieved using local field spectra signatures as endmembers. The developed methodology can be synthesised as using mainly the combination of two classification algorithms. The Spectral Angle Mapper (SAM) algorithm was followed by the application of supervised Mahalanobis distance algorithm, to avoid class mismatch in cases where spectra of materials present clusters with some differences not distinguishable by the former.

Some extra experiments were performed using Mixture Tunned Matched Filtering (MTMF) algorithm, however final results were not satisfactory. Therefore, SAM arises as more robust algorithm for classifying images that present illumination effects, showing however some limitations by different spectra that cannot be distinguished.

The use of field spectra signatures together with image spectra allowed the accurate identification of type and extension of the following mining materials over the area of study:

Mixed sulphur materials
Metallurgical slag and leached rock
Fine material associated to metallurgical slag
Yellowish ferricrete
Reddish ferricrete
Whitish leached rock
Red rock dump
Contaminated soils and sediments
Contaminated soils with shale fragments
Mixed leached fragment rocks

Although they generally represent materials with significant content of pollutants such as S, Zn, Pb, Sb, Cu, As, Hg and Cd, the first five classes correspond to the highest contents registered in local chemical samples, associated to high acidic potential. Therefore, they are crucial in detecting main dispersion of pollutants, and highlight the potentialities of imaging sensors for discriminate chemical differences in imaged ground surface.

Validation of output results was obtained by comparing waste material field mapping, mineralogy and geochemistry results with classified image. In general, the field spectra and spectra of classified image match well.

The results obtained identify areas of high risk related to AMD allowing further prioritisation for remediation processes.

AMD mineral mapping

The extension of AMD minerals was achieved using the standard laboratory measurements of USGS spectral libraries.

Based on MTMF (Mixture Tuned Map Filtering) and SAM (Spectral Angle Mapping) algorithms it was possible to delineate the spatial location of soils containing copiapite, jarosite, goethite, hematite

and alunite. Characterising and mapping jarosite and alunite enables thus to retrieve areas exhibiting pyrite, secondary salts (sulphates) deposition and efflorescent crusts which are still very active in acid drainage production.

Both mapping methods led to the identification of AD-generating minerals, with convergent results, although the extension of each class is different in the two classifications. The combined classification results show global class separability in the spectral feature space.

Validation of classification results with AD field mapping and mineralogical field result concludes that mineralogical content of soils can be mapped using hyperspectral-imaging sensors together with standard libraries.

Conclusion

Globally, both mapping results obtained either in AMD waste material either in AMD mineral was able to detect mineralogical/chemical characteristics of imaged ground data, validated by field data. Hyperspectral sensors, with high spectral resolutions, appear as potential tool when applied to mining environments for environmental assessment.

Observations derived during image processing highlight some decisions concerning future work, either concerning field spectra collection either image treatment.

The data treatment of hyperspectral images, in spite of several time consuming procedures related to data quality analysis and taking into account that corrections done were not the initial envisaged, has shown high potentialities for remotely assessing mining environment.

Multispectral sensors

To evaluate the contribution of hyperspectral sensors vs multispectral sensors, a Landsat ETM+ image, contemporaneous of the hyperspectral data acquisition, was processed.

The same methodology applied to obtain AMD waste mapping was tested. The results highlight the possibility of mapping some general features linked with mining activity and related pollutants in the whole area. However, the next step using field spectra show limited results, due to low spectral and spatial resolution. In fact, the variability of materials expressed on HyMap, does not appear on Landsat ETM+. Therefore, Landsat ETM+ image does not seem suitable for such local specific studies concerning AMD.

One positive characteristic of image Landsat ETM+ is the fact that it does not present strong illumination effects as in the hyperspectral image, which minimizes errors due to pre-processing steps. The use of hyperspectral satellites probably will avoid this problem.

10.1.3. GIS contribution

EO data integrated into GIS when combined with other relevant data has been able to assess the environmental impact of mining, both at local and regional scales.

GIS modeling envisages the definition of pollution-sensitivity areas by the integration of relevant environmental parameters, such as soil chemical content, physical water parameter (pH) with hyperspectral information.

Due to lack of information it was not possible to integrate other relevant data such as: hydrogeology groundwater vulnerability, vadose zone (due absence of water table level information), soil permeability, thickness and porosity, and recharge zones.

Digital terrain model (DTM) derived layers such as slope map, flow direction map, and flow accumulation map, were obtained. Although, not used because of low correlation of field measurements with DTM.

Due to the lack of samples of leached tailings solution, relation between sulphur concentrations and the distance to the nearest waste material obtained from hyperspectral classification (mixed leached fragment rock) could not be interpolated using *"Collocate-Cokriging"* geostatistical method.

Geochemical modeling was performed with soil chemical content cokriged with hyperspectral chemical signatures and water pH measurements using the interpolation of *"Collocate-Cokriging"* with the distance to the nearest highly correlated waste material (mixed sulphur material) obtained from hyperspectral classification.

Geochemical modeling using hyperspectral data emphasize the following:

- Superficial waters pH Indicator "*Collocate-Co-kriging*" interpolation with distance to the highly correlated material (mixed sulphur material) derived from hyperspectral processing showed very good results.
- GIS geochemical modeling of water pH allowed delimitation of Acide Mine Drainage (AMD) critical areas where pH reaches the lowest conditions (pH<5) favouring the enrichment of water solutions in available toxic elements and sulphur content.
- The comparison between results of the univariate ordinary kriging using only the chemical data and the geostatistical interpolation technique named cokriging using the highest correlated factors from hyperspectral information and chemical variables did not give the expected results. However, the cokriged maps compare favourably with the kriged maps, and show more variability than the kriged ones, being more realistic.

Conclusion

The GIS modeling allowed the prediction maps of areas of high risk related to AMD, determining the main pollutants pathway. When combined with hyperspectral images classification results, creates a real scenario of prioritisation for remediation processes. Additional prioritisation areas are given by hyperspectral results.

10.2. Results versus user demand

An environmental database related to an abandoned mining area and prediction tools have been developed, under a designed environmental concept. This can be very helpful, aiding in future decision-making for governmental regulatory bodies and industry concerning mitigation of the risks related.

In particular, this can facilitate the establishment of Environmental Impact Assessment and Environmental Management Plans, giving emphasis on:

- Providing data and elements for a better understanding of the environmental status and processes operating in and around mine site in an actual scenario
- Raising public awareness and setting safeguards in mining areas

10.3. Future plans

The results achieved are very positive, taking into account the difficulties that arose.

However, hyperspectral images classification results should be tested using different image corrections. The procedures developed in hyperspectral image processing, independently of the pre-processing steps, can have several improvements derived from the knowledge achieved, in spite that the main objective was generally reached, i.e. to determine the extension of AMD waste material and minerals. Selection of distinct spectral range, according to different field spectra, as well as combining other hyperspectral methodologies with SAM must be performed. Further environmental field survey should be done in areas that were prioritised from classification results.

Despite of vegetation characteristics of the Southern environment, i.e. low density and high variability, some tests should be done concerning vegetation stress. This could be performed based on methodologies developed by other MINEO partners.

The PIMA spectroradiometric measurements feed in Mineo Spectral Library could be correlated with mineralogical field data obtained and with standard reference spectral libraries, to enhance the differences of minerals related to AMD areas. Subsequently, further Image Processing should be done using this specific mineralogical data of this test site.

In GIS, further developments must be done, especially if we consider the data available that was compiled and generated for the Mineo objectives. Particularly, the results obtained from hyperspectral classification must be combined and modelled with environmental data, other then presented in this report.

Scientific papers will be produced and published in journals and reviews.
Further detailed studies will proceed under a PhD program.

11. REFERENCES

Alves, H. (1997).Mina de S. Domingos: um caso de tipologia industrial mineira. *Arquivo de Beja*, Vol. IV, Série III, Abril 97, pp.7-17.

Allan, J.C. (1965).A Mineração em Portugal na Antiguidade. Bol.Minas, Lisboa 2(3), pp. 139-175.

Aller, L., Bennet, T., Lehr, J.H. & Petty, R. J. (1987) - *DRASTIC: a standartized system for evaluating groundwater pollution potencial using hydrogeologic settings*. U.S. EPA Report 600/2-85/018.

Appelo, C. A. J., Postma, D. (1996).Geochemistry Groundwater and Pollution". Balkema Publishers, Rotterdam; 536 p.

Batista, M.J.(2000).Environmental State of the Portuguese Test Site. S. Domingos Mine:Past and Present. Report for European Comission (http://www.brgm.fr/mineo/IGM_test_site.pdf).

Barriga, F. and Carvalho, D. (1983).Carboniferous volcanogenic sulfide mineralizations in South Portugal (Iberian Pyrite Belt). In: Sousa M. J. L., Oliveira, J. T., Eds., The Carboniferous of Portugal. *Memórias dos Serviços Geológicos de Portugal,* v. 29, pp.99-113.

Boardman, J. W., and Kruse, F. A. (1994).Automated spectral analysis: a geological example using AVIRIS data, north Grapevine Mountains, Nevada: in Proceedings, ERIM Tenth Thematic Conference on Geologic Remote Sensing, Environmental Research Institute of Michigan, Ann Arbor, MI, pp. I-407 - I-418.

Boardman, J. W., Kruse, F. A., and Green, R. O., (1995). Mapping target signatures via partial unmixing of AVIRIS data: in Summaries, Fifth JPL Airborne Earth Science Workshop, JPL Publication 95-1, v. 1, pp. 23-26.

Carvalho, D. (1979).Geologia, metalogenia e metodologia da investigação de sulfuretos polimetálicos do sul de Portugal. *Comunicações dos Serviços Geológicos de Portugal,* t. 65, pp.169-191.

Chambel, A. & Duque, J. (1999) – Hard rock aquifers of Alentejo region (South Portugal): Contribution to the water and land management. Proceedings of XXIX Congress of International Association of Hydrogeologists, Bratislava, Slovak Republic, pp. 171-176.

COBA Consultores de Engenharia e Ambiente (2002). Estudo De Controlo Ambiental Na Mineira Abandonada De S. Domingos. Final Report for IGM.

ENVI (1999). *ENVI Users Guide*. Research Systems Inc.

Kruse, F. A., Lefkoff, A. B., Boardman, J. B., Heidebrecht, K. B., Shapiro, A. T., Barloon, P. J., and Goetz, A. F. H., (1993). The Spectral Image Processing System (SIPS) - Interactive Visualization and Analysis of imaging spectrometer Data: Remote Sensing of Environment, v. 44, p. 145 - 163.

Gao B.C., Heidebrecht K.B., Goetz A.F.H. (1999). Atmosphere Removal Programm (ATREM)-User´s Guide Version 3.1.

Gaspar, O. (1998) "História da Mineração dos Depósitos de Sulfuretos Maciços Vulcanogénicos da Faixa Piritosa Portuguesa". *Boletim de Minas Vol.35 N°4 Lisboa*.

Green, A. A., Berman, M., Switzer, P., and Craig, M. D., (1988). A transformation for ordering multispectral data in terms of image quality with implications for noise removal: IEEE Transactions on Geoscience and Remote Sensing, v. 26, no. 1, p. 65-74.

Grösel, K., Belocky, R. & Ahl A. (2002) MINEO Alpine Environment Test Site Hyperspectral remote sensing study in mining areas. MINEO Report on first remediation assessment and monitoring maps, EC.

Mason & Barry (1878). *Portugal-Notice sur la Mine de Pyrite Cuivreuse de S.Domingos*. Lallemant Frères, Imprimeurs, Lisbonne, 35pp.

Oliveira, J. T. & Silva, J. B. (1990).Notícia Explicativa da Carta Geológica à escala 1:50000. Folha 46-D-Mértola. Serviços Geológicos de Portugal.

Pereira, E., Moura, I., Costa, J., Mahony, J. (1993). Mina de S.Domingos: Contaminação por metais pesados na Albufeira do Chança pela Descarga de uma Antiga Mina de Pirites de Ferro Cupríferas. I.Análise preliminar da Qualidade da Água. *Gaia, 7,* pp 18-27.

Pereira, E., Moura, I., Costa, J., Mahony, J. Thomann, R. (1995). The S.Domingos Mine: A Study of Heavy Metal Contamination in the Water Column and Sediments of the Chança River Basin by Discharge from an Ancient Cupriferous Pyrite Mine (Portugal).*Mar.Freshwater Res*., 46, pp 145-51.

Sequeira (1884).Notícia sobre o estabelecimento de S.Domingos.*Revista de Obras Públicas e Minas,* 14,15, 1883,1884.

Silva, J. B., Oliveira, V., Matos, J. & Leitão, J. C. (1997) – Field Trip #2, Aljustrel and the Central Iberian Pyrite Belt. Geology and VMS Deposits of Iberian Pyrite Belt. Barriga and Carvalho, Eds., Guidebook Series, V. 27, 192p.

Swayze, G., Smith, K., Clark, R., Sutley, S., Pearson, R., Vance, J., Hageman, P., Briggs, P., Meier, A., Singleton, M. and Roth, S. (1999). Using Imaging Spectroscopy to Map Acidic Mine Waste U.S. Geological Survey http://speclab.cr.usgs.gov/PAPERS/leqdville99

Webb, J. (1958). Observations on the geology and origin of the S. Domingos Pyrite deposits, Portugal. *Com. Serv. Geol. Portugal*, Lisboa. T. 42, pp.129-143.

12. APPENDICES

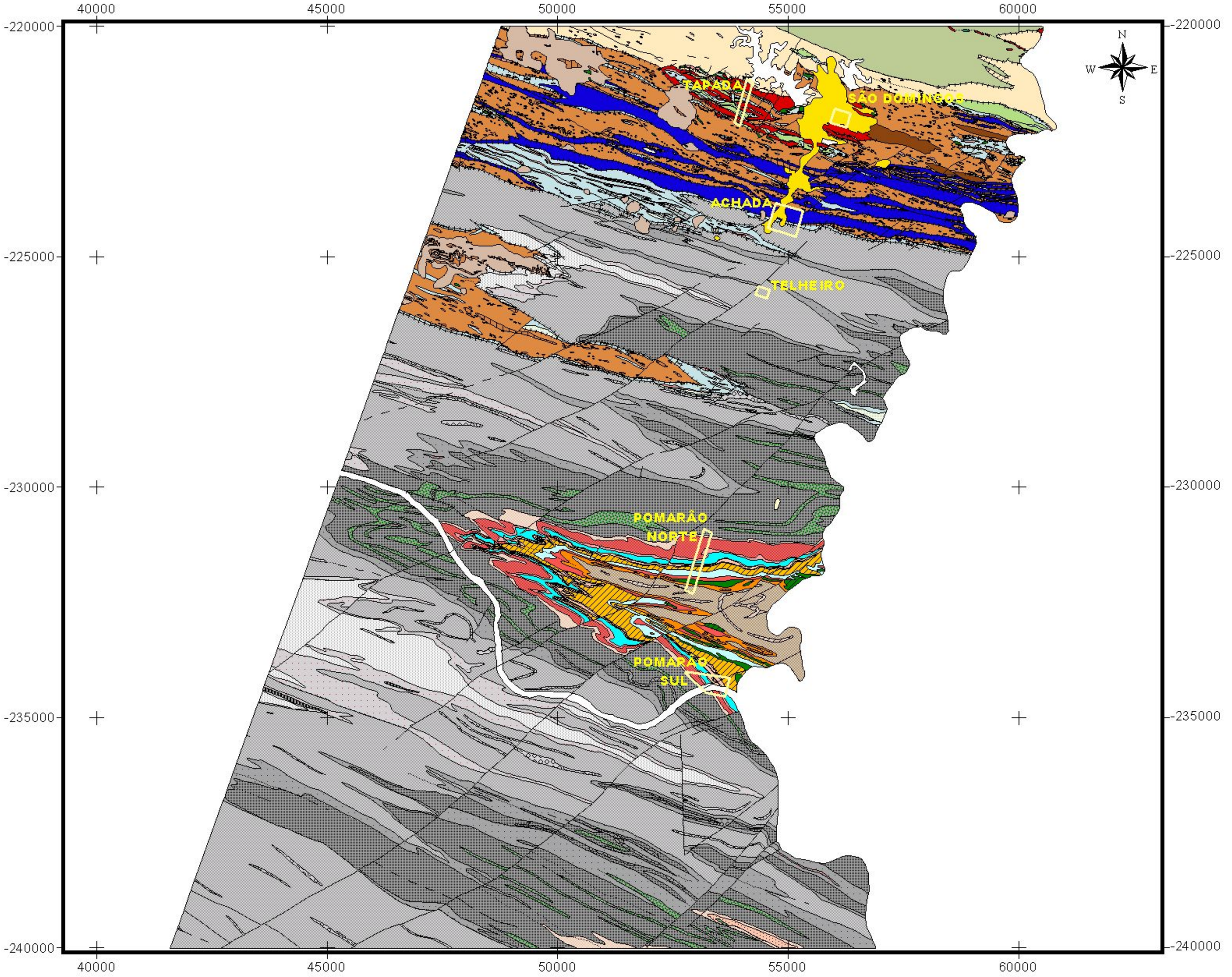

1:135 000 Scale

0 1.35 2.7 4.5 Km

LEGEND

COVER DEPOSITS

Quaternary
- Taillings and smelting products
- Fluvial terraces A
- Fluvial terraces A'

Pliocene
- Red sands and siltstones

UNCONFORMITY

CARBONIFEROUS — Upper Visean — Baixo Alentejo Flysch Group — Mértola Formation

M3 Member
- Mértola Formation M3 member
- M3 - pelites, greywackes and conglomerates
- M3 - thin bedded interbedded turbidites

M2 Member
- Mértola Formation M2 member
- M2 - thin bedded interbedded turbidites
- M2 - thin bedded interbedded turbidites
- M2 - intercalated coarser-grained greywackes
- M2 - thin bedded interbedded turbidites

M1 Member
- Mértola Formation M1 member (B1)
- M1 - pelites and thin bedded greywackes
- M1 - dominant classic turbidites
- M1 - pelites, greywackes and conglomerates
- M1 - thin interbedded turbidites

M0 Member
- Mértola Formation M0 member (B0)
- M0 - thin interbedded turbidites

CARBONIFEROUS — Tournaisian to Mid Visean — Pyrite Belt

Freixial Formation
- Freixial Formation

Volcano-Sedimentary Complex
- CVS - shales, siliceous shales, tuffites, siltstones
- CSV - jaspers, cherts
- CVS - "borra de vinho" purple and green shales
- CVS - fine grained acid tuffs
- CVS - spilites, diabases, and purple tuffs
- CVS - spilites, diabases, intermediates to basic porphyries
- CVS - rhyolites, rhyodacites, tuffs and aglomerates
- CSV - intrusive diabases
- CSV - microgranites and andesites

UPPER DEVONIAN — Middle-Upper Famennian

Phylite-Qzite Formation
- Phylite - Quartzite Formation
- PQ form - bioturbated phylites, siltstones, quartzites

Pulo do Lobo Antiform
Chança Group
- Represa Formation (RF)
- RF - rare tufites
- Gafo Formation (GF)
- GF - intrusive diabases
- GF- acidic porphyries

UPPER DEVONIAN — Famennian ? — Pyrite Belt

Barranco do Homem Formation
- Barranco do Homem Formation

Pomarão
- Aguia Formation
- Touril Formation (T0) - Achada Mina member
- T0 - Corte Machado member
- T0 - Corte Machado member
- T0 - Varjotas member
- T0 - black shales member
- Cerqueirinha Formation

- Eira Garcia member - siltstones and dark shales
- Eira Garcia member - siltst. and dark shales interc. of qzites
- Nascedios member (NM)
- NM - dark shales with lenticular limestones

FAULTS

- Fault
- Thrust Fault
- Inferred Fault
- Overthrust

MINISTÉRIO DA ECONOMIA

INSTITUTO GEOLÓGICO E MINEIRO

DEPARTAMENTO DE GEOLOGIA

GEOLOGICAL MAP OF PORTUGAL

Sheet 46-D MÉRTOLA (partial)

App.2

Mineo Sao Domingos
Mine Waste Map

Map produced in January 2001

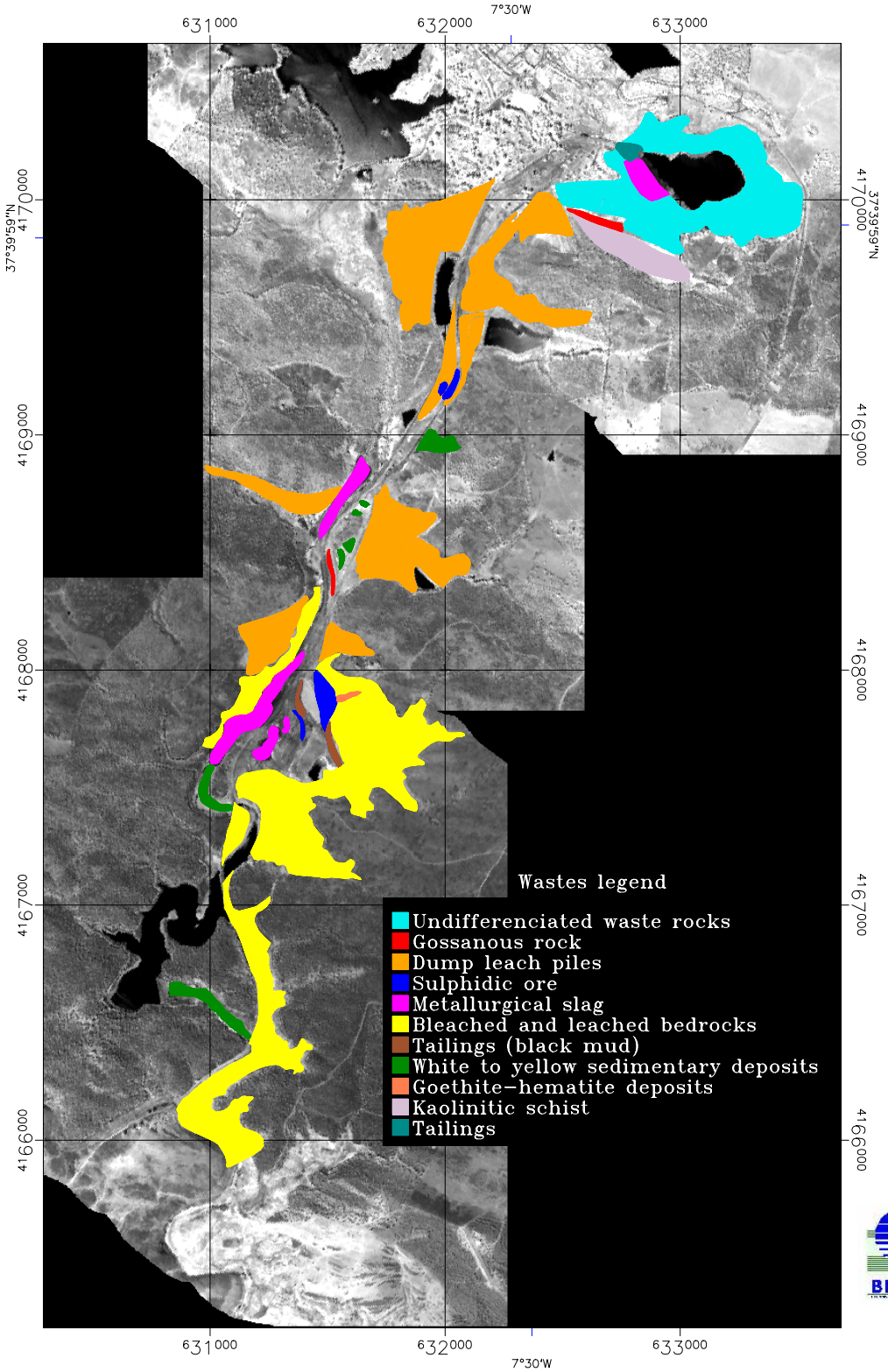

F.Cottard
projection UTM, Zone 29N
Pixel Size:4.2 Meters
Datum: WGS-84
Ellipsoid: WG 84

N
W E
S

0 1 Kilometers

App. 3.1

HyVista Corporation

Telephone: *+61 2 9878 0977*
Facsimile: *+61 2 9878 3615*
Email: *hvc@hyvista.com*
www.hyvista.com

HyMap Radiometry Report: MINEO

Prepared for: IGM October 2001

With regard to the HyMap data acquired over the MINEO test site in Portugal, IGM had some concerns about having some pixels in the images with negative radiance values and that some radiance spectra appeared distorted, possibly as a result of saturation.

By computing the scene statistics using ENVI, it is simply to identify bands with negative radiance values. To identify which pixels have these negative values, use ENVI to display a single band image (the band is selected as one having negative values) and then threshold the display stretch to highlight those pixels.

It is somewhat more difficult to identify saturation from the radiance data but thresholding the image display to only show the highest values soon highlights the pixel likely to be saturated. Those pixels are usually associated with sun glint from water bodies or specular reflections from buildings. Inspection of the radiance or reflectance spectra will also show non-typical spectral shapes if the pixel brightness is sufficient to saturate the detectors.

IGM asked HyVista Corp. to examine the data and make comment on the negative and saturated pixels. HyVista Corp. examined the raw digital number (DN) data in the assessment. IGM did not have access to raw DN data since all data delivered as part of the MINEO project had been radiometrically corrected and converted to units of radiance.

Negative Values

Negative numbers can arise in the HyMap data because of

- Statistics
- Errors in dark current correction
- Severe saturation
- "Warm detectors"

For either a constant illumination source or no source, the HyMap has noise values in the range 1 – 2.5 DN (rms). Thus for image pixels that are very dark (e.g. water, shadows or at wavelengths corresponding to strong atmospheric water vapour absorption), one may get negative numbers after the dark current has been subtracted just due to the statistical variance within the data. In DN terms, these negative DN are likely to <5.

During data acquisition, the HyMap estimates the dark current (or signal offset) by moving a shutter into a position that cuts off all radiation from the ground. This shutter is painted black and the underlying assumption is that no radiation comes from this shutter. However, the shutter has a non-zero K temperature and so a small component of blackbody radiation will be detected and will result in small radiometry errors when dark current correction is applied to the data. This error is likely to be small but could lead to some additional negativity and would only be a factor with the InSb (NIR, SWIR1 and SWIR2 modules) detector arrays.

HyVista Corporation (A.C.N. 087 620 737)
PO Box 437, Baulkham Hills NSW 1755 Australia
22 Delhi Road, North Ryde NSW 2113 Australia

Another factor that could contribute to small negative numbers is long terms (over minutes) drift in the dark current. Typically such drifts have been less than 1 DN over time periods similar to the image strip acquisition times encountered at the Portugal MINEO test site.

In the HyMap sensor, if the detectors are subjected to high levels of radiation, the system becomes over-saturated and the resultant output voltage is zero. This gives a recorded value of 0 DN. However, a typical dark current value is around 100 - 200 DN and upon dark current correction, large negative values result.

The detector arrays for the NIR, SWIR1 and SWIR2 modules are cooled by liquid nitrogen to maintain a detector temperature of around 77 – 80K. As the liquid nitrogen is depleted during the course of a survey, there can be a rapid and non-uniform increase in the dark current due to a rise in the temperature of the detectors. This event leads to a requirement that during a flight, the liquid nitrogen supply has to be replenished. The onset of this detector warming is rapid and slightly unpredictable. If the operator misjudges the timing in terms of refilling the liquid nitrogen dewars, errors in dark current could occur.

The following table shows the bands for each image strip where there was at least one pixel with a negative number.

Image Strip	**Bands with negatives**
SAO_DOM_01	63 64 126
SAO_DOM_02	63 64 65 95 126
SAO_DOM_03	63 64 65 95 126
SAO_DOM_04	63 64 65 66 94 95124 125 126
SAO_DOM_05	63 64 126
SAO_DOM_06	63 64 65 66 67 68 69 70 75 82 86 89 90 91 92 93 94 95 125 126
SAO_DOM_07	63 64 65 95 125 126
SAO_DOM_08	63 64 65 95 125 126
SAO_DOM_09	63 64 95 126
SAO_DOM_10	63 64 65 95 126
SAO_DOM_11	63 64 95 126

None of these bands have large negative DN numbers typical of severe saturation. The most common bands in the above table are 63-65 (bands in the strong 1.4 um water vapour band), 94-95 (bands in the strong 1.9 um water vapour band) and 125-126 (bands in the short wavelength wing of the strong water vapour band at 2.7 um).

Bands 63 – 94 are in the SWIR1 module and in image run, SAO_DOM_06, it can be seen that there are additional bands with a negative number and these bands are not ion the spectral region of strong water vapour absorption. This would seem to indicate a problem with detector cooling. Image SAO_DOM_07 returns to normal. The operator did refill the liquid nitrogen during the acquisition of this site but did not note when.

It is difficult to assess the impact on the radiometry of the SWIR1 bands in image SAO_DOM_06, but it would be our recommendation that the bands of the SWIR1 module be excluded from spectral analysis for this image.

It is arguable as to whether the bands in the region of strong water vapour absorption bands should be used in spectral analysis because of the low signal to noise ratio (SNR). However, if one decided to include these bands in the analysis but preclude pixels with negative radiance, a pixel mask would need to be generated (see the ENVI manuals).

In summary, the negative values encountered in the SAO_DOM image data set are not due to saturation of the detectors but represent small errors in dark current correction (SAO_DOM_06 in the SWIR1 is an exception). In terms of the mean radiance of the scenes, these radiometric errors are less than 1%. This is smaller than the radiometric inaccuracies associated with the laboratory radiometric calibration procedures where the main source of

HyVista Corporation (A.C.N. 087 620 737)
PO Box 437, Baulkham Hills NSW 1755 Australia
22 Delhi Road, North Ryde NSW 2113 Australia

error is the radiometric calibration of the standard light source used. The calibration of this standard light source is traceable to the NIST laboratory in the USA.

Correctly accounted for, the pixels with negative radiance will have no impact on the ability to detect and map spectral variability within the scene.

Saturated Values

Saturated values can occur within a scene due to sun glint from water, reflections from building windows and metal roofs and occasionally from very bright, diffuse reflecting materials (usually at high sun angles). It should be noted that not all bands or bands from all modules will saturated when viewing bright pixels.

The figure below shows the DN values (dark corrected) for the brightest pixel in each of the 11 SAO_DOM image strips. It can be seen that all but two images have saturation in the SWIR2 (bands 94-126) module but only three have saturation in the VIS (bands 1 –30) module.

The HyMap uses 12 bit analog to digital converters and so the maximum DN value recorded is 4096. The data comprising the figure below have been dark current corrected and so the maximum DN is less than 4000 (generally). It should be noted at this point that there may be some non-linearity in the response functions as the detector/amplifier combination approach saturation and so when setting a DN threshold to define saturation, it is recommended that one is a bit more conservative. A dark corrected DN value of around 3600 is reasonable for defining saturation.

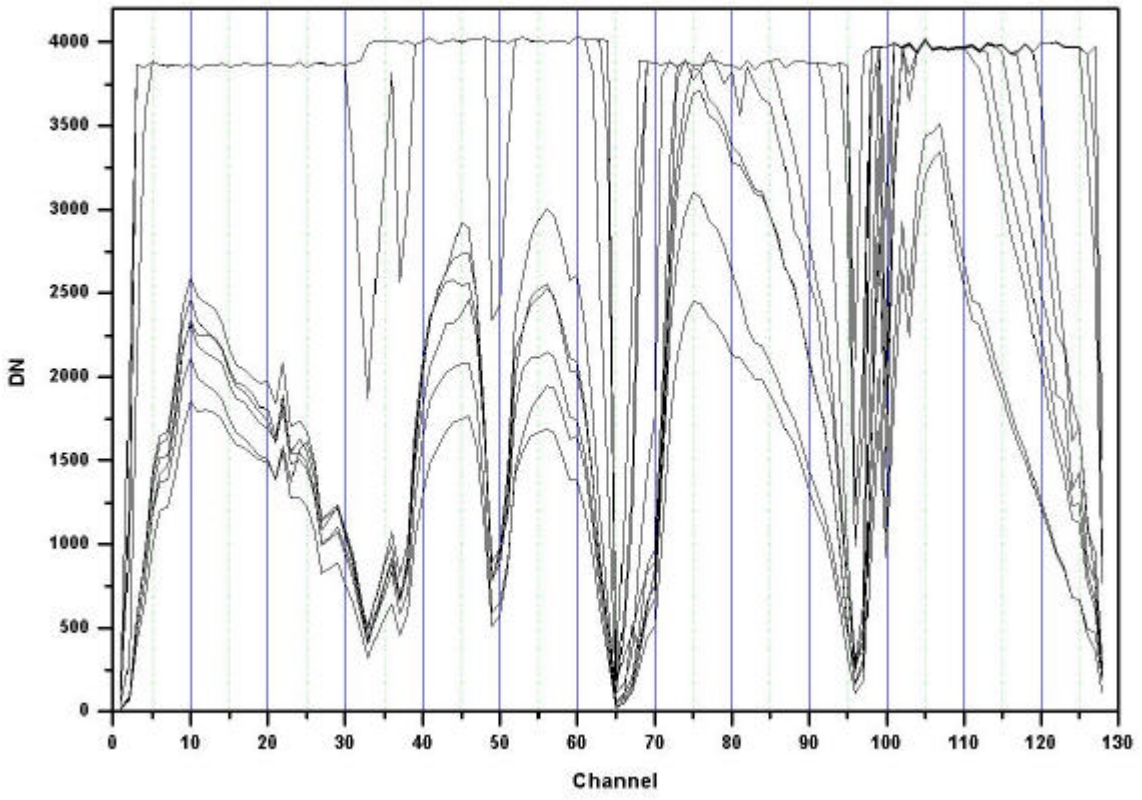

HyVista Corporation (A.C.N. 087 620 737)
PO Box 437, Baulkham Hills NSW 1755 Australia
22 Delhi Road, North Ryde NSW 2113 Australia

During pre-processing, the DN data is converted to radiance by basically multiplying the DN values by a DN_to_radiance conversion factor determined by the laboratory radiance calibration of the HyMap. There is an extra step in the pre-processing which uses the on-board calibration lamp to make corrections to the laboratory conversion factors. These corrections are required because some of the optical components are sensitive to temperature and humidity, which are different during aircraft operations than at the time of laboratory calibration.

If we assume that a DN value of 3600 be used to define saturation, then the "at sensor" radiance that will yield a DN value of 3600 for each band is given in the figure below.

Note that the HyMap radiance data has units of uW cm^{-2} nm^{-1} sr^{-1}.

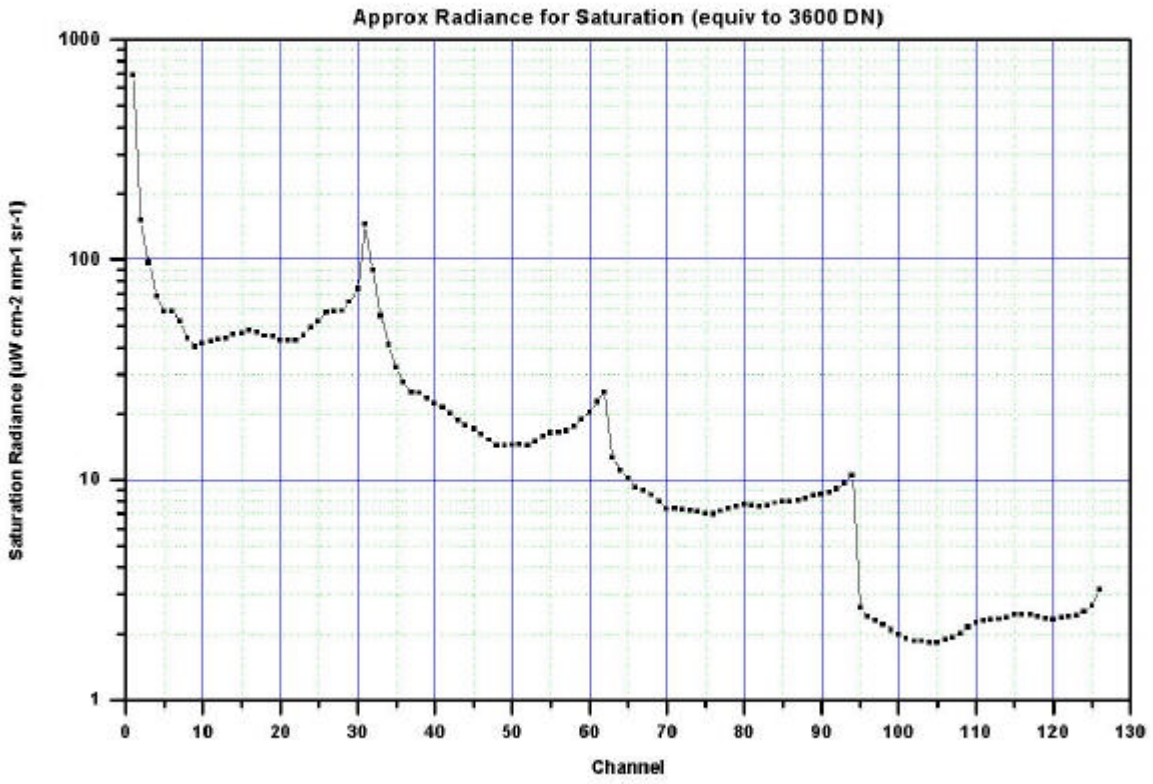

The radiance values derived from the above figure could be used when defining thresholds for the creation of pixel masks.

Attached Data Files

Two tab delimited ASCII files are attached as part of this report.

The first file, ***SAO_DOM_min_max_DN_126_stats.txt***, has the band number in column 1, the band wavelength in column 2, the DN_to_radiance multipliers in column 4 and then a series of DN values representing the minimum

HyVista Corporation (A.C.N. 087 620 737)
PO Box 437, Baulkham Hills NSW 1755 Australia
22 Delhi Road, North Ryde NSW 2113 Australia

and maximum DN value for the nominated image strip (SAO_DOM_01 to SAO_DOM_11). Note that these DN values are dark corrected values.

This file makes it simple to identify which bands have either saturated (ie. greater than 3600) or negative values.

The second file, ***SAO_DOM_saturation_radiances.txt***, gives the radiance (in units of uW cm^{-2} sr^{-1} nm^{-1}) for which a given band is saturated. (column 4).

It should be noted that if one wishes to use the DN_to_radiance conversion factors to revert the radiance data to DN, there will be a difference between the original DN and these derived values because the on-board calibration lamp will not have been taken into consideration.

Conclusion

The HyMap data of the MINEO test site in Portugal does have negative radiance values that at worst are given by a relatively few pixels at wavelengths associated with very low signals (ie near strong water vapour absorption bands). These negative values represent small radiometric errors that are easily removed from downstream spectral processing and will not compromise the overall quality of the data.

The HyMap data of the MINEO test site in Portugal does contain saturated pixels which are primarily associated with sun glint from water bodies and buildings. Again, these pixels can be easily masked.

In the image strip, SAO_DOM_06, the data in bands of the SWIR1 module appear to be unusable due to warming of the detector array during that acquisition.

HyVista Corporation (A.C.N. 087 620 737)
PO Box 437, Baulkham Hills NSW 1755 Australia
22 Delhi Road, North Ryde NSW 2113 Australia

Negative Pixel Distribution

Negative pixels predominately occur in water bodies such as rivers, dams and ponds.
Negative pixels displayed in red (subsetted scene SAO_DOM_01).

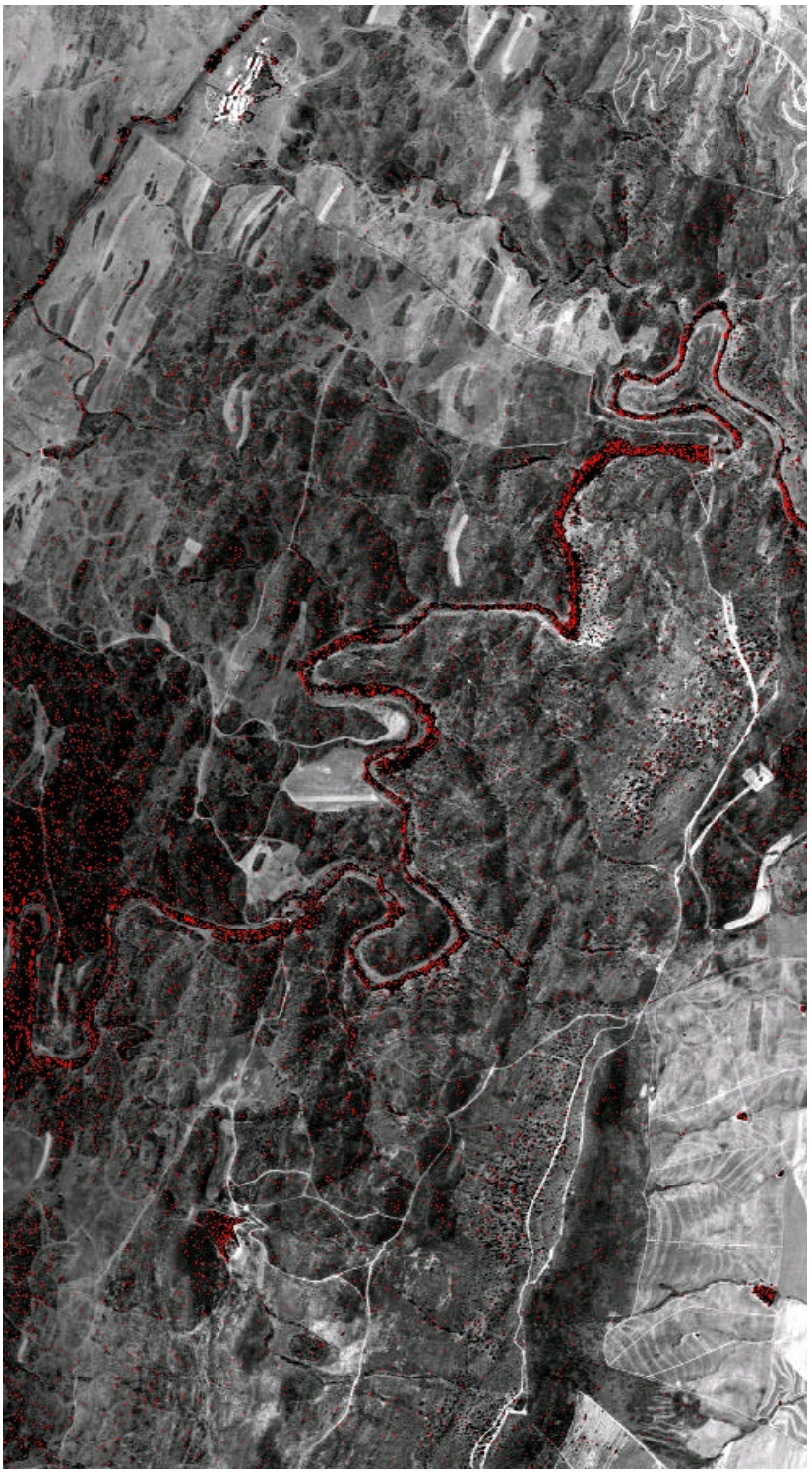

HyVista Corporation (A.C.N. 087 620 737)
PO Box 437, Baulkham Hills NSW 1755 Australia
22 Delhi Road, North Ryde NSW 2113 Australia

Saturated Pixel Distribution

Saturated pixels occur predominately from reflections from building windows, metal roofs etc.
Saturated pixels displayed in red (subsetted scene SAO_DOM_02).

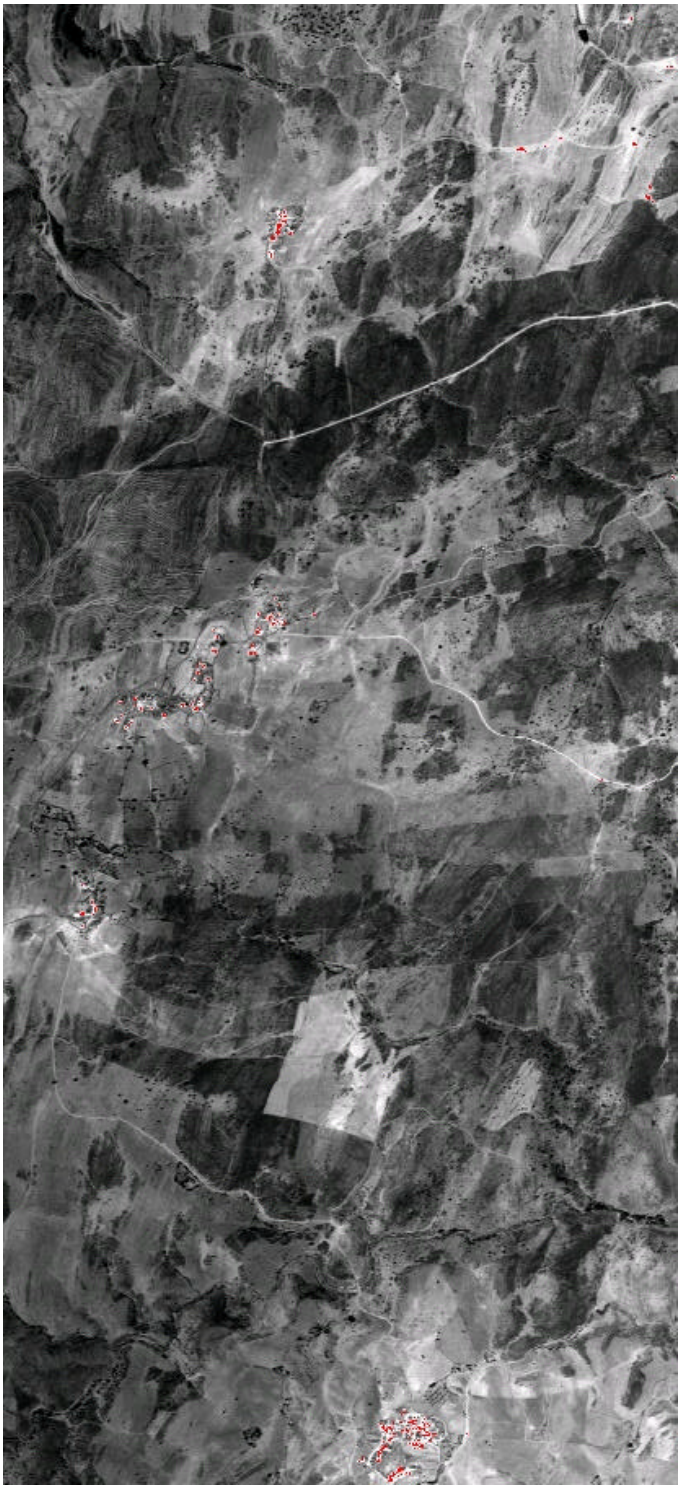

HyVista Corporation (A.C.N. 087 620 737)
PO Box 437, Baulkham Hills NSW 1755 Australia
22 Delhi Road, North Ryde NSW 2113 Australia

Attached files

File 1 - SAO_DOM_min_max_DN_126_stats.txt

File 2 - SAO_DOM_saturation_radiances.txt

HyVista Corporation (A.C.N. 087 620 737)
PO Box 437, Baulkham Hills NSW 1755 Australia
22 Delhi Road, North Ryde NSW 2113 Australia

Attached files

File 1 - SAO_DOM_min_max_DN_126_stats.txt

			SD_01		SD_02		SD_03		SD_04		SD_05		SD_06		SD_07		SD_08		SD_09		SD_10		SD_11	
Wavelength (nm)	Module Band	DN_to_ Rad_mult	MIN	MAX	MIN	MAX	MIN	MAX	MIN	MAX	MIN	MAX	MIN	MAX	MIN	MAX	MIN	MAX	MIN	MAX	MIN	MAX	MIN	MAX
437	VIS01	0.1917887	3	65	1	77	1	77	1	78	2	87	1	94	2	1002	1	87	0	1962	2	305	2	1273
448.9	VIS02	0.0417966	36	407	28	478	28	478	28	474	35	552	30	551	35	3865	32	557	34	3865	32	2004	30	3865
461.3	VIS03	0.0267761	58	656	46	784	46	784	44	783	56	918	50	889	58	3846	50	926	54	3846	51	3569	47	3846
477.3	VIS04	0.0190023	87	990	65	1191	65	1191	65	1213	81	1436	71	1338	85	3883	73	1402	76	3883	74	3883	70	3883
492.3	VIS05	0.0161205	95	1199	73	1372	73	1372	71	1415	91	1647	78	1514	94	3862	78	1597	84	3862	81	3862	76	3862
507.4	VIS06	0.0161798	93	1223	74	1380	74	1380	71	1464	90	1672	80	1527	93	3854	76	1628	87	3855	80	3855	73	3855
523.4	VIS07	0.01464	109	1423	86	1632	86	1632	86	1765	113	1995	97	1813	111	3865	91	1940	104	3865	97	3865	91	3865
538.8	VIS08	0.0121862	136	1682	105	1971	105	1971	103	2154	137	2408	116	2172	134	3851	111	2313	128	3852	119	3852	108	3852
554.2	VIS09	0.0111095	148	1856	113	2112	113	2112	108	2336	150	2590	122	2320	149	3869	117	2468	139	3869	127	3869	119	3869
569.5	VIS10	0.0115756	136	1796	104	1993	104	1993	101	2254	136	2478	112	2184	140	3831	114	2326	128	3831	119	3831	109	3831
584.7	VIS11	0.0117561	134	1805	102	1952	102	1952	99	2251	123	2440	100	2143	128	3863	111	2283	125	3863	112	3864	106	3863
600.1	VIS12	0.0120857	133	1786	99	1914	99	1914	91	2232	108	2402	84	2115	114	3860	107	2220	122	3860	110	3860	104	3860
615.7	VIS13	0.012195	130	1748	96	1868	96	1868	83	2181	100	2325	80	2084	107	3867	103	2166	119	3868	106	3867	102	3868
631.3	VIS14	0.0126865	123	1651	88	1745	88	1745	76	2041	92	2164	71	1950	98	3852	95	2023	112	3852	96	3852	91	3852
646.6	VIS15	0.0127953	120	1591	83	1667	83	1667	68	1964	85	2066	65	1863	91	3860	90	1937	105	3860	94	3860	86	3860
661.7	VIS16	0.0132433	117	1575	82	1630	82	1630	63	1943	80	2042	61	1839	85	3867	86	1908	98	3867	91	3868	84	3867
676.9	VIS17	0.0130146	114	1532	81	1575	81	1575	59	1895	76	1994	59	1784	83	3862	81	1843	92	3862	92	3862	84	3862
692.4	VIS18	0.0125127	123	1503	87	1526	87	1526	58	1818	77	1964	56	1727	81	3856	79	1794	92	3856	98	3856	98	3856
707.8	VIS19	0.0123946	130	1490	104	1506	104	1506	58	1812	76	1966	56	1688	81	3867	78	1739	89	3867	102	3868	102	3867
722.9	VIS20	0.0119494	125	1394	95	1379	95	1379	53	1643	72	1834	50	1619	76	3865	72	1606	81	3865	91	3866	96	3866
738.1	VIS21	0.0118825	139	1585	109	1559	109	1559	61	1874	83	2082	57	1887	85	3863	81	1815	93	3863	101	3863	110	3863
753.4	VIS22	0.0119048	116	1371	94	1276	94	1276	50	1542	69	1710	47	1550	71	3853	67	1481	79	3853	83	3853	92	3853
768.5	VIS23	0.0126219	117	1567	95	1277	95	1277	50	1542	70	1741	48	1628	72	3884	68	1504	78	3884	85	3884	93	3884
783.5	VIS24	0.0137482	116	1610	95	1230	95	1230	49	1492	67	1676	46	1560	70	3847	65	1450	77	3847	84	3848	92	3847
798.8	VIS25	0.0146238	104	1459	85	1079	85	1079	44	1310	59	1489	41	1396	63	3871	59	1287	69	3871	74	3871	82	3871
814.1	VIS26	0.015994	79	1154	63	826	63	826	34	1002	46	1142	31	1085	48	3872	46	992	53	3873	57	3873	64	3873
829.2	VIS27	0.0160734	82	1192	65	854	65	854	35	1045	48	1184	32	1155	50	3856	46	1032	54	3856	58	3856	65	3856
844.4	VIS28	0.0162283	86	1234	68	883	68	883	35	1105	49	1213	34	1223	52	3867	48	1072	55	3867	58	3867	66	3867
859.8	VIS29	0.0179043	74	1076	59	771	59	771	32	982	43	1061	29	1094	44	3863	43	944	50	3864	52	3864	60	3864

HyVista Corporation (A.C.N. 087 620 737)
PO Box 437, Baulkham Hills NSW 1755 Australia
22 Delhi Road, North Ryde NSW 2113 Australia

File 1 - SAO_DOM_min_max_DN_126_stats.txt (continuation)

			SD_01		SD_02		SD_03		SD_04		SD_05		SD_06		SD_07		SD_08		SD_09		SD_10		SD_11	
Wavelength (nm)	Module Band	DN_to_ Rad_mult	MIN	MAX	MIN	MAX	MIN	MAX	MIN	MAX	MIN	MAX	MIN	MAX	MIN	MAX	MIN	MAX	MIN	MAX	MIN	MAX	MIN	MAX
875	VIS30	0.0205219	64	907	50	655	50	655	27	846	37	893	26	944	39	3869	37	799	41	3869	45	3307	52	3869
872.6	NIR01	0.040106	28	480	21	320	21	320	8	426	17	502	9	404	16	3985	14	399	19	3985	21	1864	23	3985
890.3	NIR02	0.0250182	42	695	34	447	34	447	15	606	25	690	15	573	25	4008	23	570	29	4008	29	2633	35	4008
905.6	NIR03	0.0154962	54	899	42	562	42	562	19	774	32	878	20	772	33	4000	30	711	37	4000	39	3235	44	4000
922.2	NIR04	0.0114039	65	1071	50	643	50	643	24	917	37	989	23	886	38	4006	36	837	42	4006	45	3813	53	4006
938	NIR05	0.0089561	47	814	33	457	33	457	14	660	25	686	15	666	28	3997	23	584	30	3997	32	2569	36	3997
953.6	NIR06	0.0077339	56	1004	43	596	43	596	20	848	35	880	20	926	35	4004	31	715	39	4004	42	3041	47	4004
969.3	NIR07	0.0069026	104	1682	80	1028	80	1028	39	1541	62	1483	40	1609	61	3983	56	1268	68	3983	76	3983	85	3983
984.8	NIR08	0.0068844	134	2102	103	1294	103	1294	53	2025	79	1826	53	2050	82	4002	75	1639	90	4002	99	4002	110	4002
1000.9	NIR09	0.0064935	156	2354	117	1480	117	1480	62	2329	91	2059	61	2317	93	4028	86	1859	102	4028	114	4028	127	4028
1016.5	NIR10	0.0061752	165	2473	126	1581	126	1581	67	2509	98	2182	66	2519	99	3989	93	1948	110	3989	122	3989	135	3989
1032	NIR11	0.0059366	172	2565	132	1672	132	1672	69	2626	100	2311	68	2617	102	4002	96	2024	114	4002	128	4002	141	4002
1047.5	NIR12	0.0055585	177	2581	134	1727	134	1727	71	2704	103	2315	70	2774	104	4013	97	2052	118	4013	131	4013	145	4013
1063	NIR13	0.005175	183	2546	135	1750	135	1750	73	2740	105	2375	70	2922	106	3999	101	2078	119	3999	134	4000	147	3999
1078	NIR14	0.0048981	181	2560	135	1770	135	1770	72	2735	105	2463	71	2886	105	4014	101	2082	120	4014	134	4015	147	4014
1093.1	NIR15	0.0047274	161	2327	118	1581	118	1581	63	2478	94	2243	61	2460	94	4013	87	1850	106	4013	117	4013	130	4013
1108	NIR16	0.0044653	110	1636	79	1079	79	1079	41	1694	62	1601	41	1679	65	4029	59	1255	71	4029	77	4029	87	4029
1122.9	NIR17	0.0042182	53	894	36	508	36	508	17	794	27	783	15	799	28	4008	25	594	32	4008	34	2338	37	4008
1137.6	NIR18	0.0039668	53	975	37	576	37	576	17	879	31	969	17	929	30	4011	26	647	33	4011	38	2427	42	4011
1152.2	NIR19	0.0039783	77	1175	55	864	55	864	26	1251	43	1441	27	1364	45	3999	40	900	50	3999	55	3356	61	3999
1166.7	NIR20	0.0040007	123	1797	91	1442	91	1442	45	1994	72	2336	47	2164	74	4017	66	1409	81	4017	91	4017	100	4017
1181.4	NIR21	0.0040183	140	2048	101	1652	101	1652	52	2293	79	2596	53	2278	83	4025	77	1556	91	4025	103	4025	112	4025
1196.1	NIR22	0.0039753	151	2113	107	1804	107	1804	56	2430	85	2837	57	2478	86	4005	82	1646	96	4005	110	4006	118	4005
1210.3	NIR23	0.0041563	153	2115	110	1874	110	1874	59	2470	86	2929	59	2518	89	4009	84	1664	100	4010	113	4010	121	4010
1224.5	NIR24	0.0043752	158	2148	113	1943	113	1943	62	2524	89	3001	60	2556	90	3996	87	1693	100	3996	116	3996	125	3996

HyVista Corporation (A.C.N. 087 620 737)
PO Box 437, Baulkham Hills NSW 1755 Australia
22 Delhi Road, North Ryde NSW 2113 Australia

File 1 - SAO_DOM_min_max_DN_126_stats.txt (continuation)

			SD_01		SD_02		SD_03		SD_04		SD_05		SD_06		SD_07		SD_08		SD_09		SD_10		SD_11	
Wavelength (nm)	Module Band	DN_to_ Rad_mult	MIN	MAX	MIN	MAX	MIN	MAX	MIN	MAX	MIN	MAX	MIN	MAX	MIN	MAX	MIN	MAX	MIN	MAX	MIN	MAX	MIN	MAX
1238.7	NIR25	0.0045236	156	2118	111	1931	111	1931	61	2485	86	2959	59	2468	89	4011	86	1663	100	4011	114	4011	124	4011
1253.2	NIR26	0.0045591	144	1951	102	1792	102	1792	55	2272	80	2797	53	2322	82	4004	76	1533	93	4004	104	4004	114	4004
1267.3	NIR27	0.0046382	132	1765	91	1629	91	1629	50	2037	73	2575	50	2112	75	3997	71	1384	83	3997	96	3998	104	3998
1281.4	NIR28	0.0048435	131	1746	91	1647	91	1647	50	2035	73	2608	49	2092	75	4033	70	1382	84	4033	96	4033	104	4033
1295.4	NIR29	0.005221	115	1533	79	1449	79	1449	44	1784	62	2301	44	1828	66	4015	62	1207	73	4015	83	4015	90	4015
1309.4	NIR30	0.0056357	89	1188	61	1110	61	1110	33	1367	48	1777	32	1389	50	4013	47	920	55	4013	62	3818	68	4013
1323.6	NIR31	0.0062495	57	821	40	729	40	729	21	912	30	1168	20	880	32	4011	30	613	36	4012	40	2532	44	4012
1336.8	NIR32	0.0069391	30	471	19	388	19	388	10	499	16	628	9	503	16	3375	14	333	18	4006	19	1361	22	4006
1406.4	SW1_01	0.0035065	-8	178	-8	22	-8	22	-8	27	-13	51	-26	61	-33	119	-9	22	-52	253	-33	109	-60	180
1420.6	SW1_02	0.0030619	-2	327	-5	57	-5	57	-6	77	-3	111	-124	86	-5	462	-5	50	-10	1054	-4	165	-7	551
1434.4	SW1_03	0.0028019	4	463	-1	138	-1	138	-4	167	0	201	-124	517	-2	1123	-2	119	0	2434	-1	345	0	1339
1448.5	SW1_04	0.0025598	14	663	5	326	5	326	-1	385	7	467	-61	364	5	2600	5	263	5	3886	7	898	7	3115
1462.6	SW1_05	0.0025011	25	828	13	574	13	574	3	654	15	866	-160	617	13	3880	12	439	14	3880	14	1415	15	3880
1476.6	SW1_06	0.0023725	31	891	17	676	17	676	5	759	17	969	-4	849	17	3868	17	511	17	3868	18	1774	21	3868
1490.3	SW1_07	0.0022209	64	1390	43	1408	43	1408	19	1562	39	1886	-30	1702	42	3864	41	1022	44	3864	45	3797	51	3864
1503.9	SW1_08	0.0020397	114	2267	83	2490	83	2490	40	2697	72	3290	-90	2803	75	3879	69	1729	79	3879	80	3879	90	3879
1517.2	SW1_09	0.002049	142	2707	107	3104	107	3104	53	3290	90	3849	64	3773	96	3849	92	2116	100	3849	102	3848	116	3849
1530.7	SW1_10	0.0020369	161	2972	123	3489	123	3489	61	3664	102	3882	55	3892	108	3882	102	2341	114	3882	117	3882	131	3882
1544.1	SW1_11	0.0020048	169	3103	130	3694	130	3694	64	3843	109	3858	86	3779	114	3858	110	2446	120	3858	123	3857	140	3858
1557.6	SW1_12	0.0019917	170	3077	131	3710	131	3710	66	3829	107	3863	71	3821	114	3862	107	2439	122	3862	124	3862	140	3862
1570.6	SW1_13	0.0019536	166	2934	127	3563	127	3563	64	3655	105	3884	-136	3939	110	3884	101	2349	117	3884	119	3883	138	3884
1583.5	SW1_14	0.0019452	163	2883	125	3525	125	3525	61	3610	103	3881	68	3853	108	3881	103	2309	117	3881	117	3881	135	3881
1596.5	SW1_15	0.001994	159	2784	123	3446	123	3446	62	3521	99	3863	80	3755	105	3863	105	2242	114	3863	112	3862	132	3863
1609.5	SW1_16	0.00205	154	2625	115	3275	115	3275	58	3371	94	3856	68	3820	99	3856	97	2128	107	3856	108	3856	126	3856
1622.3	SW1_17	0.0020966	156	2484	118	3273	118	3273	58	3324	94	3835	-86	3562	100	3835	105	2116	108	3835	111	3834	128	3835
1635.1	SW1_18	0.0021364	150	2296	115	3185	115	3185	56	3222	91	3887	59	3851	96	3887	90	2051	105	3887	105	3887	124	3887
1647.8	SW1_19	0.0021152	145	2205	111	3092	111	3092	56	3121	88	3833	77	3747	93	3833	91	1988	101	3833	100	3832	120	3833
1660.3	SW1_20	0.0021016	143	2185	110	3085	110	3085	55	3105	87	3876	-3	3663	93	3876	84	1981	99	3876	102	3876	119	3876
1672.7	SW1_21	0.0021235	136	2085	101	2959	101	2959	50	2961	82	3883	62	3632	87	3883	84	1890	95	3883	95	3882	111	3882

HyVista Corporation (A.C.N. 087 620 737)
PO Box 437, Baulkham Hills NSW 1755 Australia
22 Delhi Road, North Ryde NSW 2113 Australia

File 1 - SAO_DOM_min_max_DN_126_stats.txt (continuation)

			SD_01		SD_02		SD_03		SD_04		SD_05		SD_06		SD_07		SD_08		SD_09		SD_10		SD_11	
Wavelength (nm)	Module Band	DN_to_ Rad_mult	MIN	MAX	MIN	MAX	MIN	MAX	MIN	MAX	MIN	MAX	MIN	MAX	MIN	MAX	MIN	MAX	MIN	MAX	MIN	MAX	MIN	MAX
1685.1	SW1_22	0.0021763	128	1974	96	2819	96	2819	47	2841	77	3739	51	3417	81	3901	76	1799	88	3901	90	3901	104	3901
1697.5	SW1_23	0.0022203	117	1844	90	2648	90	2648	45	2639	72	3546	51	3252	77	3844	73	1684	81	3844	82	3843	97	3844
1709.9	SW1_24	0.0022042	108	1753	82	2532	82	2532	43	2548	67	3342	-159	2872	71	3881	65	1603	76	3881	76	3881	91	3881
1722.1	SW1_25	0.0022349	100	1610	74	2336	74	2336	38	2337	62	3138	37	2801	66	3884	63	1480	70	3884	69	3883	81	3884
1734.1	SW1_26	0.0022948	88	1438	65	2092	65	2092	31	2110	54	2809	10	2576	58	3874	59	1318	61	3874	59	3873	71	3874
1746.5	SW1_27	0.0023598	79	1310	58	1880	58	1880	29	1882	49	2554	-45	2414	52	3877	55	1186	55	3877	55	3876	65	3877
1758.4	SW1_28	0.0023923	71	1187	51	1730	51	1730	25	1722	42	2389	-154	2017	46	3873	42	1089	49	3873	49	3719	57	3873
1770.3	SW1_29	0.0024426	57	972	41	1379	41	1379	20	1373	36	1944	-12	1809	37	3852	39	875	39	3852	38	2856	46	3852
1782.2	SW1_30	0.0025275	39	705	25	948	25	948	11	961	24	1342	-5	1232	24	3876	25	608	27	3876	26	1915	30	3876
1794	SW1_31	0.0026613	21	483	13	529	13	529	5	541	12	778	-45	766	12	3106	13	344	13	3855	13	968	15	3855
1805.7	SW1_32	0.0029131	6	262	2	164	2	164	-2	173	2	245	-68	320	1	986	2	110	2	2099	1	271	2	1238
1951.6	SW2_01	0.0007285	2	420	-1	276	-1	276	-6	319	0	503	-1	349	-2	1677	-3	184	-21	3919	-6	630	-9	2064
1970.7	SW2_02	0.0006629	46	1186	28	1535	28	1535	11	1596	28	2201	16	1546	28	3967	25	939	29	3969	29	3650	31	3971
1989.5	SW2_03	0.000634	89	2045	60	2897	60	2897	28	2834	54	3967	36	3419	58	3969	53	1735	59	3971	61	3974	62	3972
2008.2	SW2_04	0.0006076	44	1076	27	1480	27	1480	12	1453	27	2059	16	1819	25	3965	24	920	30	3967	30	2943	30	3968
2027.1	SW2_05	0.0005777	95	2205	67	3198	67	3198	32	3174	60	3991	38	3278	62	3993	59	1887	65	3995	65	3999	70	3997
2045.9	SW2_06	0.0005513	130	2926	91	3975	91	3975	46	3975	85	3961	56	3973	89	3963	83	2643	93	3965	91	3969	96	3967
2064.5	SW2_07	0.0005286	105	2483	69	3805	69	3805	35	3654	69	3981	45	3994	71	3983	66	2239	75	3985	72	3989	80	3987
2082.7	SW2_08	0.0005138	130	3158	92	3946	92	3946	48	3946	85	3931	58	3944	92	3933	87	2881	95	3935	92	3939	100	3937
2100.8	SW2_09	0.0005133	141	3440	104	4023	104	4023	55	4023	94	4008	65	4020	101	4010	95	3204	106	4012	102	4016	108	4014
2118.7	SW2_10	0.0005051	140	3460	101	3963	101	3963	52	3963	90	3948	61	3960	99	3950	93	3295	101	3952	99	3956	104	3954
2136.7	SW2_11	0.0005034	149	3515	109	3974	109	3974	56	3973	96	3959	67	3971	104	3961	100	3343	104	3963	105	3967	111	3965
2154.7	SW2_12	0.0005199	134	3201	95	3963	95	3963	51	3962	85	3948	60	3960	93	3950	87	3035	95	3952	94	3956	99	3954
2172.2	SW2_13	0.0005357	121	2907	89	3973	89	3973	45	3973	78	3958	53	3970	83	3960	79	2757	86	3962	85	3966	91	3964
2189.2	SW2_14	0.0005595	111	2678	81	3975	81	3975	40	3974	71	3960	48	3972	73	3962	70	2535	77	3964	77	3968	81	3966
2206.6	SW2_15	0.0005962	103	2452	74	3985	74	3985	36	3895	64	3970	42	3982	65	3971	61	2335	72	3974	71	3978	76	3976
2224.8	SW2_16	0.0006204	103	2435	78	3953	78	3953	36	3842	60	3937	42	3950	67	3939	64	2307	73	3942	73	3946	78	3944
2241.7	SW2_17	0.0006363	95	2290	68	3935	68	3935	33	3641	57	3984	41	3997	62	3986	58	2171	65	3988	65	3992	70	3990
2259.4	SW2_18	0.0006401	79	2111	60	3665	60	3665	28	3345	51	3970	35	3983	55	3972	52	2018	58	3975	54	3978	61	3977

HyVista Corporation (A.C.N. 087 620 737)
PO Box 437, Baulkham Hills NSW 1755 Australia
22 Delhi Road, North Ryde NSW 2113 Australia

File 1 - SAO_DOM_min_max_DN_126_stats.txt (continuation)

			SD_01		SD_02		SD_03		SD_04		SD_05		SD_06		SD_07		SD_08		SD_09		SD_10		SD_11	
Wavelength (nm)	Module Band	DN_to_ Rad_mult	MIN	MAX	MIN	MAX	MIN	MAX	MIN	MAX	MIN	MAX	MIN	MAX	MIN	MAX	MIN	MAX	MIN	MAX	MIN	MAX	MIN	MAX
2276.6	SW2_19	0.0006454	69	1966	52	3420	52	3420	24	3130	45	3976	30	3934	48	3978	45	1881	50	3980	48	3984	53	3982
2293.5	SW2_20	0.000655	62	1806	45	3141	45	3141	21	2859	38	3929	27	3665	43	3931	41	1734	45	3933	43	3937	47	3935
2310	SW2_21	0.0006768	55	1672	40	2948	40	2948	18	2716	38	3915	25	3276	37	3937	36	1609	40	3939	38	3943	38	3941
2326.3	SW2_22	0.000679	50	1559	36	2746	36	2746	16	2515	33	3656	22	3112	35	3984	33	1499	37	3986	35	3990	36	3988
2342.8	SW2_23	0.0006771	42	1404	31	2481	31	2481	14	2272	31	3346	19	2838	29	3941	26	1359	32	3943	31	3947	32	3945
2359.7	SW2_24	0.0006604	39	1257	26	2236	26	2236	12	2064	26	2987	14	2494	24	3995	22	1219	29	3998	24	3655	29	3999
2375.8	SW2_25	0.0006465	32	1106	22	1974	22	1974	8	1788	23	2669	13	2290	21	3989	20	1075	24	3992	22	2995	25	3993
2391.8	SW2_26	0.0006443	28	955	17	1716	17	1716	6	1594	19	2272	10	1887	18	3997	16	940	21	4000	17	2659	19	4001
2407.6	SW2_27	0.0006536	24	856	15	1556	15	1556	5	1400	17	2172	8	1848	14	3969	14	844	18	3972	15	2199	17	3973
2423.6	SW2_28	0.0006614	19	678	8	1236	8	1236	1	1149	11	1619	5	1324	10	3967	8	678	12	3969	10	1836	11	3971
2439.3	SW2_29	0.0006706	19	674	10	1241	10	1241	1	1125	10	1707	4	1430	8	3966	6	672	10	3968	9	1696	10	3970
2455	SW2_30	0.0006984	7	494	3	834	3	834	-2	771	3	1084	1	902	3	3338	2	455	5	3924	4	1136	3	3926
2470.5	SW2_31	0.0007444	5	470	1	665	1	665	-4	613	0	953	-2	774	-1	2617	0	365	1	3972	1	792	1	3276
2485.9	SW2_32	0.0008786	-4	203	-7	186	-7	186	-8	190	-5	256	-6	214	-11	764	-8	111	-19	1499	-5	194	-7	930

HyVista Corporation (A.C.N. 087 620 737)
PO Box 437, Baulkham Hills NSW 1755 Australia
22 Delhi Road, North Ryde NSW 2113 Australia

Attached files

File 2 - SAO_DOM_saturation_radiances.txt

Nominal_Saturation (DN) =	3600			
Band	Wavelength (nm)	Module_Band	DN_to_Radiance_mult	Saturation_level_Radiance (uW cm-2 nm-1 sr-1)
1	437	VIS01	0.1917887	690.43932
2	448.9	VIS02	0.0417966	150.46776
3	461.3	VIS03	0.0267761	96.39396
4	477.3	VIS04	0.0190023	68.40828
5	492.3	VIS05	0.0161205	58.0338
6	507.4	VIS06	0.0161798	58.24728
7	523.4	VIS07	0.01464	52.704
8	538.8	VIS08	0.0121862	43.87032
9	554.2	VIS09	0.0111095	39.9942
10	569.5	VIS10	0.0115756	41.67216
11	584.7	VIS11	0.0117561	42.32196
12	600.1	VIS12	0.0120857	43.50852
13	615.7	VIS13	0.012195	43.902
14	631.3	VIS14	0.0126865	45.6714
15	646.6	VIS15	0.0127953	46.06308
16	661.7	VIS16	0.0132433	47.67588
17	676.9	VIS17	0.0130146	46.85256
18	692.4	VIS18	0.0125127	45.04572
19	707.8	VIS19	0.0123946	44.62056
20	722.9	VIS20	0.0119494	43.01784
21	738.1	VIS21	0.0118825	42.777
22	753.4	VIS22	0.0119048	42.85728
23	768.5	VIS23	0.0126219	45.43884
24	783.5	VIS24	0.0137482	49.49352
25	798.8	VIS25	0.0146238	52.64568
26	814.1	VIS26	0.015994	57.5784
27	829.2	VIS27	0.0160734	57.86424
28	844.4	VIS28	0.0162283	58.42188
29	859.8	VIS29	0.0179043	64.45548
30	875	VIS30	0.0205219	73.87884
31	872.6	NIR01	0.040106	144.3816
32	890.3	NIR02	0.0250182	90.06552
33	905.6	NIR03	0.0154962	55.78632
34	922.2	NIR04	0.0114039	41.05404
35	938	NIR05	0.0089561	32.24196
36	953.6	NIR06	0.0077339	27.84204
37	969.3	NIR07	0.0069026	24.84936
38	984.8	NIR08	0.0068844	24.78384
39	1000.9	NIR09	0.0064935	23.3766
40	1016.5	NIR10	0.0061752	22.23072
41	1032	NIR11	0.0059366	21.37176
42	1047.5	NIR12	0.0055585	20.0106
43	1063	NIR13	0.005175	18.63
44	1078	NIR14	0.0048981	17.63316
45	1093.1	NIR15	0.0047274	17.01864
46	1108	NIR16	0.0044653	16.07508
47	1122.9	NIR17	0.0042182	15.18552
48	1137.6	NIR18	0.0039668	14.28048
49	1152.2	NIR19	0.0039783	14.32188

HyVista Corporation (A.C.N. 087 620 737)
PO Box 437, Baulkham Hills NSW 1755 Australia
22 Delhi Road, North Ryde NSW 2113 Australia

File 2 - SAO_DOM_saturation_radiances.txt (continuation)

Nominal_Saturation (DN) =	3600			
Band	Wavelength (nm)	Module_Band	DN_to_Radiance_mult	Saturation_level_Radiance (uW cm-2 nm-1 sr-1)
50	1166.7	NIR20	0.0040007	14.40252
51	1181.4	NIR21	0.0040183	14.46588
52	1196.1	NIR22	0.0039753	14.31108
53	1210.3	NIR23	0.0041563	14.96268
54	1224.5	NIR24	0.0043752	15.75072
55	1238.7	NIR25	0.0045236	16.28496
56	1253.2	NIR26	0.0045591	16.41276
57	1267.3	NIR27	0.0046382	16.69752
58	1281.4	NIR28	0.0048435	17.4366
59	1295.4	NIR29	0.005221	18.7956
60	1309.4	NIR30	0.0056357	20.28852
61	1323.6	NIR31	0.0062495	22.4982
62	1336.8	NIR32	0.0069391	24.98076
63	1406.4	SW1_01	0.0035065	12.6234
64	1420.6	SW1_02	0.0030619	11.02284
65	1434.4	SW1_03	0.0028019	10.08684
66	1448.5	SW1_04	0.0025598	9.21528
67	1462.6	SW1_05	0.0025011	9.00396
68	1476.6	SW1_06	0.0023725	8.541
69	1490.3	SW1_07	0.0022209	7.99524
70	1503.9	SW1_08	0.0020397	7.34292
71	1517.2	SW1_09	0.002049	7.3764
72	1530.7	SW1_10	0.0020369	7.33284
73	1544.1	SW1_11	0.0020048	7.21728
74	1557.6	SW1_12	0.0019917	7.17012
75	1570.6	SW1_13	0.0019536	7.03296
76	1583.5	SW1_14	0.0019452	7.00272
77	1596.5	SW1_15	0.001994	7.1784
78	1609.5	SW1_16	0.00205	7.38
79	1622.3	SW1_17	0.0020966	7.54776
80	1635.1	SW1_18	0.0021364	7.69104
81	1647.8	SW1_19	0.0021152	7.61472
82	1660.3	SW1_20	0.0021016	7.56576
83	1672.7	SW1_21	0.0021235	7.6446
84	1685.1	SW1_22	0.0021763	7.83468
85	1697.5	SW1_23	0.0022203	7.99308
86	1709.9	SW1_24	0.0022042	7.93512
87	1722.1	SW1_25	0.0022349	8.04564
88	1734.1	SW1_26	0.0022948	8.26128
89	1746.5	SW1_27	0.0023598	8.49528
90	1758.4	SW1_28	0.0023923	8.61228
91	1770.3	SW1_29	0.0024426	8.79336
92	1782.2	SW1_30	0.0025275	9.099
93	1794	SW1_31	0.0026613	9.58068
94	1805.7	SW1_32	0.0029131	10.48716
95	1951.6	SW2_01	0.0007285	2.6226
96	1970.7	SW2_02	0.0006629	2.38644
97	1989.5	SW2_03	0.000634	2.2824
98	2008.2	SW2_04	0.0006076	2.18736
99	2027.1	SW2_05	0.0005777	2.07972
100	2045.9	SW2_06	0.0005513	1.98468
101	2064.5	SW2_07	0.0005286	1.90296
102	2082.7	SW2_08	0.0005138	1.84968
103	2100.8	SW2_09	0.0005133	1.84788

HyVista Corporation (A.C.N. 087 620 737)
PO Box 437, Baulkham Hills NSW 1755 Australia
22 Delhi Road, North Ryde NSW 2113 Australia

File 2 - SAO_DOM_saturation_radiances.txt (continuation)

Nominal_Saturation (DN) =	3600			
Band	Wavelength (nm)	Module_Band	DN_to_Radiance_mult	Saturation_level_Radiance (uW cm-2 nm-1 sr-1)
104	2118.7	SW2_10	0.0005051	1.81836
105	2136.7	SW2_11	0.0005034	1.81224
106	2154.7	SW2_12	0.0005199	1.87164
107	2172.2	SW2_13	0.0005357	1.92852
108	2189.2	SW2_14	0.0005595	2.0142
109	2206.6	SW2_15	0.0005962	2.14632
110	2224.8	SW2_16	0.0006204	2.23344
111	2241.7	SW2_17	0.0006363	2.29068
112	2259.4	SW2_18	0.0006401	2.30436
113	2276.6	SW2_19	0.0006454	2.32344
114	2293.5	SW2_20	0.000655	2.358
115	2310	SW2_21	0.0006768	2.43648
116	2326.3	SW2_22	0.000679	2.4444
117	2342.8	SW2_23	0.0006771	2.43756
118	2359.7	SW2_24	0.0006604	2.37744
119	2375.8	SW2_25	0.0006465	2.3274
120	2391.8	SW2_26	0.0006443	2.31948
121	2407.6	SW2_27	0.0006536	2.35296
122	2423.6	SW2_28	0.0006614	2.38104
123	2439.3	SW2_29	0.0006706	2.41416
124	2455	SW2_30	0.0006984	2.51424
125	2470.5	SW2_31	0.0007444	2.67984
126	2485.9	SW2_32	0.0008786	3.16296

HyVista Corporation (A.C.N. 087 620 737)
PO Box 437, Baulkham Hills NSW 1755 Australia
22 Delhi Road, North Ryde NSW 2113 Australia

3.2. DATA QUALITY CHECKING PROBLEMS ENCOUNTERED

3.2.1. Data quality checking, problems encountered

HyVista Corp (HVC) Company delivered radiance data to IGM in end of January 2001. Due to anomalies verified in the data, further re-processing was done by this company at IGM request and was secondly delivered in end of June 2001, with additional reflectance data and geocorrection files. An explanatory report was delivered in October 2001 (App. 3.1). Anomalies verified are due to negative and saturated pixels as representative of lost data.

Data quality checking presented show slight differences, compared to HVC report, once it excludes data calibration laboratory.

3.2.1.1. Negative numbers

According to explanatory report (App. 3.1), radiance data negative numbers from São Domingos images could arise due to the following 3 factors:

(i) Dark current correction: result in small radiometry errors when dark current correction is applied to the data. This error is likely to be small but could lead to some additional negativity ;

(ii) Saturation of the detectors - if the detectors are subjected to high levels of radiation, large negative values result after dark current correction;

(iii) Warming of the detectors - detector arrays for IR modules are cooled by liquid nitrogen. If the operator misjudges the timing in terms of refilling the liquid nitrogen, errors in dark current could occur and there can be a rapid and non-uniform increase in the dark current. The onset of this detector warming is rapid and slightly unpredictable.

According to HVC report (App. 3.1), the operator did refill the liquid nitrogen during the acquisition of this site but did not note when.

To identify occurrence of negative numbers each image was analyzed per band and results are shown in Table 1, Figures 3.2.1a) and 3.2.1b) and in Table 3.2.2.

Table 3.2.1 resumes the bands where at least one negative pixel occurs.

Table 3.2.1 – Occurrence of negative pixels in images per band

Image Strip	Bands with negatives
SAO_DOM_01	63 64, 126
SAO_DOM_02	63-65, 126
SAO_DOM_03	63-64, 126
SAO_DOM_04	63-66, 94-95, 124-126
SAO_DOM_05	63-64, 80, 82-84, 126
SAO_DOM_06	63-70, 75, 79, 82, 86, 89-95, 125 126
SAO_DOM_07	1-35, 63-65, 67-69, 80, 92-93, 95, 126
SAO_DOM_08	63-65, 95, 126
SAO_DOM_09	1-35, 63 64, 66-69, 83-93, 95, 126
SAO_DOM_10	1-34, 63-65, 80, 82-90, 95, 126
SAO_DOM_11	1-35, 63 64, 67-69,80, 82-93, 95, 126

Graphics from Figures 3.2.1 and 3.2.2 shows the distribution of negative values along spectral bands, for images strip 1 to 6 and images strip 7 to strip 11, respectively.

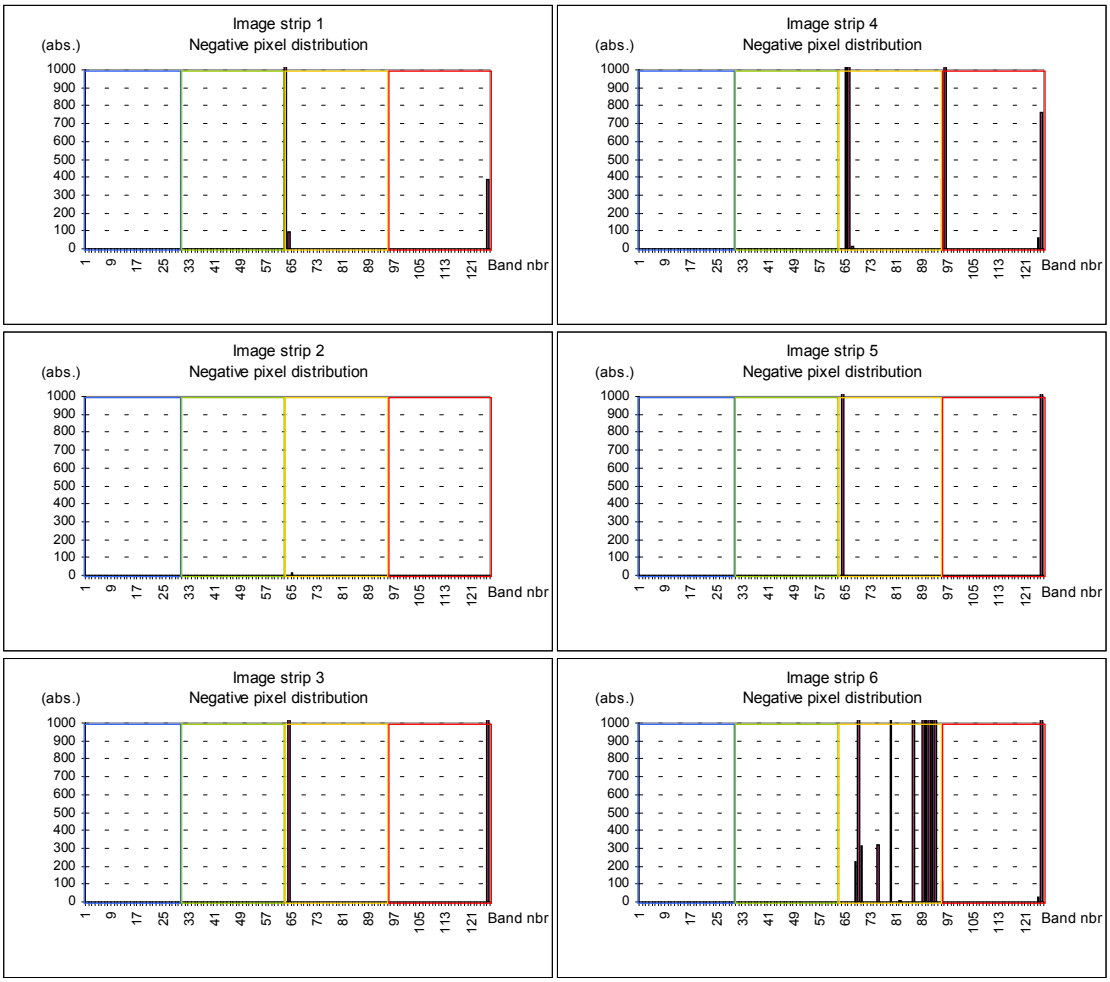

Figure 3.2.1a) – Distribution of negative pixel along spectral wavelength for images strip1, strip2, strip3, strip4, strip5 and strip 6.

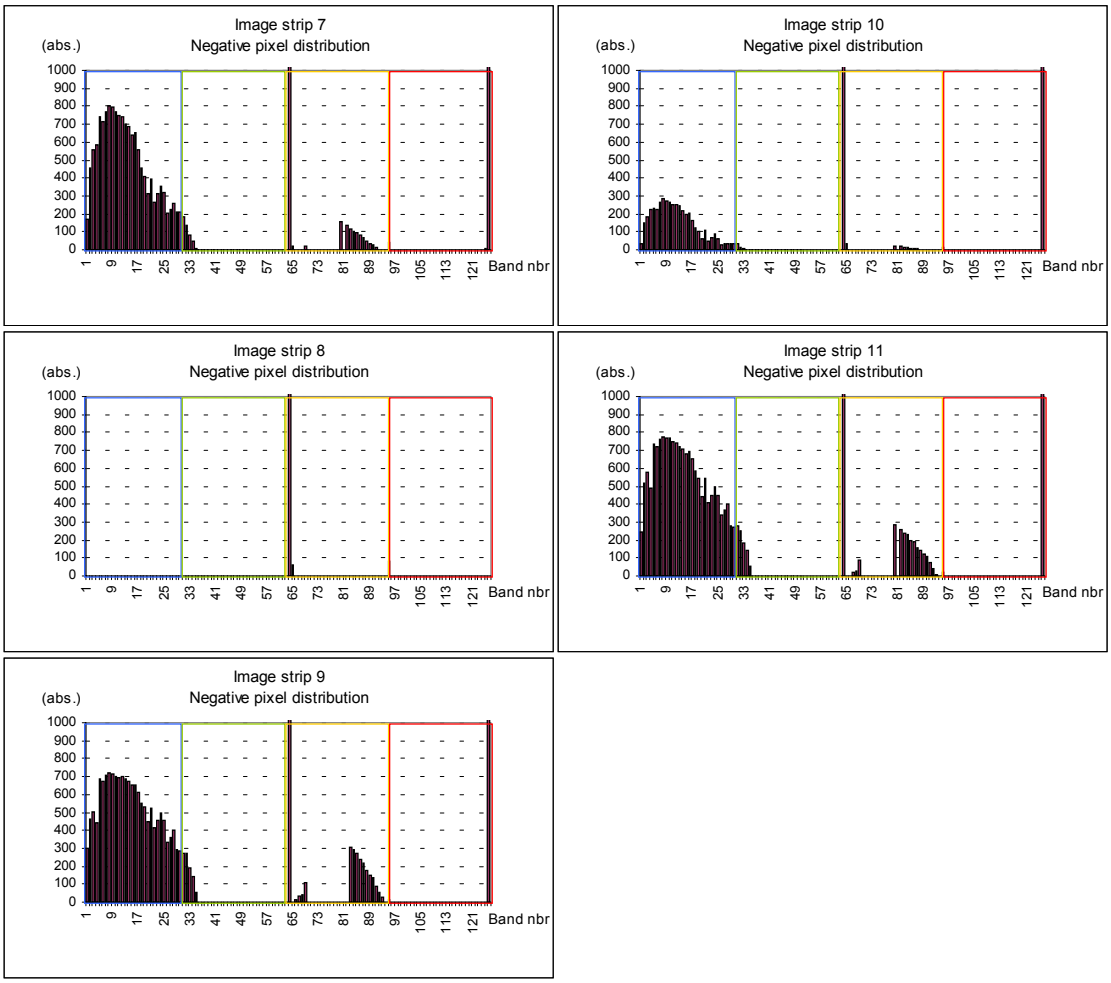

Figure 3.2.1b) – Distribution of negative pixel along spectral wavelength for images strip7, strip8, strip9, strip10 and strip 11.

Analyzing negative pixel distribution of Figures 3.2.1a) and 3.2.1b), it is clearly evident that negative values present two distinct distributions:

- Images from strip 1 to strip 5 – negative values mainly arise on bands 63 to 94 from SWIR1 module (orange color in the a.m. figures) and bands 125-126 in SWIR2 module (red color area). These bands correspond to regions of strong water vapor bands: at 1.4 μm for bands 63 to 65, bands 94-95 correspond to the 1.9 μm strong water vapor bands and band 126 to water vapor band at 2.7 μm.
- Image strip 6, have additional bands with negative numbers in SWIR1 region, however these bands are not in the spectral region of strong water vapor absorption. This would seem to indicate a problem with detector cooling.
- Images from strip 7 to strip 11 – excluding strip 8, these images present negative pixels not only in strong water absorption bands (as do strips 1 to 5) but they also have negative data along the entire VIS region (see Figure 3.2.1b and Table 3.2.1), NIR region, SWIR1 and SWIR2. To explain this fact one could think that new distribution of negative pixels from images 7 to 11 occur due to cooling of the detectors after strip 6 survey (see App. 3.1). In the other hand, similar distribution of negative pixels observed on strip 7, strip 10 and strip 11 against the one's from strips 8 and 10, suggests that negative pixels could too be influenced by flight direction for south-east direction.

Table 3.2.2 show the statistics of negative pixels distribution for each image per band.

Table 3.2.2 - Statistics of negative pixels distribution

	Strip1	Strip2	Strip3	Strip4	Strip5	Strip6	Strip7	Strip8	Strip9	Strip10	Strip11
Aver per bnd.	400	0.3	1429	3720	766	124352	1705	4664	1680	2820	2908
Sdv	2221	1.4	72134	17208	4043	331140	6590	18360	7042	14556	14302
min	0	0	0	0	0	0	0.	0	0	0	0
Max. freq.	24928	15	80587	191642	45349	2522371	72997	146326	79019	163322	160686
Tot neg.	25410	20	90749	236239	48637	7896335	108233	296179	106681	179076	184682
% neg	0.01%	0.00%	0.02%	0.05%	0.01%	1.55%	0.02%	0.07%	0.02%	0.04%	0.04%
Dim image ($x10^8$)	4.57	4.71	5.11	5.03	4.69	5.10	4.68	4.49	5.14	4.87	4.42

As it could be seen in Table 3.2.2, globally negative pixels occurrence is less than 1% for each total image, except in strip 6, where it reaches 1.55% of total image pixels.

In the image strip 6, the data in bands of the SWIR1 module appear to be unusable due to warming of the detector array during data acquisition.

As it is difficult to assess the impact on the radiometry of the SWIR1 bands in image strip 6, HVC recommend that, for this image, the bands of the SWIR1 module should be excluded.

In summary, negative pixels are distributed with major importance in atmospheric bands (ie near strong water vapor absorption bands), however, strips 7, 9 and 11 present negative data along the whole VIS and part of the NIR region, maybe due to changes in detectors cooling conditions and influence of flight direction illumination.

As negative pixels are more often distributed in image water bodies, spatial masks for water bodies where create in order to reduce the influence of anomalous pixels in subsequent image processing.

According to HVC report, negative values encountered in São Domingos image data set are not due to saturation of the detectors but represent small errors in dark current correction (image Strip 6 (SAO_DOM_06) in the SWIR1 is an exception). In terms of the mean radiance of the scenes, these radiometric errors are less than 1%. This is smaller than the radiometric inaccuracies associated with the laboratory radiometric calibration procedures where the main source of error is the radiometric calibration of the standard light source used. The calibration of this standard light source is traceable to the NIST laboratory in the USA.

Correctly accounted for, the pixels with negative radiance will have no impact on the ability to detect and map spectral variability within the scene.

3.2.1.2. Saturated pixels

Saturated pixels are image data which radiance value exceeds the maximum radiance the sensor could register. These pixels represent lost data, and are usually associated with sun glint from water bodies or specular reflections, from building windows and metal roofs and, occasionally, from very bright, diffuses reflecting materials (usually at high sun angles).

The HyMap data of the MINEO test site in Portugal does contain saturated pixels, which are primarily associated with sun glint from water bodies and buildings.

To identify occurrence of saturated pixels it was done the same analysis as in 3.2.1.1.. Each image was analyzed per band and results are shown in Figures 3.2.2a) and 3.2.2b) and Table 3.2.3.

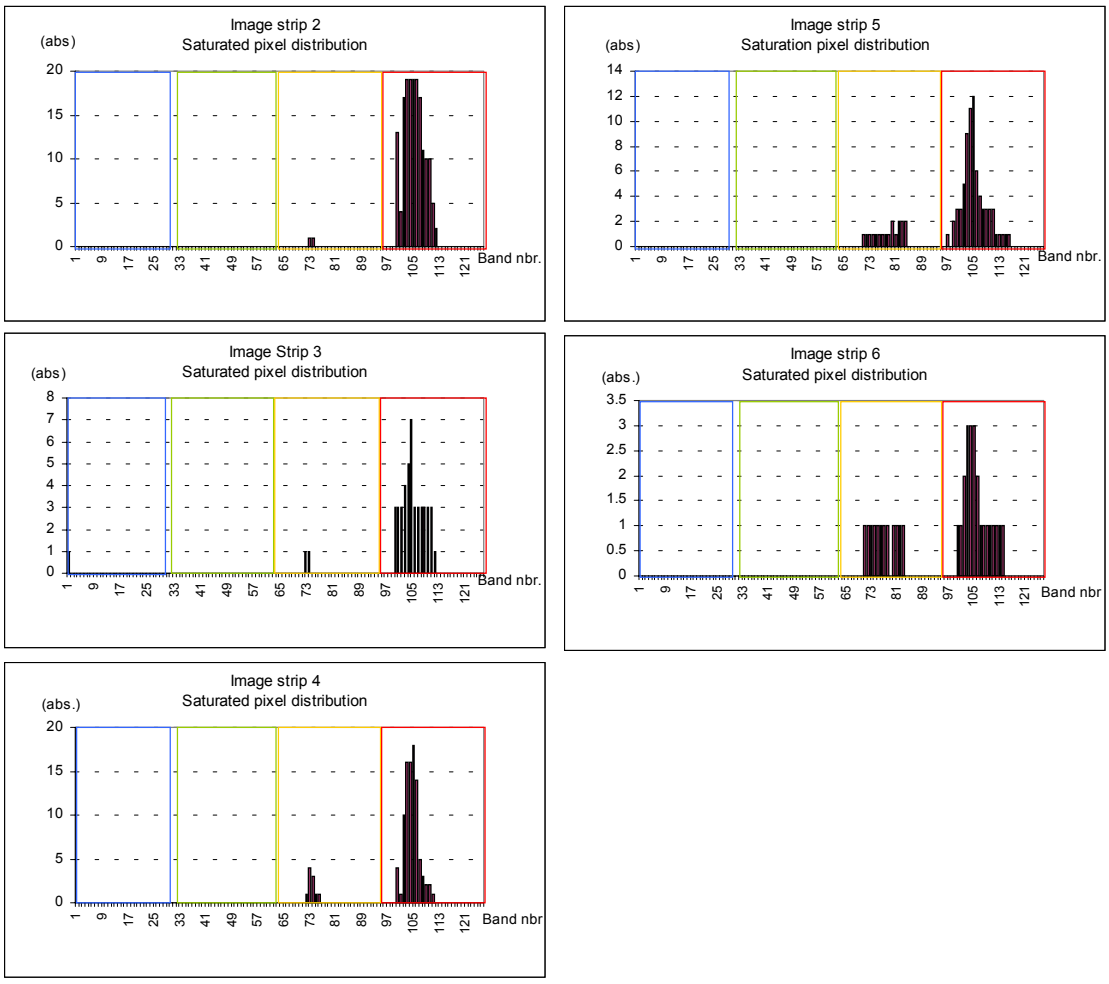

Figure 3.2.2a) – Distribution of saturated pixel along spectral wavelength for images strip2, strip3, strip4, strip5 and strip 6.

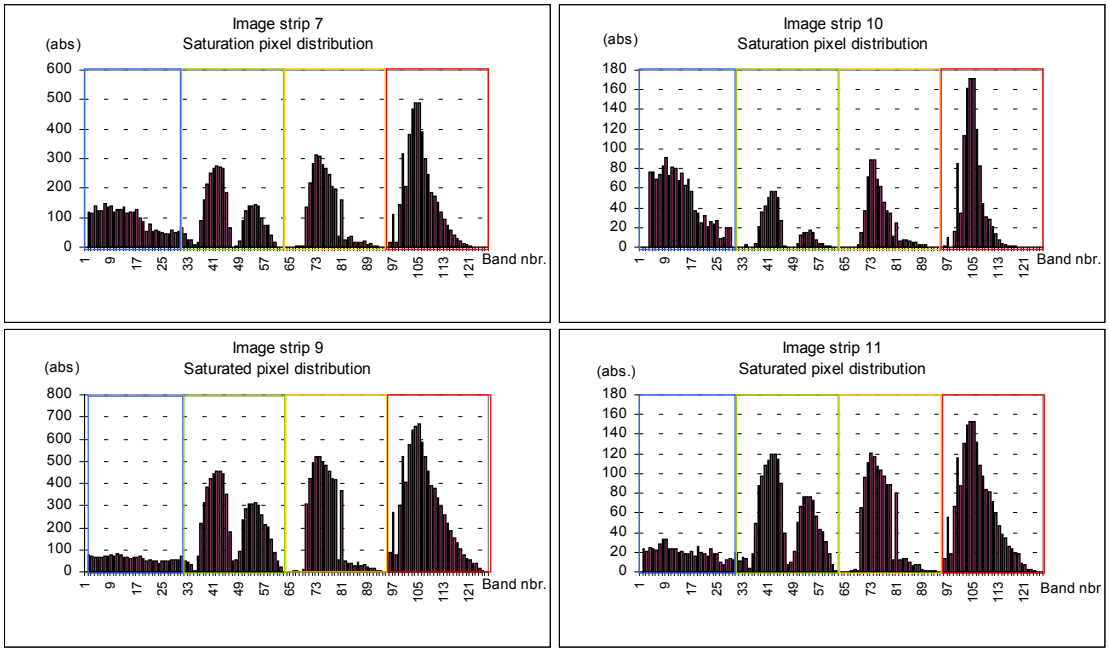

Figure 3.2.2b) – Distribution of saturated pixel along spectral wavelength for images Strip7, strip9, strip10 and strip 11.

Comparing saturated pixel distribution of Figure 3.2.2a) with the ones on Figure 3.2.2b) it is clear that, excluding strips 2 and strip 8 (which don't have saturated pixel), saturated pixels present 2 distinct distributions.

Images from strip 2 to strip 6: saturated pixels present bimodal distribution along spectral bands, corresponding to SWIR1 region and mainly to SWIR2 region (orange and red colors, respectively).

Images from strip 7 to strip 11: saturated pixels occur along the whole spectral range, from VIS, NIR, SWIR1 and SWIR2. It is evident that detectors cooling done during strip 6 survey has affected the occurrence of saturated pixels in posterior images acquisition, as referenced in 3.2.1.1. for the negative values.

Table 3.2.3 shows statistics of saturated pixels distribution.

Table 3.2.3 - Statistics of saturated pixels

	Strip1	Strip2	Strip3	Strip4	Strip5	Strip6	Strip7	Strip8	Strip9	Strip10	Strip11
Aver per bnd.	0	1	0.4	1	0.7	0.3	108	0	179	28	42
Sdv	0	2338	157	1137	447	47	1564587	0	4277459	172455	222645
min	0	0	0	0	0	0	0	0	0	0	0
Max. freq.	0	19	7	18	12	3	491	0	668	171	153
Tot sat.	0	167	46	102	72	35	13552	0	22500	3523	5237
% sat.	0	0.00004	0.00001	0.00002	0.00002	0.00001	0.0029	0	0.0044	0.0007	0.001
Dim image ($x10^8$)	4.57	4.71	5.11	5.03	4.69	5.10	4.68	4.49	5.14	4.87	4.42

As it could be seen in table 3, globally saturated pixels occurrence is not representative for each image. Strip 7, 9 and 11 are those with higher number of saturated pixels, but less than 0.004% of total image.

Hence, flight direction seems to slightly influence the existence of saturated pixels, as suggested for negative values (see 3.2.1.1.).

3.2.1.3. Conclusions

Negative pixels are distributed with major importance in atmospheric bands (ie near strong water vapor absorption bands), however, strips 7, 9 and 11 present negative data along the whole VIS and part of the NIR region, maybe due to changes in detectors cooling conditions and influence of flight direction illumination.

Globally negative pixels occurrence is less than 1% for each total image, except in band 6, where it reaches 1.55% of total image pixels. Concerning saturated pixels strips 7, 9 and 11 are the one with highest number of saturated pixels, but less than 0.004% of total image.

Saturated pixels are mainly distributed with in SWIR1 and SWIR2 spectral regions, however, strips 7, 9 and 11 present increasing of saturated data along the whole VIS and part of the NIR region, again, maybe due to variation of detectors temperature conditions and due to the influence of flight direction.

APPENDIX 4

GEOCHEMICAL MODELLING USING HYPERSPECTRAL DATA

A.4.1. Basic statistics for some soil characteristics

A.4.2. Basic statistics for some elements

A.4.3. Soils and sediments

A.4.4. Geochemical background reference targets: multivariate analysis (PCA) and elements spacial distribution

Basic statistics for some soils characteristics of the six subareas

Units					Particle size distribution (<2mm)			
ACHADA		**pH_H2O**	**Orgcarb**	**FeMJ**	**coarse_sand**	**fine_sand**	**silt**	**clay**
	Valid N	36	36	36	32	32	32	32
	Mean	4,26	15,34	28,41	287,44	366,63	189,50	156,41
	Median	4,00	7,1	20,79	289	386,5	171	148
	Minimum	1,62	0	7,77	2	2	2	3
	Maximum	7,78	106,2	99,60	993	583	458	426
	Std.Dev.	1,11	20,02	19,84	181,16	117,68	82,39	84,89
TELHEIRO		**pH_H2O**	**Orgcarb**	**FeMJ**	**coarse_sand**	**fine_sand**	**silt**	**clay**
	Valid N	37	37	37	37	37	37	37
	Mean	4,65	16,20	26,49	194,62	426,16	204,03	175,19
	Median	4,45	17,1	15,24	154	435	193	169
	Minimum	2,66	1,9	3,30	7	105	71	81
	Maximum	7,40	57,8	85,47	728	714	362	379
	Std.Dev.	1,35	12,47	20,60	162,76	114,73	71,74	67,69
S.DOMINGOS		**pH_H2O**	**Orgcarb**	**FeMJ**	**coarse_sand**	**fine_sand**	**silt**	**clay**
	Valid N	23	23	23	21	21	21	21
	Mean	4,25	23,26	37,79	310,33	318,14	206,00	165,52
	Median	4,44	16,9	30,45	326	321	193	170
	Minimum	2,52	4	2,18	52	133	81	22
	Maximum	5,81	137,4	79,89	509	539	390	336
	Std.Dev.	0,92	27,82	26,03	126,19	91,51	88,76	87,28
POMARÃON		**pH_H2O**	**Orgcarb**	**FeMJ**	**coarse_sand**	**fine_sand**	**silt**	**clay**
	Valid N	30		30	30	30	30	30
	Mean	5,93		11,03	31,85	33,71	19,40	15,05
	Median	6,10		11,39	32,05	33,55	19,55	14,7
	Minimum	4,60		2,46	5,4	23,6	7,5	9,4
	Maximum	6,80		16,62	52,6	41,1	49,7	22,6
	Std.Dev.	0,55		3,12	9,94	4,90	8,35	3,21
TAPADA		**pH_H2O**	**Orgcarb**	**FeMJ**	**coarse_sand**	**fine_sand**	**silt**	**clay**
	Valid N	34	34	34	34	34	34	34
	Mean	5,82	15,39	11,91	293,32	375,94	184,56	140,85
	Median	5,78	15,15	11,69	307,5	385	173	130,5
	Minimum	5,09	5,3	2,48	3	246	85	20
	Maximum	6,68	38,7	23,32	410	556	493	303
	Std.Dev.	0,37	6,48	5,34	79,29	85,01	74,04	58,47
POMARÃOS		**pH_H2O**	**Orgcarb**	**FeMJ**	**coarse_sand**	**fine_sand**	**silt**	**clay**
	Valid N	18		18	18	18	18	18
	Mean	6,28		16,31	19,65	33,42	17,28	14,21
	Median	6,6		14,73	23	33,4	18,6	13,6
	Minimum	1,1		4,68	-9,9	-9,9	-9,9	-9,9
	Maximum	8		57,04	54,3	76,6	39,4	34,7
	Std.Dev.	1,77		11,19	16,70	22,06	13,58	11,13

FeMJ (iron Mehra &Jackson)

Basic statistics for some elements of the six subareas

	%	ppm	ppb	ppm	ppm	ppm	ppm	ppm		ppm	ppm	%	ppm	ppm
ACHADA	**Al**	**As**	**Au**	**Ba**	**Cd**	**Co**	**Cr**	**Cu**	**Fe**	**Hg**	**Pb**	**S**	**Sb**	**Zn**
Valid N	36	36	36	36	36	36	36	36	36	36	36	36	36	36
Mean	4,39	1443,99	85,86	452,08	4,95	22,60	72,33	542,40	7,47	459,11	3984,12	1,34	458,71	917,14
Median	4,29	544,00	30,50	470,00	0,59	11,50	66,50	209,48	5,27	1,25	779,95	0,62	96,70	104,04
Min	1,32	25,90	1,00	25,00	0,15	0,50	29,00	56,63	1,85	0,50	95,71	0,01	6,00	28,00
Max	7,93	14200,0	820,00	800,00	80,01	265,00	195,00	6207,33	39,70	9300,00	32170,00	7,93	5640,0	14850,00
Std.Dev.	1,44	3135,92	161,77	177,28	14,19	44,51	29,16	1084,92	7,44	1922,15	7627,54	1,83	1153,8	2568,21
TELHEIR	**Al**	**As**	**Au**	**Ba**	**Cd**	**Co**	**Cr**	**Cu**	**Fe**	**Hg**	**Pb**	**S**	**Sb**	**Zn**
Valid N	37	37	37	37	37	37	37	37	37	37	37	37	37	37
Mean	4,37	1727,09	26,58	502,43	2,64	12,41	75,49	104,22	5,68	29,32	1000,65	0,62	236,12	140,69
Median	4,38	277,00	5,00	490,00	0,96	12,00	75,00	50,31	4,90	0,50	156,11	0,37	68,90	88,74
Min	3,07	28,00	0,15	290,00	0,15	0,50	49,00	7,64	1,56	0,50	47,16	0,02	3,50	17,29
Max	6,14	15900,0	194,00	1100,00	22,78	32,00	100,00	690,74	15,10	420,00	7315,18	2,81	2400,0	494,95
Std.Dev.	0,66	2792,62	44,68	152,65	4,10	8,55	12,98	134,77	3,02	81,24	1694,03	0,73	466,76	121,80
S.DOM	**Al**	**As**	**Au**	**Ba**	**Cd**	**Co**	**Cr**	**Cu**	**Fe**	**Hg**	**Pb**	**S**	**Sb**	**Zn**
Valid N	23	23	23	23	23	23	23	23	23	23	23	23	23	23
Mean	4,18	1141,38	372,83	566,96	1,58	6,91	84,04	295,30	7,94	2,93	2971,10	0,97	236,05	141,36
Median	4,14	504,00	172,00	550,00	0,65	5,00	96,00	214,47	6,20	3,00	1597,00	0,94	145,00	118,01
Min	2,27	41,80	7,00	380,00	0,15	2,00	-5,00	25,21	1,16	0,50	149,88	0,01	9,10	33,17
Max	6,94	11600,0	2600,0	850,00	14,17	28,00	150,00	1275,38	31,30	11,00	24930,00	2,10	2150,0	754,25
Std.Dev.	1,28	2334,97	574,06	145,33	2,90	6,39	42,21	299,06	6,91	2,73	5052,64	0,76	431,61	147,03
POM N	**Al**	**As**	**Au**	**Ba**	**Cd**	**Co**	**Cr**	**Cu**	**Fe**	**Hg**	**Pb**	**S**	**Sb**	**Zn**
Valid N	30	30	30	30	30	30	30	30	30	30	30	30	30	30
Mean	5,61	19,13	2,13	564,33	0,26	19,93	63,97	43,24	3,92	0,50	44,02	0,02	2,07	86,26
Median	5,10	19,00	1,00	505,00	0,15	20,00	46,50	32,93	4,08	0,50	32,88	0,02	1,70	76,09
Min	3,39	8,90	1,00	250,00	0,15	4,00	-5,00	15,55	1,45	0,50	12,47	0,01	0,60	28,85
Max	12,68	40,50	7,00	1500,0	0,57	43,00	247,00	116,67	6,92	0,50	183,32	0,06	4,80	312,04
Std.Dev.	1,73	8,15	2,18	236,68	0,15	10,54	57,62	24,18	1,35	0,00	32,89	0,01	1,11	50,35
TAPADA	**Al**	**As**	**Au**	**Ba**	**Cd**	**Co**	**Cr**	**Cu**	**Fe**	**Hg**	**Pb**	**S**	**Sb**	**Zn**
Valid N	34	34	34	34	34	34	37	34	34	34	34	34	34	34
Mean	3,66	21,51	7,49	440,00	0,16	14,71	69,24	27,29	2,71	0,57	64,50	0,01	5,39	63,09
Median	3,59	18,75	4,00	440,00	0,15	15,00	68,00	25,29	2,72	0,50	50,39	0,01	3,10	56,52
Min	2,60	7,40	0,15	150,00	0,15	2,00	13,00	8,94	1,02	0,50	22,02	0,00	1,50	26,93
Max	5,25	77,60	65,00	700,00	0,34	31,00	292,00	78,44	5,22	3,00	256,69	0,04	19,70	212,26
Std.Dev.	0,58	13,63	12,37	120,03	0,04	7,59	48,51	15,23	1,03	0,43	43,38	0,01	5,16	32,03
POM S	**Al**	**As**	**Au**	**Ba**	**Cd**	**Co**	**Cr**	**Cu**	**Fe**	**Hg**	**Pb**	**S**	**SB**	**ZN**
Valid N	18	18	18	18	18	18	18	18	18	18	18	18	18	18
Mean	6,19	155,97	19,94	475,83	0,21	31,33	65,44	360,36	4,77	1,8056	641,96	1,38	20,49	278,21
Median	5,57	59,75	15	505	0,15	27	67,5	125,69	3,99	0,5	118,148	0,084	7,3	116,388
Min	1,66	12,2	1	25	-0,3	14	25	20,727	2,83	0,5	5,53888	0,013	1,7	53,57855
Max	12,7	1580	112	750	0,8951	81	108	2727,4	15,8	24	9063,35	16,97	239	1808,096
Std.Dev.	2,52	363,785	25,014	170,21	0,2713	17,0259	23,971	720,66	2,862	5,539	2106,77	4,167	54,912	470,3619

4.3-GEOCHEMICAL MULTIVARIATE APPROACH (PRINCIPAL COMPONENT ANALYSIS)) AND MAPPING:

After univariate statistic analysis some geochemical data and soil characteristics were choosen for Principal Components Analysis (PCA). This step reduces the volume of data creating 6 main composite variables in place of original 34 .in order to improve the interpretation of geochemical patterns and meaningful anomalies related with environmental problems or lithological background.

Two axis (components), more clearly correlated with meaningful geochemical elements association and dispersion, were choosen:

Potential non contaminated areas -Tapada and Pomarão N

TAPADA	CORRELATIONS (+)	CORRELATIONS (-)
AXIS 1 (37%)	V, Fe(MJ), Ni, Co, P, Mn, Cu,Cr, Al, S, Zn, pH	Y
AXIS 4 (7%)	Sb, Pb, As, S, Zn	

POMARÃO N	CORRELATIONS (+)	CORRELATIONS (-)
AXIS 1 (36.0%)	Al,Ca,(Cd),Co,Cr,Fe,Mg,Na,Ni,Sr,V,pH	K,Th,U,
AXIS 2 (19.5%)	As,(Co),Cu,Ni,P,S,Sb, (V,FeMJ)	Na

Potential contaminated areas –S. Domingos, Achada, Telheiro and Pomarão S.

S. DOMINGOS	CORRELATIONS (+)	CORRELATIONS (-)
AXIS 1 (38%)	Hg, Sb, Pb, Au, Cd, As, Se, Fe, Ag	Mg, K, Na, U
AXIS 4 (10%)	Ca, Br, Cu, Corg, Mn, Co, Zn	Ti

ACHADA	CORRELATIONS (+)	CORRELATIONS (-)
AXIS 1 (33%)	Ag, As, Pb, S, Sb, Se (Hg, Cd)	V, Al, Th, U, FeMJ, (K, Mg)
AXIS 2 (19%)	(K)	Ca, Co, Cu, Fe, pH, Zn

TELHEIRO	CORRELATIONS (+)	CORRELATIONS (-)
AXIS 1 (37%)	S, FeMJ, Cd, As, Sb, Pb, K, Au, Ag	Mg, Mn, Ni, Co, Cr, Th, U, pH
AXIS 2 (16%)	K,V	P, Ca, Cu, Corg, pH

POMARÃO S	CORRELATIONS (+)	CORRELATIONS (-)
AXIS 1 (%)	V, Al, U, Th, K, P, pH	S, As, FeMJ, Sb, Zn, Pb, Fe, Au, Co, Cu
AXIS 2 (%)	Na, Ca, Sr, Mg	Mn, Ni, Th, K

The geochemical mapping using geostatistic interpolation (ordinary kriging) of selected axis improves the identification and interpretation of geochemical patterns.

4.4-GEOCHEMICAL BACKGROUND REFERENCE TARGETS: MULTIVARIATE ANALYSIS (PCA) AND ELEMENTS SPATIAL DISTRIBUTION.

The maps estimated for Tapada and Pomarão N, were based on two axes more clearly correlated with meaningful patterns (Figures 4.4.1 and 4.4.2.). The results validate these two subareas as environmental background reference targets.

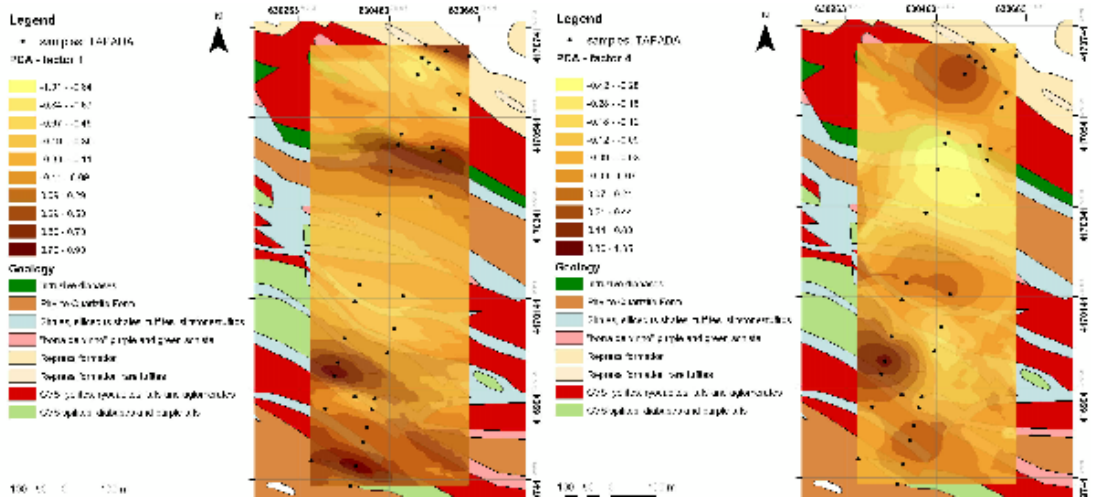

Figure. 4.4.1 - 1 st and 4th PCA kriging interpolation for Tapada related with geology.

Tapada PCA 1st axis represents highly correlated parameters such as V, FeMJ, Ni, Co, Mn, Cu, Cr, S, Zn, and also soil pH. The spatial distribution shows that it is probably associated with local geochemical backgrounds related to lithology, namely basic volcanic rocks, where Cu, Cr, Co, Ni, Fe, and Mn have usually a high background contrasting with acid ones.

On the 4th axis the highly correlated elements, Sb, Pb, As, S, Zn, probably represents local small concentration of disperse sulphides.

Similar conclusions were inferred for Pomarão N, where high values of the 1st axis separate the basic volcanic rocks *versus* acid ones. The 2nd axis seems to characterize greywakes and quartzwakes of Touril formation.

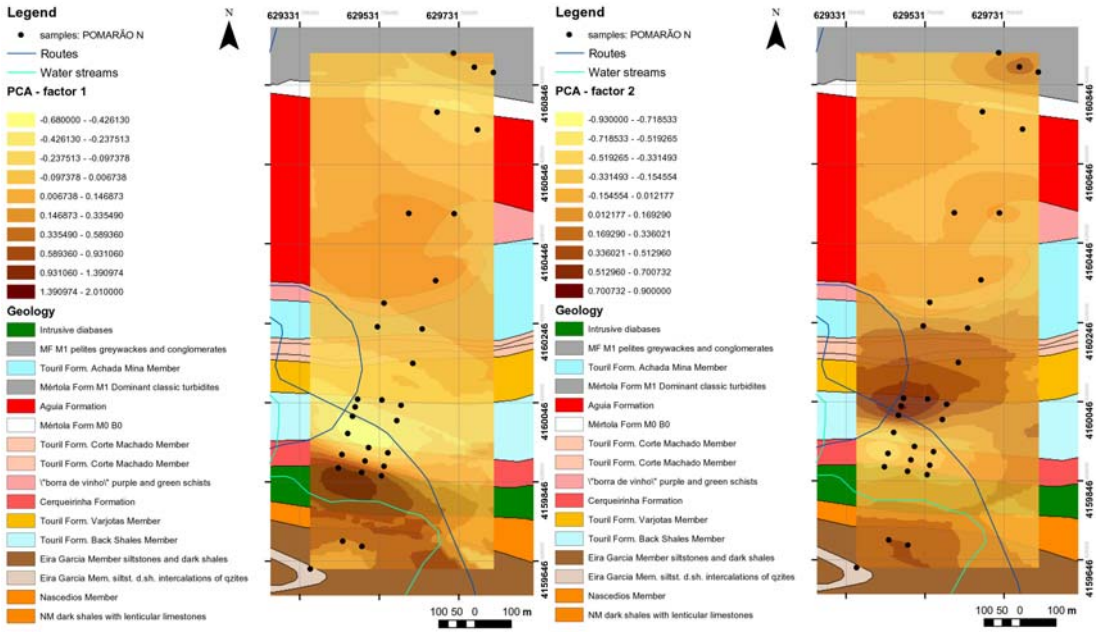

Figure 4.4.2 - 1st and 2nd PCA kriging interpolation for Pomarão N related with geology

Water Sampling Location

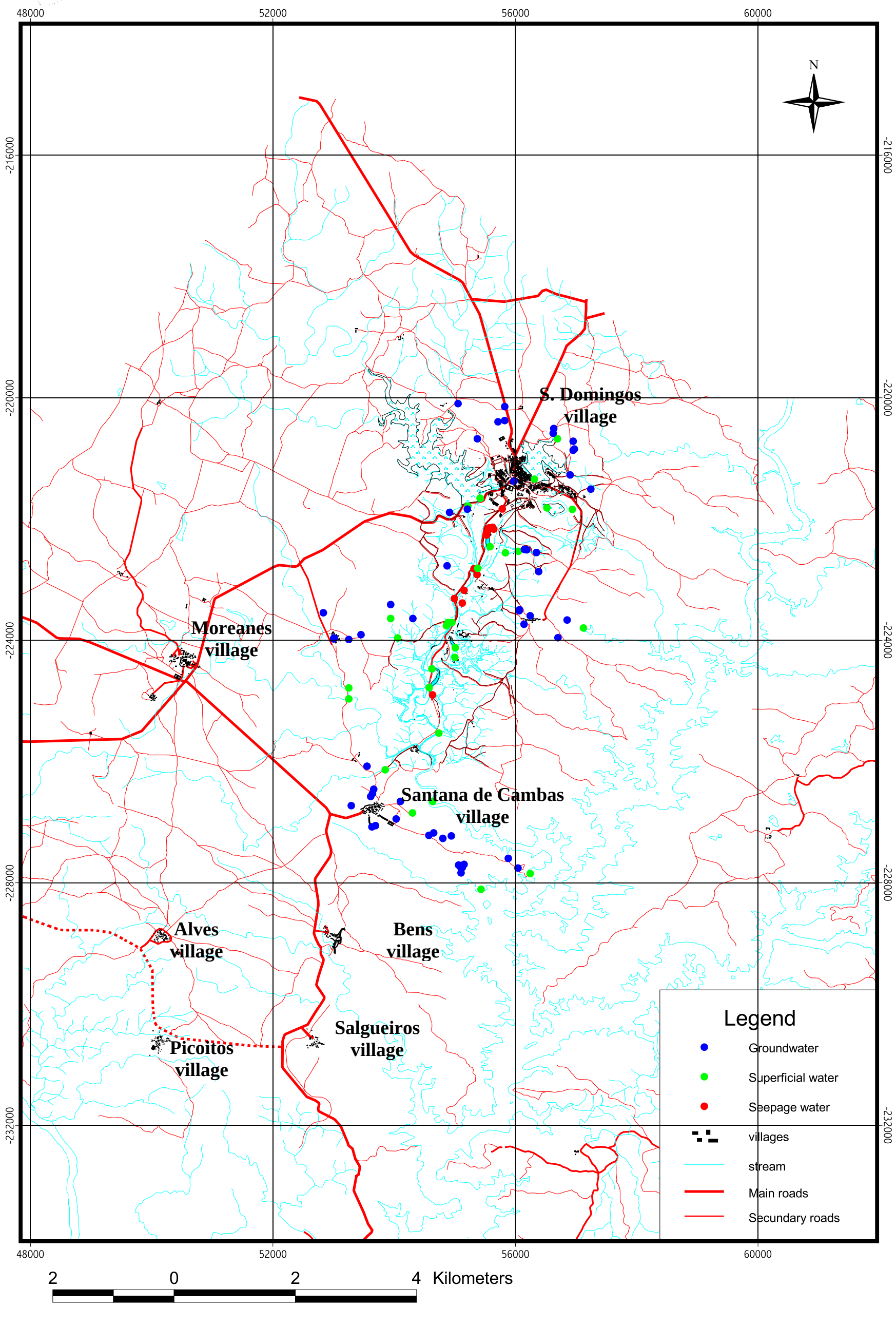

MINEO São Domingos
AMD waste material
(Spectral Angle Mapper)

Map produced in September 2002

IGM

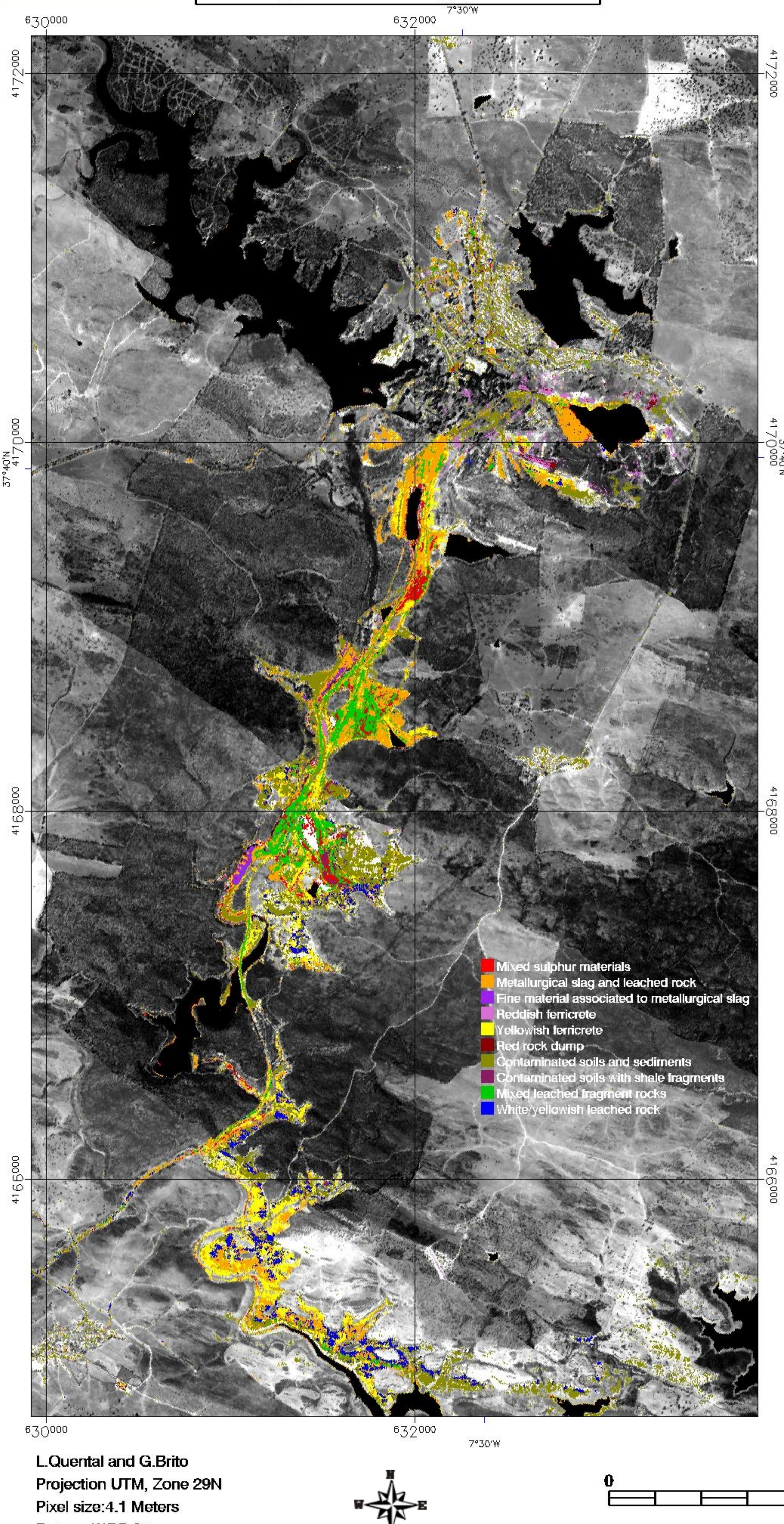

L.Quental and G.Brito

Projection UTM, Zone 29N

Pixel size:4.1 Meters

Datum: WGS-84

Ellipsoid: WG 84

N W E S

0 1 Km

MINEO São Domingos
AMD waste material
(Spectral Angle Mapper)

Map produced in September 2002

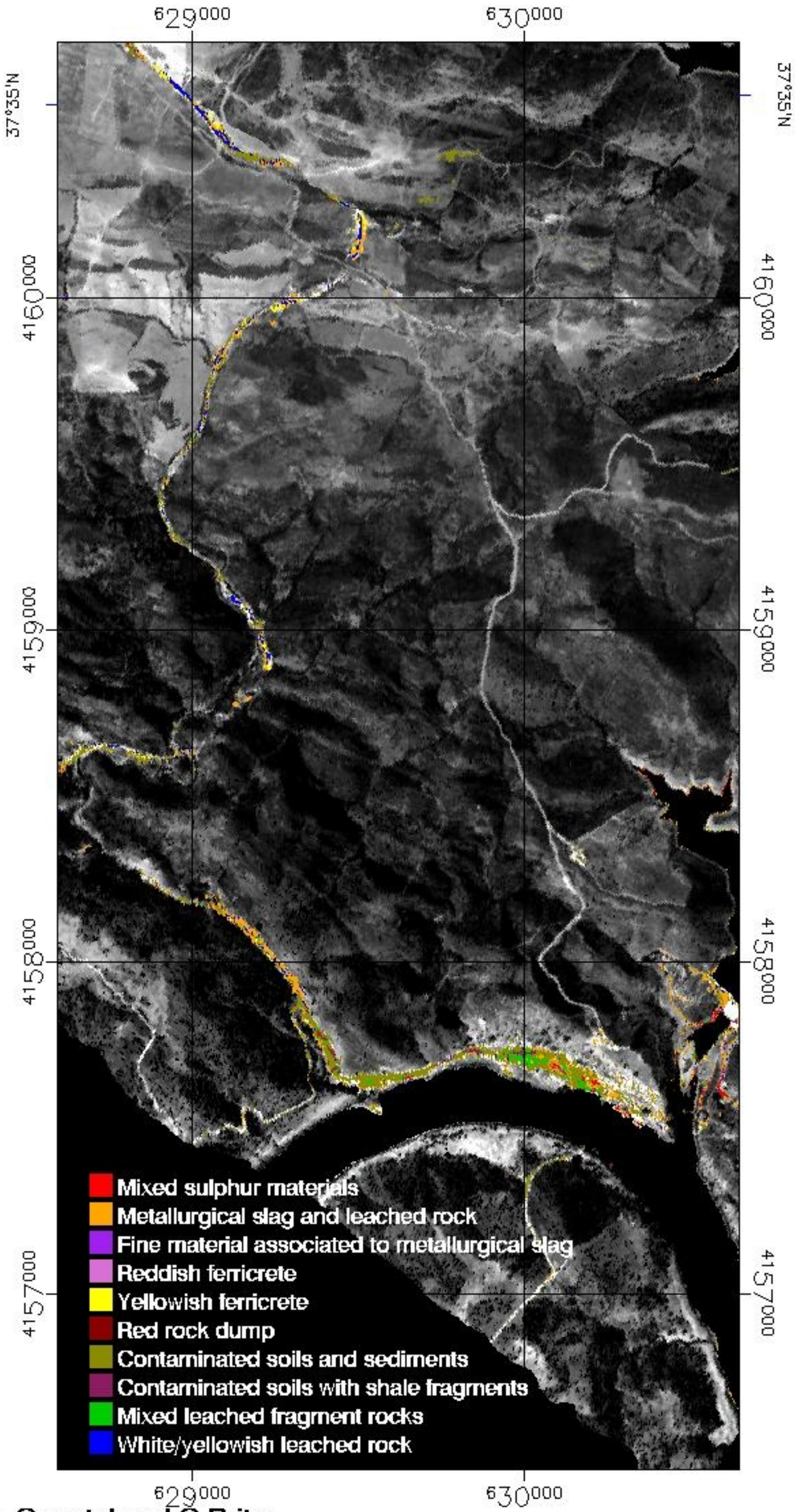

L.Quental and G.Brito

Projection UTM, Zone 29N

Pixel size: 4.1 Meters

Datum: WGS-84

Ellipsoid: WG 84

N W E S

0 0.5 km

Mineo Sao Domingos
AMD mineral mapping
(Mixture Tuned Matched Filtering)

Map produced in September 2002

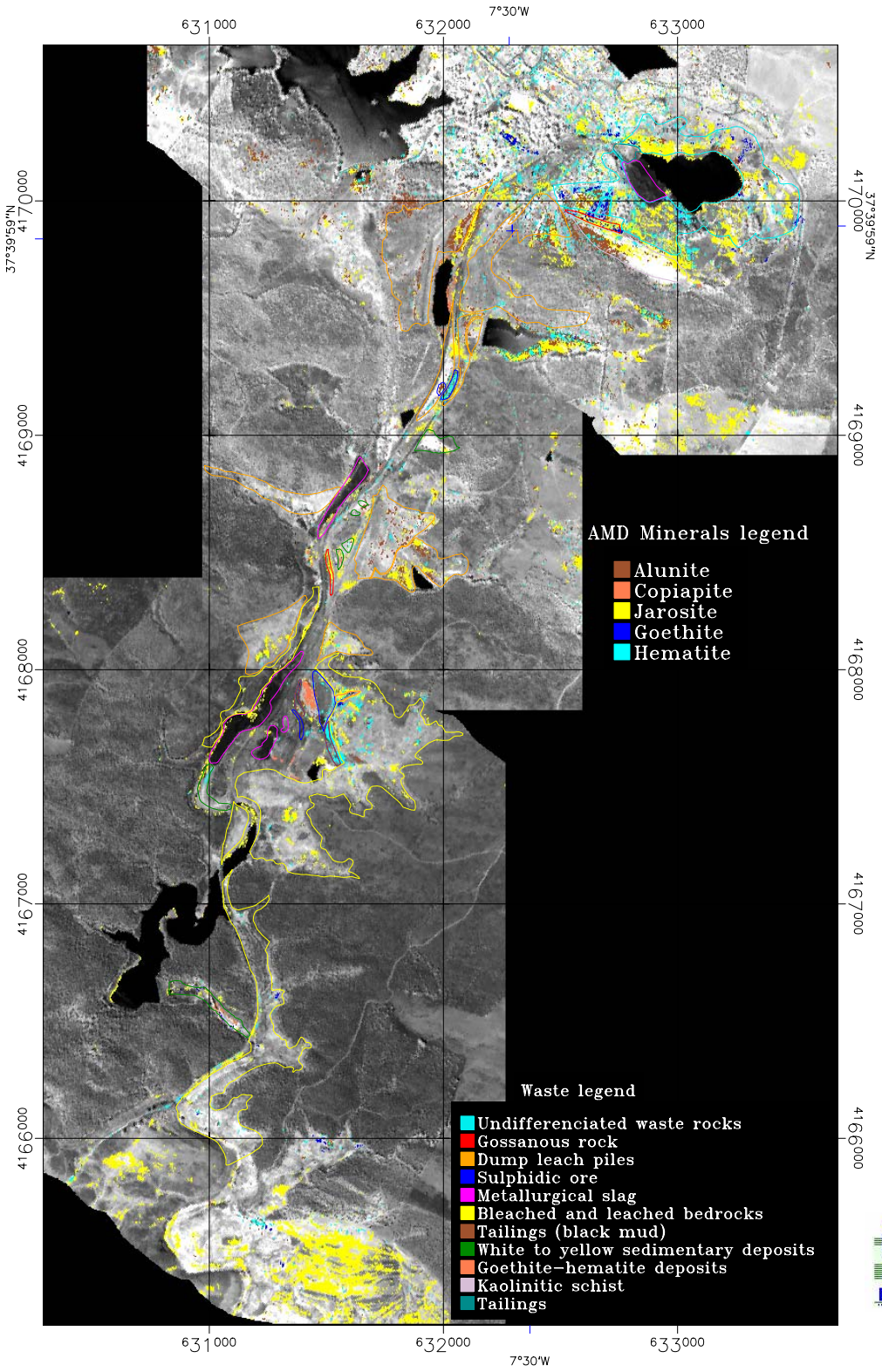

BRGM

A. Bourguignon
projection UTM, Zone 29N
Pixel Size:4.2 Meters
Datum: WGS-84
Ellipsoid: WG 84

N
W
E
S

0 1 Kilometers

Mineo Sao Domingos
AMD mineral mapping
(Spectral Angle Mapper)

Map produced in May 2001

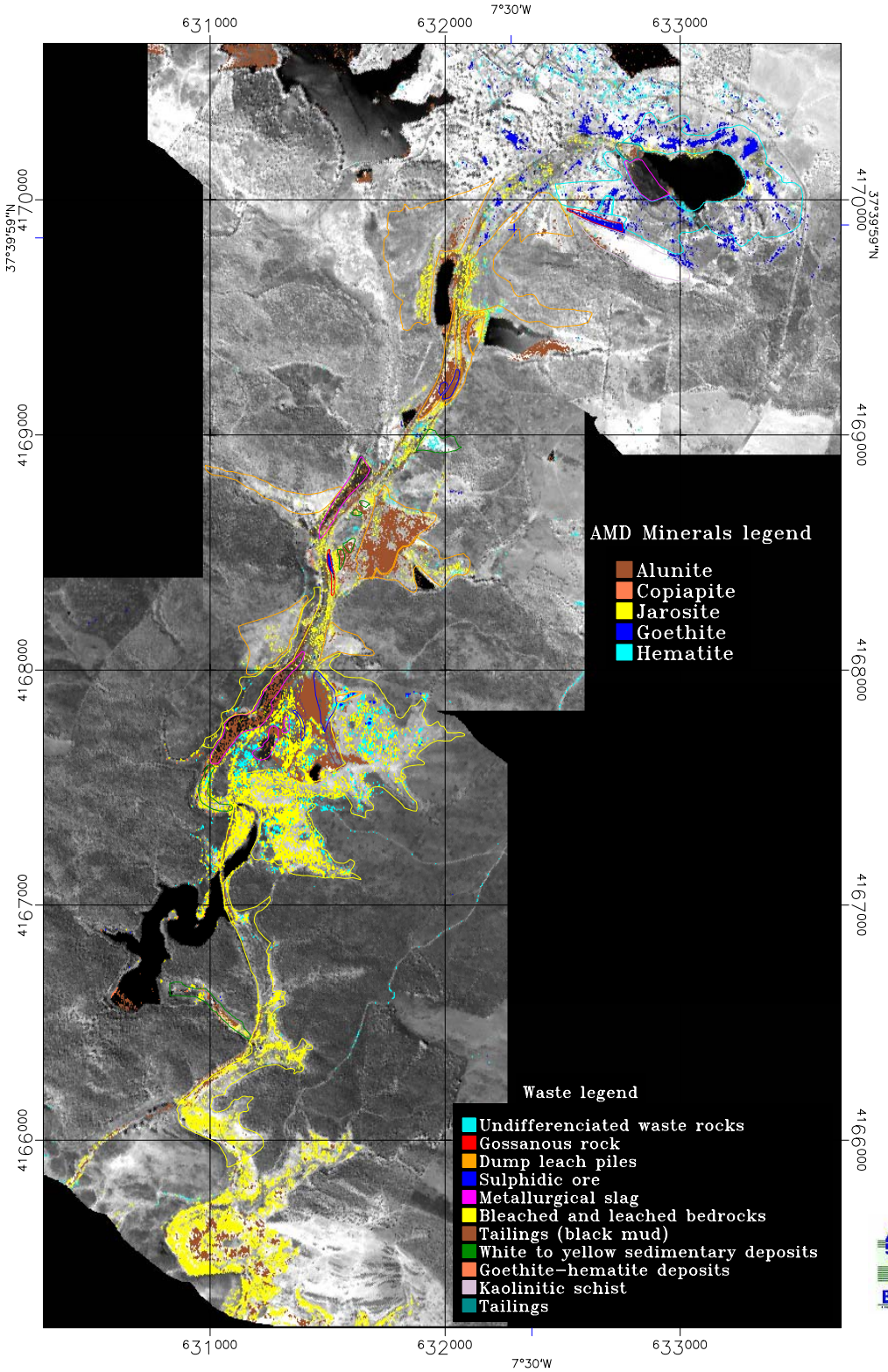

BRGM

A. Bourguignon
projection UTM, Zone 29N
Pixel Size:4.2 Meters
Datum: WGS-84
Ellipsoid: WG 84

N
W
E
S

0 1 Kilometers

Mineo Sao Domingos
AMD mineral mapping
Intersection pixels mapped with MTMF and SAM

Map produced in September 2002

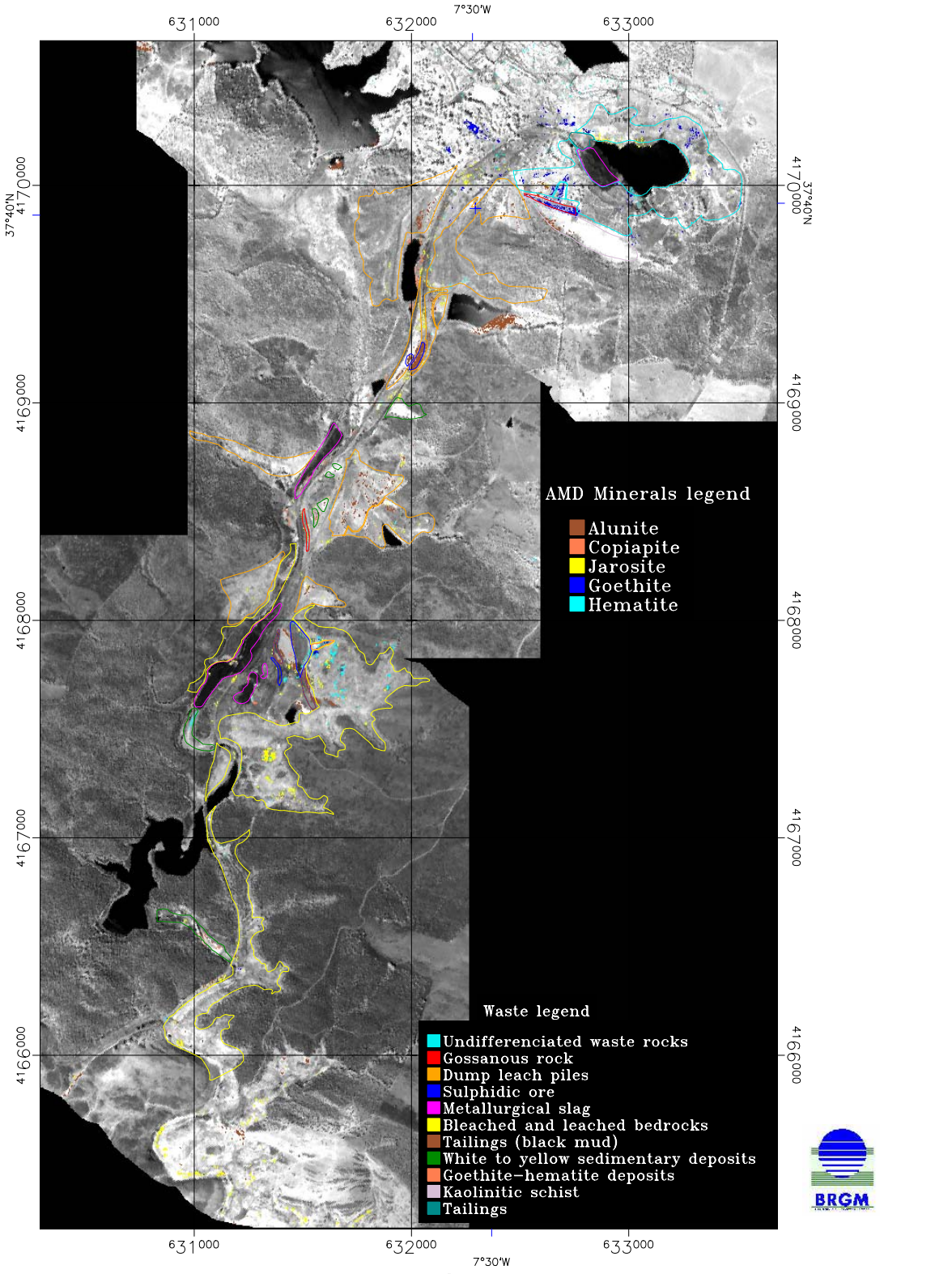

BRGM

A. Bourguignon
projection UTM, Zone 29N
Pixel Size:4.2 Meters
Datum: WGS-84
Ellipsoid: WG 84

N
W
E
S

0 1 Kilometers

MINEO S. Domingos Test Site

Indicator "Collocate Co-kriging" of pH

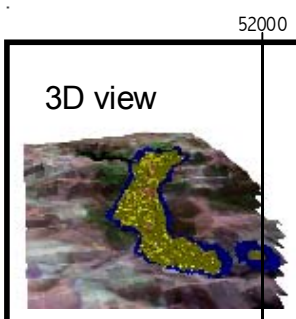

APPENDICE 8

GEOCHEMICAL MODELLING USING HYPERSPECTRAL DATA

A.8.0. Geostatistical modelling

A.8.1. Basic statistics of soil data

A.8.2. Correlation Coefficients of soil data

A.8.3. Correlation Coefficients between soil and hyperspectral data

A.8.4. Contamination maps (S. Domingos)

A.8.5. Contamination maps (Tapada)

A.8.6. Contamination maps (Achada)

A.8.7. Contamination maps (Telheiro)

A.8.0. GEOSTATISTICAL MODELLING

ABSTRACT

The aim of the geostatistical analysis task was the production of soil pollution maps based on the combination of the ground geochemical data and the hyperspectral images. To achieve this objective, a two step methodology using, respectively, multivariate data analysis on hyperspectral maps and multivariate geostatistical techniques to estimate the soil pollution variables, was developed.

The cross-validation tests show that the inclusion of the hyperspectral images in the estimation procedure only slightly improve the results. The contamination maps obtained by cokriging present more variability than the maps obtained based only on geochemical data.

A.8.0.1 INTRODUCTION

The main objective of the geostatistical task is the development of a methodology to incorporate the hyperspectral images, in order to improve the geochemical cartography based only on ground samples and the delineation of the contaminated areas.

The main assumption is that there is some correlation between ground chemical composition and the spectral signature of the hyperspectral images.

A.8.0.2 METHODOLOGY

In order to improve the estimation of the ground chemical concentrations using the spectral signatures of the hyperspectral image, a two step methodology was developed:

- Treatment of the hyperspectral images aiming at the identification of image factors with high correlations with chemical soil composition;
- Estimation and/or stochastic simulation of the soil concentrations using these high-correlated factors combined with the soil chemical data.

The first step was based on multivariate data analysis methods, namely Principal Components Analysis (PCA), Minimum Noise Fraction (MNF) and Factorial Correspondence Analysis (FCA), applied to the spectral signatures of pixels corresponding to the ground samples. Then the correlation between the image factors extracted by those analyses and the ground data were calculated.

The second step was based on multivariate geostatistical techniques. Full and co-located cokriging (Wackernagel, 2003) were tested and compared with the results of the univariate ordinary kriging using only the ground geochemical data. These techniques are based on the direct and cross spatial correlations ground data (primary variables) and image factors (secondary variables). Kriging with external drift was another geostatistical technique that could be used. However, in this case study, the assumption of linear dependency between primary and secondary variables is too strong.

The comparison between multivariate techniques and the improvement introduced by the hyperspectral images was measured by the root mean square error (RMSE) of the cross validation techniques (Goovaerts, 1997).

Indicator cokriging and stochastic co-simulation can after be used to define the contaminated areas.

A.8.0.3 MAIN RESULTS

The described methodology was used to map the geochemical contents of the soils of the 4 areas presented in the previous reports of the MINEO Southern environment test site: S. Domingos (23 soil samples), Tapada (34 soil samples), Achada (36 soil samples) and Telheiro (37 soil samples).

According to the samples spatial distribution, it was decided to divide the whole mining area into two main areas:

- Area 1 – S. Domingos sub-area
- Area 2 – includes Tapada, Achada and Telheiro sub-areas.

Due to the type of the contamination, 11 variables were selected: pH and concentrations of As, Cu Fe, Hg, Pb, S, U, Zn, Corg (organic carbon) and Fe*MJ* (free iron). In the Appendix 6.1, the basic statistics of the selected variables are presented for each sub-area. Looking for the median, S. Domingos and Tapada present the highest values of the variables related with pollution. However, some of the highest grades belong to samples located in Telheiro.

In the Appendix 8.2, the correlation coefficients between those variables are shown. As can be seen, there are high correlation values between the variables related with pollution due to mining and metallurgical activity.

In order to include hyperspectral images in the estimation of the chemical concentrations, the first step of the developed methodology was based on multivariate factorial data analysis of those images. So, Principal Component Analysis, Minimum Noise Fraction and Factorial Correspondence Analysis were applied to the spectral signatures of pixels corresponding to the ground samples. To avoid image 'noise', strong water absorption bands (1, 62 to 69, 93 to 96 and 126) were excluded from these analysis.

Due to spatial deviations between the ground samples locations and correspondent image pixels, this procedure was repeated for a neighbourhood of 11x11 pixels centred in each sample location. However, as the results were inconclusive, the values of the central pixel (the pixel 'corresponding' to the sample) were retained.

Table 8.0.1 and 8.0.2 show the factors that present the highest correlation coefficient (bold) with each variable in the two areas (more detailed results are presented in Appendix 8.3). Other relatively high correlation coefficients are also presented in the same tables. In general, the factors from PCA present the highest values of correlation coefficients with the chemical variables. However, those coefficients are not very high[1], probably due to some problems related with the hyperspectral images. Namely, the significant number of saturated pixels, the

[1] In S. Domingos area, most of the variables present a high correlation coefficient with the second principal component (PCA2). However, this principal component represents a small proportion of the total variability.

spatial calibration of the hyperspectral images and the number and clustering of the soil samples could be responsible for these relatively low coefficients.

	As	Cu	Fe	Hg	Pb	S	U	Zn	Corg	Fe*MJ*	pH
PCA1						0.41			-0.55		
PCA4				-0.49	**-0.54**						
PCA5		0.52	0.48								
PCA6								**-0.46**			-0.41
PCA9							**-0.47**		**0.61**		**0.73**
MNF1					-0.42	**-0.72**					
MNF2			**-0.64**							**0.60**	
MNF5							**0.47**				
MNF6	0.38										
AFC2						-0.42					0.52
AFC3				0.50	0.52				0.49		
AFC4	**0.53**	**0.58**	0.63							0.56	
AFC8	0.43			**0.52**					0.43	0.56	

Tables 8.0.1 – Highest (bold) correlation coefficients between soil chemical variables and hyperspectral factors (S. Domingos area).

	As	Cu	Fe	Hg	Pb	S	U	Zn	Corg	Fe*MJ*	pH
PCA1								**-0.47**			
PCA2	**-0.79**	**-0.68**	**-0.56**	**-0.53**	**-0.76**	**-0.79**			0.50	**-0.63**	**0.77**
MNF1		-0.55	**-0.57**								
MNF2	-0.73		-0.51		-0.59	-0.71	**0.54**			-0.55	0.54
AFC1	-0.61	-0.53		-0.51	-0.68	-0.64			**0.58**	-0.53	0.71
AFC2								**0.47**			

Tables 8.0.2 – Highest (bold) correlation coefficients between soil chemical variables and hyperspectral factors (Tapada, Telheiro and Achada area)

So, those factors (Table 8.0.1 and 8.0.2) were selected to improve the estimation[2] of the chemical grades in soils (second step of the methodology used). The cross validation results of multivariate techniques using those factors as secondary variables and of the (univariate) kriging results were compared using the RMSE (root mean square error) parameter.

	Kriging	Cokriging		
		AFC	ACP	MNF
As	2475.00	**2420.00**	-	2440.00
Cu	264.80	253.30	**252.00**	-
Fe	6.56	6.34	5.78	**5.70**
Hg	2.69	**2.59**	2.72	-
Pb	5392.00	**4996.00**	5396.00	5454.00
S	0.73	0.67	0.66	**0.63**
U	1.68	-	-	**1.53**
Zn	147.90	-	**147.80**	-
Corg	**25.58**	28.55	26.27	28.18
Fe*MJ*	21.61	19.97	20.34	**18.61**
PH	0.83	0.67	0.69	**0.64**

Table 8.0.3 – Lowest (bold) RMSE parameters of the cross - validation tests (S. Domingos area)

In general, to estimate chemical soils content, the geostatistical interpolation technique named cokriging using the highest (spatial) correlated factors improves the results, as presented in

[2] The geostatistical tool of the ArcMap 8.2 was used to perform the geostatistical estimation.

Table 8.0.3. In the case of Fe, S, U, Fe*MJ* and pH variables, the best results of the RMSE parameter are obtained with the MNF factors. However, the improvement introduced by the use of the hyperspectral images was not so important as we expected.

	Kriging	Cokriging		
		AFC	ACP	MNF
As	2150,00	**2106,00**	2139,00	2121,00
Cu	696,30	732,90	**696,20**	716,80
Fe	**4,67**	4,95	5,72	4,98
Hg	1007,00	**999,40**	1023,00	1026,00
Pb	3490,00	**3358,00**	3369,00	-
S	**0,91**	0,92	0,92	**0,91**
U	**1,33**	-	-	1,35
Zn	1711,00	1892,00	**1702,00**	1721,00
Corg	**14,47**	14,55	14,75	14,70
Fe*MJ*	**14,81**	15,57	-	15,73
pH	0,89	0,80	0,83	**0,79**

Table 8.0.4 – Lowest (bold) RMSE parameters of the cross - validation tests (Tapada, Telheiro and Achada area)

Table 8.0.4 shows the values of the RMSE parameter in the case of the second area. As can be seen, we obtain worst results. The improvement introduced by the hyperspectral images was not significant.

Figure 8.0.1 shows the maps of the As grades in S. Domingos obtained by kriging and cokriging using AFC4 as secondary variable. As can be seen the maps are similar. However, the map obtained by cokriging shows higher variability, introduced by the hyperspectral image.

In the Appendix 8.4 the estimated maps of S. Domingos area are presented for each chemical concentration and pH. In the Appendices 8.5, 8.6 and 8.7, the same type of maps are presented, showing the spatial interpolation of the same variables in the sub-areas Tapada, Achada and Telheiro, respectively. The cokriging maps were estimated with the image factors presenting the best RMSE.

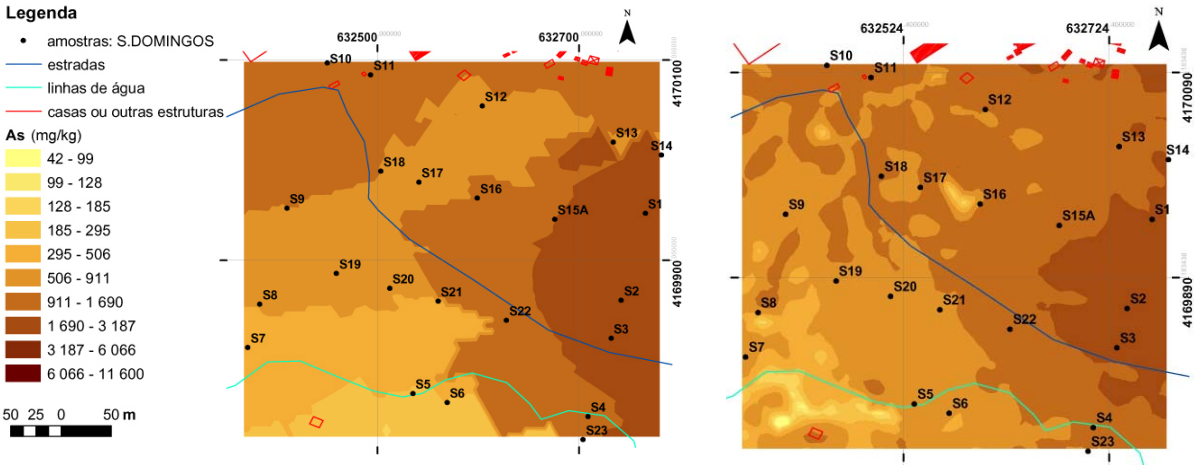

Figure 8.0.1 - As map (S. Domingos) estimated by kriging (left) and cokriging (right)

In most the cases, the cokriging maps present more variability than the kriging ones, giving a more 'realistic' picture introduced by the hyperspectral image. However, we must remember the results of the cross validation tests. Similar results were obtained in the other sub-areas, Tapada, Achada and Telheiro.

From the maps of the pollution variables, the contaminated areas can be delineated. Given the smoothing effect introduced by kriging, the cokriging maps must be used for this effect.

Alternative methods, like stochastic co-simulation and indicator cokriging, could be use used to help the delineation of the contaminated areas. However, given the improvement introduced by the image in the estimation procedure, these techniques present marginal benefits compared with the equivalent univariate ones, and don't justify their use.

A.8.0.4 CONCLUSIONS

In the MINEO Southern environment test, the improvement introduced in the estimation of the pollution-related variables and the delineation of the contaminated areas were very marginal. The cokriged maps seem more realistic, however more validation ground data and another site tests are necessary.

The aspects related with the low correlation coefficients between hyperspectral information and chemical variables mentioned before could explain this performance, which remains behind that would be expected.

A.8.0.5 REFERENCES

Goovaerts, P., 1997. *Geoestatistics for Natural Resources Evaluation*, Oxford University Press, New York.

Wackernagel, H., 2003. *Multivariate Geoestatistics*, 3rd edition, Springer-Verlag, Berlin, 259pp.

A.8.1 - BASIC STATISTICS OF SOIL DATA

	Area	n	Average	Median	Min.	Max.	Variance	Coef. variation	Skewness
As	Tapada	34	21.51	18.80	7.40	77.60	185.83	0.63	2.74
	S. Domingos	23	1141.38	504.00	41.80	11600.00	5452084.92	2.05	4.44
	Achada	36	1443.99	545.00	25.90	14200.00	9833977.76	2.17	3.61
	Telheiro	37	1727.09	277.00	28.00	15900.00	7798739.31	1.62	3.79
Cu	Tapada	34	27.29	25.31	8.94	78.44	231.83	0.56	1.60
	S. Domingos	23	295.30	214.47	25.21	1275.38	89434.18	1.01	2.23
	Achada	36	542.40	224.00	56.63	6207.33	1177053.71	2.00	4.53
	Telheiro	37	104.22	50.31	7.64	690.74	18163.79	1.29	2.93
Fe	Tapada	34	27.1	27.30	10.20	52.20	10.60	3.8	4.5
	S. Domingos	23	79.4	62.00	11.60	313.00	477.50	8.7	19
	Achada	36	74.7	52.80	18.50	397.00	553.50	10	31.6
	Telheiro	37	56.8	49.00	15.60	151.00	91.30	5.3	18.2
Hg	Tapada	34	0.57	0.50	0.50	3.00	0.18	0.75	5.83
	S. Domingos	23	2.93	3.00	0.50	11.00	7.44	0.93	1.42
	Achada	36	459.11	2.00	0.50	9300.00	3694674.26	4.19	4.18
	Telheiro	37	29.32	0.50	0.50	420.00	6599.68	2.77	3.81
Pb	Tapada	34	64.50	51.70	22.02	256.70	1882.30	0.67	2.89
	S. Domingos	23	2971.10	1597.00	149.88	24930.00	25529167.50	1.70	4.04
	Achada	36	3984.12	803.89	95.71	32170.00	58179399.50	1.91	2.88
	Telheiro	37	1000.65	156.11	47.16	7315.20	2869746.80	1.69	2.27
S	Tapada	34	100	100.00	3.30	400.00	0.00	5.7	25.6
	S. Domingos	23	970	9400.00	100.00	21000.00	5700.00	7.8	1.00
	Achada	36	1340	6500.00	100.00	79300.00	33400.00	13.7	21.8
	Telheiro	37	6200	3700.00	200.00	28100.00	5300.00	11.8	14.7
U	Tapada	34	3.75	3.90	0.25	5.80	1.47	0.32	-0.50
	S. Domingos	23	3.08	3.10	0.25	5.80	2.62	0.53	-0.57
	Achada	36	2.26	2.40	0.25	4.70	1.89	0.61	-0.29
	Telheiro	37	2.03	2.20	0.25	5.00	2.03	0.70	0.08
Zn	Tapada	34	63.09	57.15	26.93	212.26	1025.82	0.51	3.19
	S. Domingos	23	141.36	118.01	33.17	754.25	21618.51	1.04	3.52
	Achada	36	917.14	109.79	28.00	14850.00	6595675.96	2.80	4.88
	Telheiro	37	140.69	88.74	17.29	494.95	14834.27	0.87	1.90
Corg	Tapada	34	15.39	15.40	5.30	38.70	41.93	0.42	1.37
	S. Domingos	23	23.26	16.90	4.00	137.40	773.80	1.20	3.40
	Achada	36	15.34	7.30	0.00	106.20	400.75	1.30	3.02
	Telheiro	37	16.20	17.10	1.90	57.80	155.43	0.77	1.21
Fe*MJ*	Tapada	34	11.91	11.74	2.48	23.32	28.53	0.45	0.17
	S. Domingos	23	37.79	30.45	2.18	79.89	677.58	0.69	0.13
	Achada	36	28.41	21.45	7.77	99.60	393.73	0.70	2.19
	Telheiro	37	26.49	15.24	3.30	85.47	424.48	0.78	1.57
pH	Tapada	34	5.82	5.78	5.09	6.68	0.14	0.06	0.19
	S. Domingos	23	4.25	4.44	2.52	5.81	0.85	0.22	-0.09
	Achada	36	4.26	4.01	1.62	7.78	1.24	0.26	0.69
	Telheiro	37	4.65	4.50	2.66	7.40	1.81	0.29	0.17

A.8.2 - CORRELATION COEFFICIENTS OF SOIL DATA

	As	Cu	Fe	Hg	Pb	S	U	Zn	Corg	Fe*MJ*	pH
As	1.000	0.142	0.823	0.751	0.966	0.015	-0.456	-0.039	-0.055	0.377	-0.129
Cu	0.142	1.000	0.505	0.404	0.099	0.421	-0.536	0.679	0.670	0.504	-0.104
Fe	0.823	0.505	1.000	0.797	0.759	0.229	-0.484	0.222	0.184	0.756	-0.074
Hg	0.751	0.404	0.797	1.000	0.782	0.372	-0.458	0.018	0.350	0.610	-0.185
Pb	0.966	0.099	0.759	0.782	1.000	0.086	-0.429	-0.136	-0.028	0.312	-0.245
S	0.015	0.421	0.229	0.372	0.086	1.000	-0.225	0.119	0.209	0.383	-0.720
U	-0.456	-0.536	-0.484	-0.458	-0.429	-0.225	1.000	-0.275	-0.347	-0.180	0.240
Zn	-0.039	0.679	0.222	0.018	-0.136	0.119	-0.275	1.000	0.131	0.227	0.134
Corg	-0.055	0.670	0.184	0.350	-0.028	0.209	-0.347	0.131	1.000	0.225	0.041
Fe*MJ*	0.377	0.504	0.756	0.610	0.312	0.383	-0.180	0.227	0.225	1.000	-0.023
pH	-0.129	-0.104	-0.074	-0.185	-0.245	-0.720	0.240	0.134	0.041	-0.023	1.000

Table A.8.2.1 - Correlation coefficients (S. Domingos area)

	As	Cu	Fe	Hg	Pb	S	U	Zn	Corg	FeMJ	pH
As	1.000	0.008	0.030	0.602	0.649	0.584	-0.436	0.119	-0.075	0.209	-0.578
Cu	0.008	1.000	0.737	0.006	0.193	0.314	-0.128	0.554	-0.071	0.134	-0.066
Fe	0.030	0.737	1.000	-0.070	0.115	0.384	-0.279	0.759	-0.131	0.463	-0.200
Hg	0.602	0.006	-0.070	1.000	0.923	0.758	-0.191	0.234	0.189	-0.058	-0.313
Pb	0.649	0.193	0.115	0.923	1.000	0.892	-0.426	0.429	0.016	0.392	-0.652
S	0.584	0.314	0.384	0.758	0.892	1.000	-0.566	0.423	-0.288	0.700	-0.685
U	-0.436	-0.128	-0.279	-0.191	-0.342	-0.426	1.000	-0.105	0.095	-0.476	0.466
Zn	0.119	0.554	0.759	0.234	0.297	0.429	-0.105	1.000	-0.011	-0.033	-0.023
Corg	-0.075	-0.071	-0.131	0.189	0.118	0.016	0.095	-0.011	1.000	-0.158	0.370
FeMJ	0.209	0.134	0.463	-0.058	0.111	0.392	-0.476	-0.033	-0.158	1.000	-0.573
pH	-0.578	-0.066	-0.200	-0.313	-0.494	-0.652	0.466	-0.023	0.370	-0.573	1.000

Table A.8.2.2 - Correlation coefficients (Tapada, Telheiro and Achada areas)

A.8.3 - CORRELATION BETWEEN SOIL VARIABLES AND IMAGE FACTORS

	As	Cu	Fe	Hg	Pb	S	U	Zn	Corg	Fe*MJ*	pH
PCA1	-0.11	-0.24	-0.06	0.00	0.01	0.41	0.30	-0.16	**-0.55**	0.06	-0.36
PCA2	-0.17	-0.29	-0.45	-0.11	-0.14	0.15	0.04	-0.32	-0.13	-0.41	-0.14
PCA3	-0.20	0.10	0.16	-0.08	-0.36	-0.34	0.32	-0.18	0.51	0.19	0.47
PCA4	-0.36	-0.13	-0.20	-0.49	**-0.54**	-0.10	0.34	0.30	-0.12	-0.06	0.35
PCA5	0.39	0.52	0.48	0.16	0.13	0.34	-0.32	0.16	-0.01	0.34	-0.39
PCA6	0.05	0.14	0.21	0.30	0.31	0.28	-0.14	**-0.46**	0.02	0.26	-0.41
PCA7	-0.38	-0.12	-0.26	-0.50	-0.22	-0.11	-0.18	0.11	-0.37	-0.54	-0.11
PCA8	0.15	0.02	0.12	0.26	0.09	0.00	-0.09	0.18	0.15	0.11	0.20
PCA9	0.10	0.42	0.14	-0.01	-0.05	-0.05	**-0.47**	0.20	0.20	-0.11	0.02

Table A.8.3.1 - Correlation coefficients between soil chemical variables and PCA factors (S. Domingos area)

	As	Cu	Fe	Hg	Pb	S	U	Zn	Corg	Fe*MJ*	pH
PCA1	-0.11	-0.26	-0.39	0.07	-0.09	-0.17	0.11	**-0.47**	-0.24	-0.06	-0.09
PCA2	**-0.79**	**-0.68**	**-0.56**	**-0.53**	**-0.76**	**-0.79**	0.39	-0.18	**0.50**	**-0.63**	**0.77**

Tables A.8.3.2 - Correlation coefficients between soil chemical variables and ACP factors (Tapada, Telheiro and Achada areas)

	As	Cu	Fe	Hg	Pb	S	U	Zn	Corg	Fe*MJ*	pH
MNF1	-0.35	-0.08	-0.17	-0.26	-0.42	**-0.72**	0.17	-0.02	**0.61**	-0.19	**0.73**
MNF2	-0.20	-0.41	**-0.64**	-0.29	-0.07	0.16	-0.17	-0.04	-0.58	**-0.60**	-0.35
MNF3	0.03	-0.11	-0.11	0.09	0.32	0.25	-0.32	-0.05	-0.24	-0.18	-0.46
MNF4	-0.02	0.08	0.09	-0.01	-0.24	-0.31	0.26	0.19	0.53	0.21	0.62
MNF5	-0.36	-0.26	-0.17	-0.29	-0.22	0.16	**0.47**	0.21	-0.44	-0.09	-0.05
MNF6	0.38	0.21	0.25	0.22	0.19	-0.04	-0.35	0.38	0.01	0.30	0.05

Table A.8.3.3 - Correlation coefficients between soil chemical variables and MNF factors (S. Domingos area)

	As	Cu	Fe	Hg	Pb	S	U	Zn	Corg	Fe*MJ*	pH
MNF1	-0.51	-0.55	-0.57	-0.25	-0.49	-0.57	0.34	-0.46	0.11	-0.39	0.40
MNF2	-0.73	-0.48	-0.51	-0.49	-0.59	-0.71	**0.54**	-0.29	0.31	-0.55	0.54
MNF3	-0.74	-0.40	-0.55	-0.44	-0.55	-0.66	0.46	-0.39	0.16	-0.51	0.58
MNF4	0.60	0.43	0.21	0.48	0.64	0.56	-0.23	0.02	-0.46	0.47	-0.75

Table A.8.3.4 - Correlation coefficients between soil chemical variables and MNF factors (Tapada, Telheiro and Achada areas)

	As	Cu	Fe	Hg	Pb	S	U	Zn	Corg	Fe*MJ*	pH
AFC1	-0.14	-0.06	-0.28	-0.13	-0.23	-0.29	-0.05	-0.12	0.44	-0.24	0.32
AFC2	-0.14	0.17	0.27	-0.05	-0.29	-0.42	0.26	-0.03	0.49	0.32	**0.52**
AFC3	-0.38	-0.25	-0.33	-0.50	-0.52	-0.15	0.34	0.20	-0.20	-0.12	0.33
AFC4	**0.53**	**0.58**	0.63	0.35	0.23	0.40	-0.23	0.03	0.11	**0.56**	-0.32
AFC5	0.40	0.17	0.24	0.23	0.04	0.05	0.04	0.22	0.17	0.25	0.11
AFC6	0.31	0.44	0.37	0.08	0.15	0.29	-0.30	0.08	-0.10	0.20	-0.45
AFC7	0.22	0.33	0.29	-0.06	-0.02	0.16	-0.18	0.27	-0.13	0.14	-0.28
AFC8	0.43	0.18	0.29	**0.52**	0.21	0.08	0.04	-0.06	0.43	**0.56**	0.17

Table A.8.3.5 - Correlation coefficients between soil chemical variables and FCA factors (S. Domingos area)

	As	Cu	Fe	Hg	Pb	S	U	Zn	Corg	Fe*MJ*	pH
AFC1	-0.61	-0.53	-0.39	-0.51	-0.68	-0.64	0.29	-0.02	**0.58**	-0.53	0.71
AFC2	0.38	0.41	0.45	0.15	0.32	0.48	-0.33	**0.47**	0.13	0.26	-0.06

Tables A.8.3.6 - Correlation coefficients between soil chemical variables and FCA factors (Tapada, Telheiro and Achada areas)

A.8.4 - ESTIMATED MAPS IN S. DOMINGOS AREA

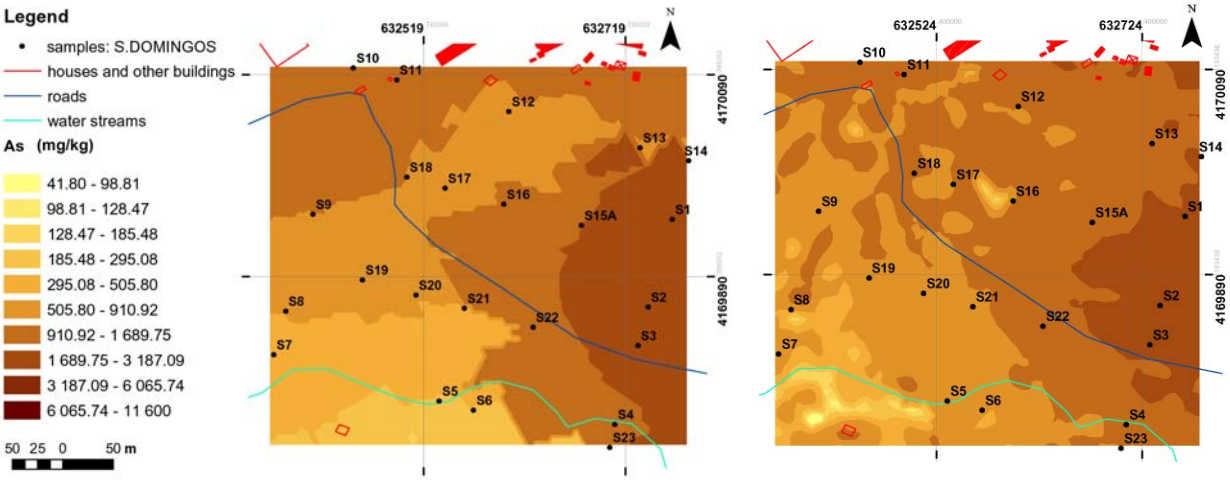

Figure A.8.4.1 - As map (S. Domingos) estimated by kriging (left) and cokriging (right)

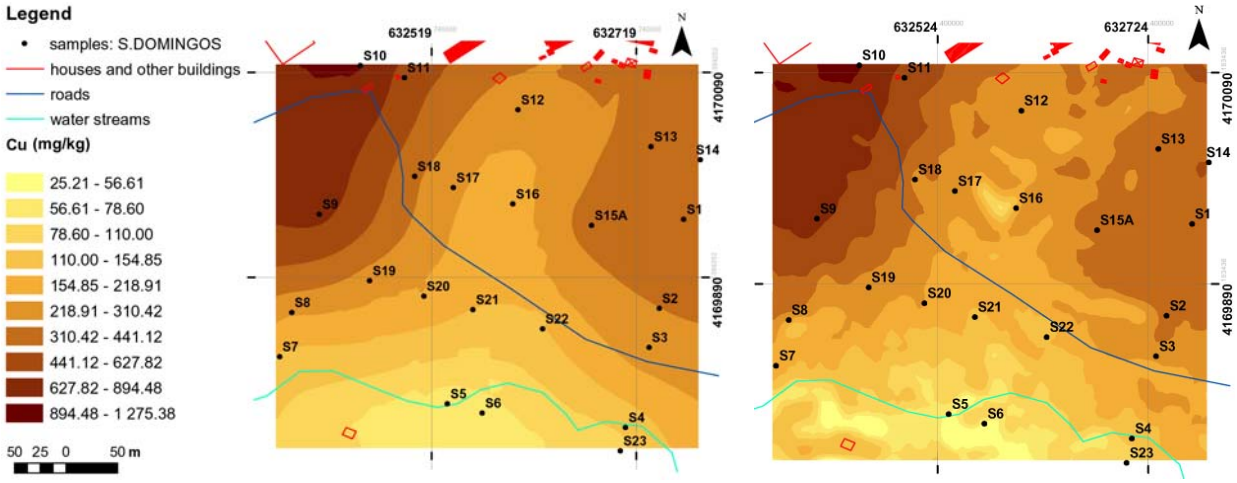

Figure A.8.4.2 - Cu map (S. Domingos) estimated by kriging (left) and cokriging (right)

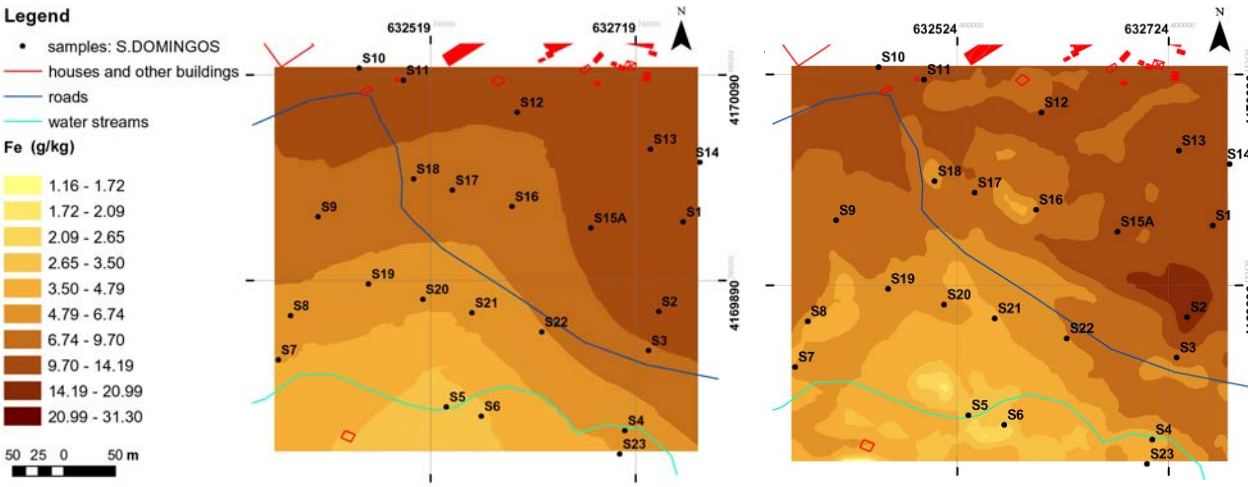

Figura A.8.4.3 - Cartografia do Fe em S. Domingos por krigagem normal (esq.) e por cokrigagem (dir.)

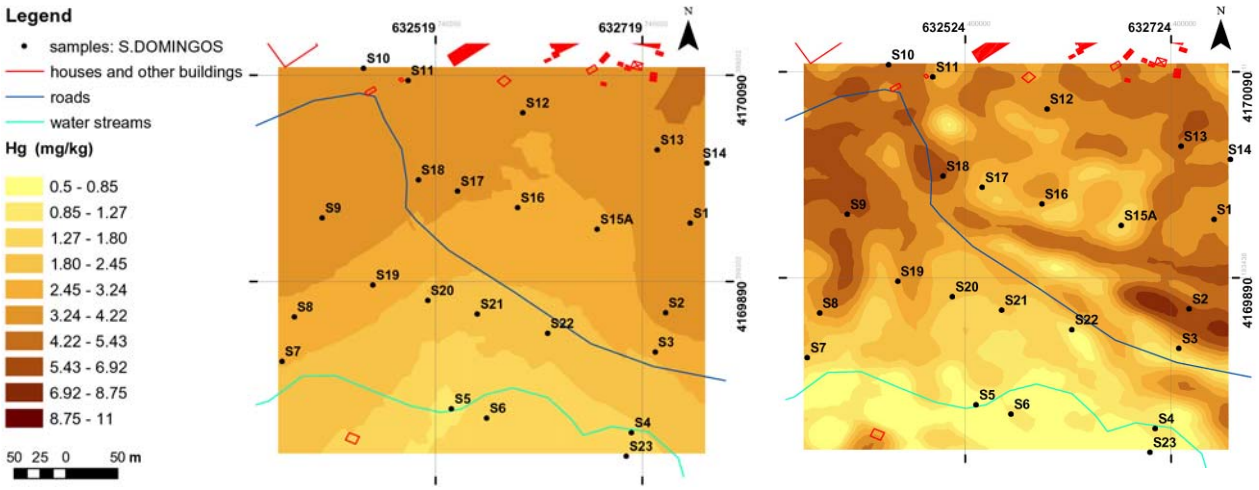

Figure A.8.4.4 - Hg map (S. Domingos) estimated by kriging (left) and cokriging (right)

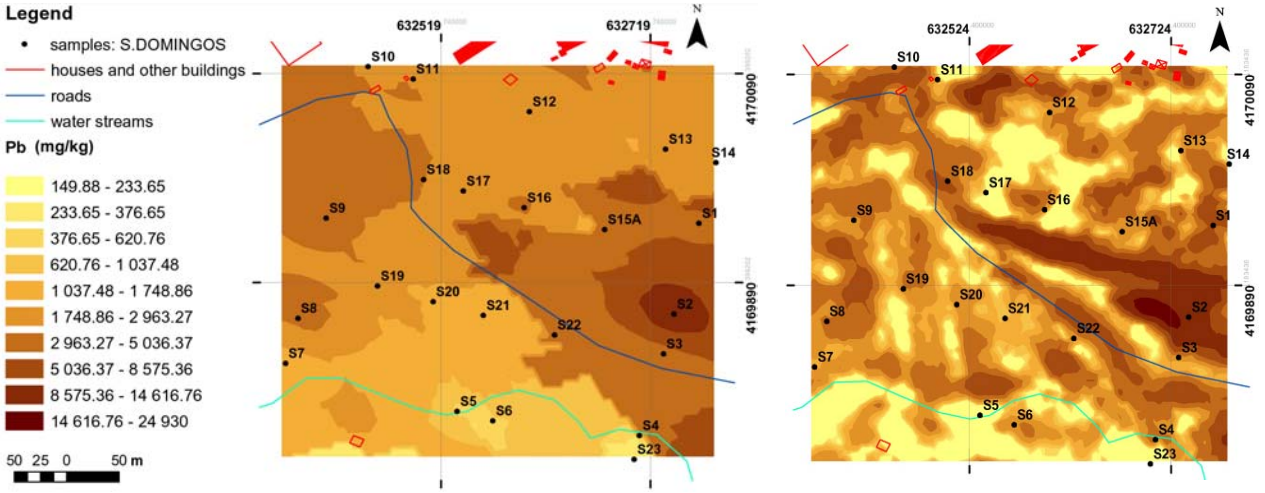

Figure A.8.4.5 - Pb map (S. Domingos) estimated by kriging (left) and cokriging (right)

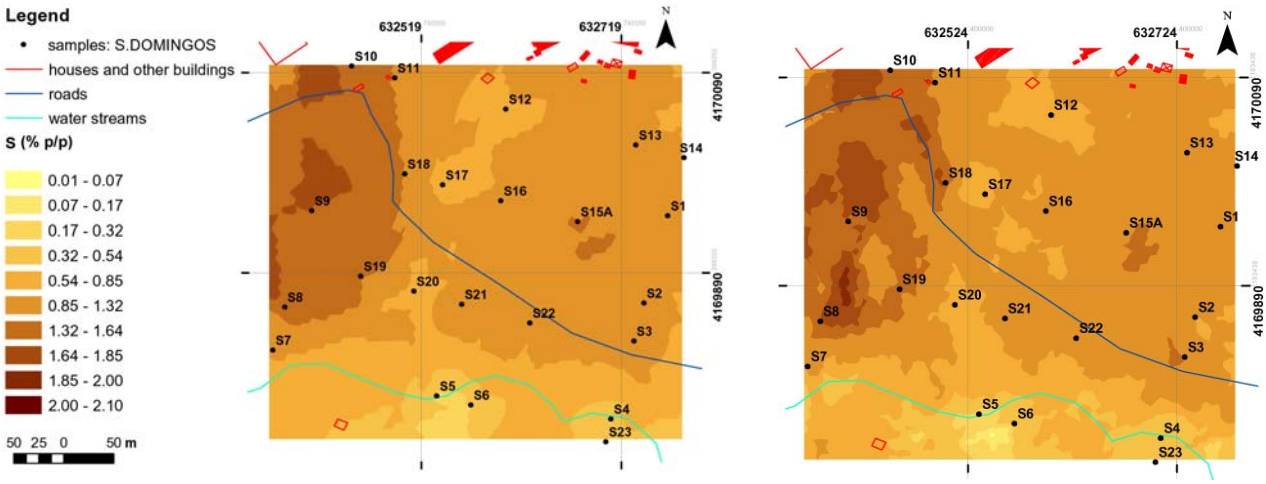

Figure A.8.4.6 - S map (S. Domingos) estimated by kriging (left) and cokriging (right)

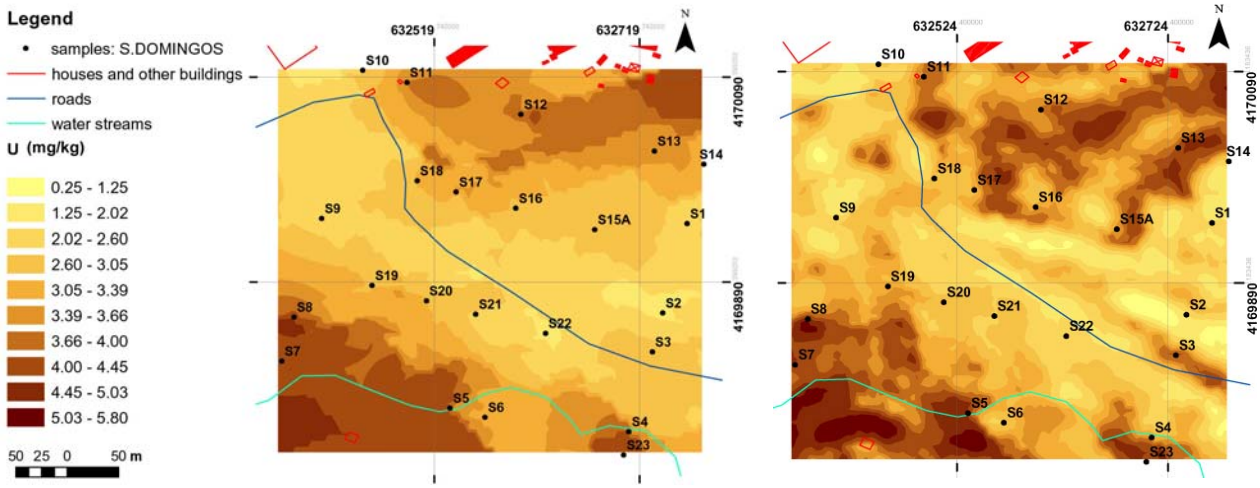

Figura A.8.4.7 – U map (S. Domingos) estimated by kriging (left) and cokriging (right)

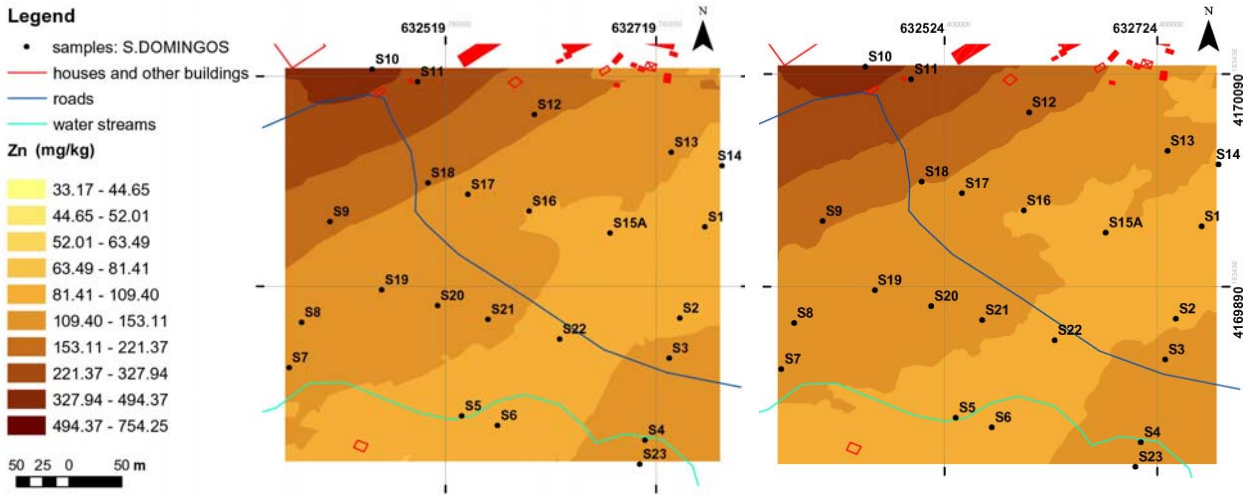

Figure A.8.4.8 - Zn map (S. Domingos) estimated by kriging (left) and cokriging (right)

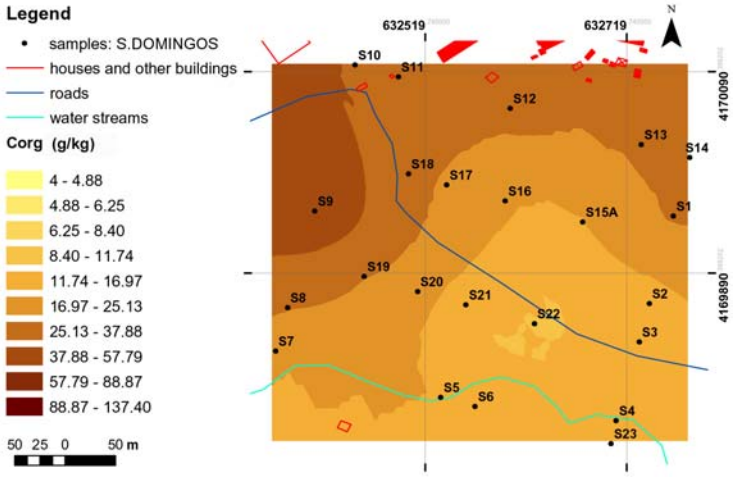

Figure A.8.4.9 – Corg map (S. Domingos) estimated by kriging (left) and cokriging (right)

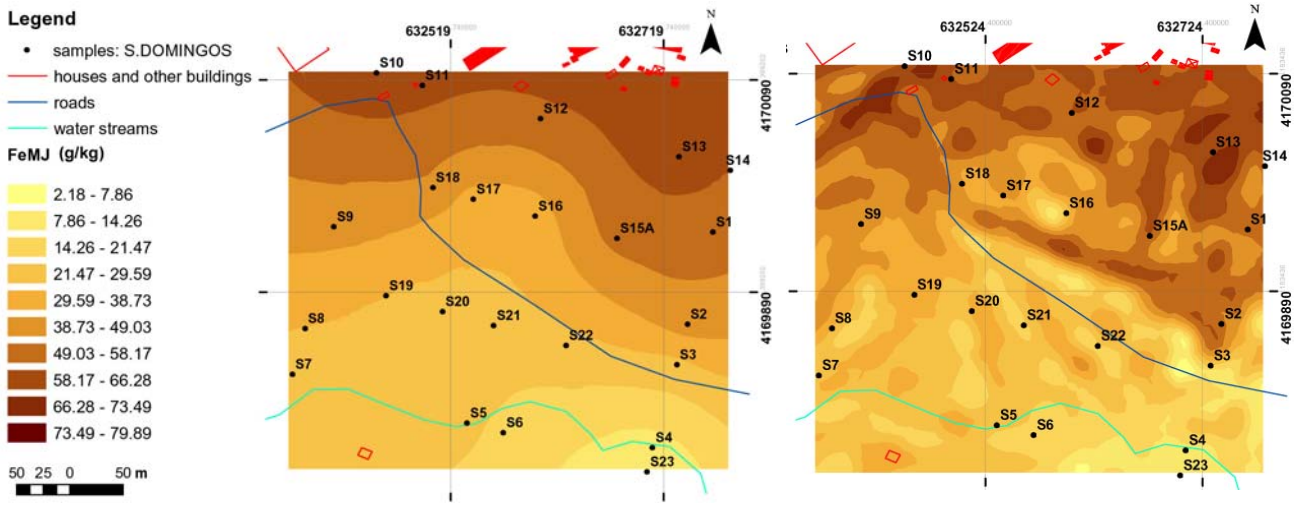

Figura A.8.4.10 - Fe*MJ* map (S. Domingos) estimated by kriging (left) and cokriging (right)

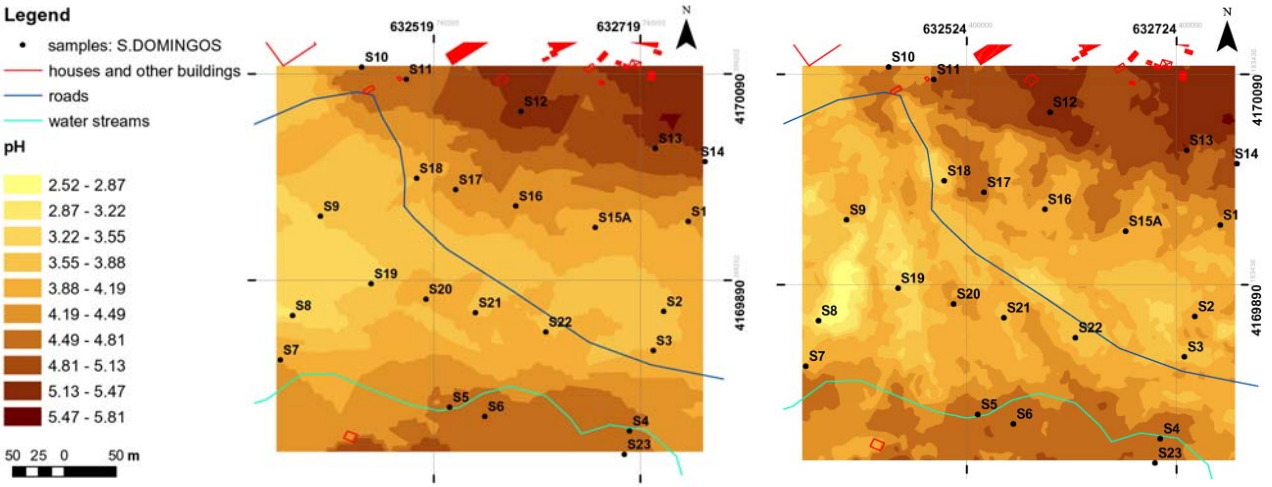

Figura A.8.4.11 – pH map (S. Domingos) estimated by kriging (left) and cokriging (right)

A.8.5 - ESTIMATED MAPS IN TAPADA SUB-AREA

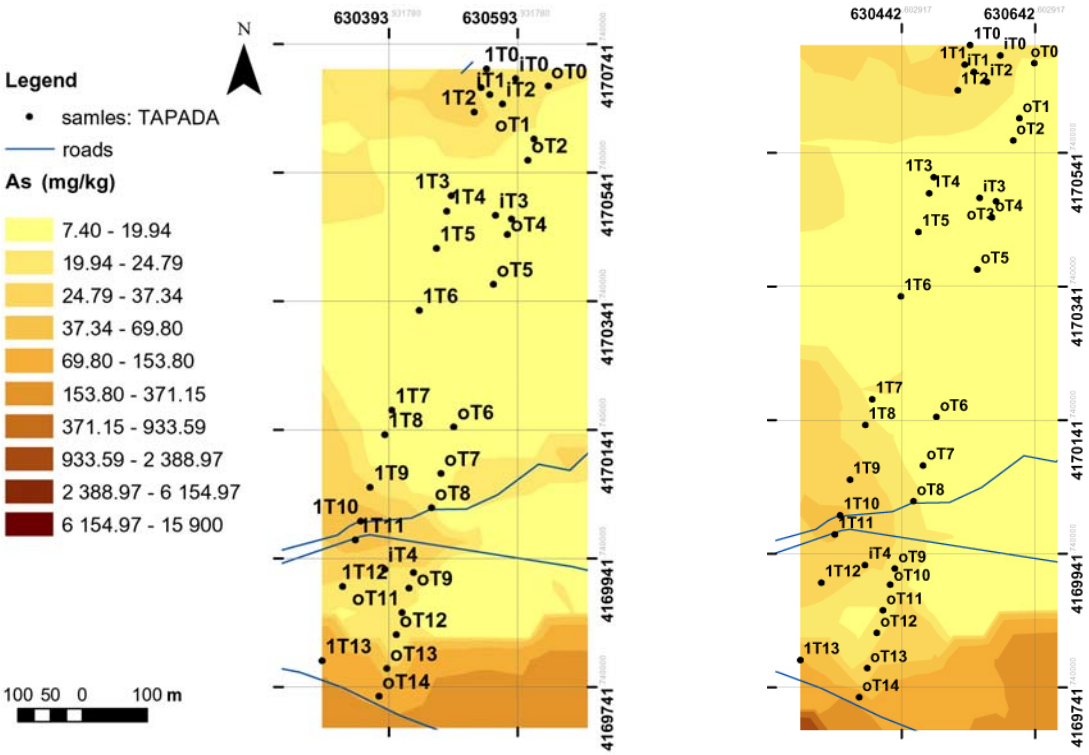

Figure A.8.5.1 - As map (Tapada) estimated by kriging (left) and cokriging (right)

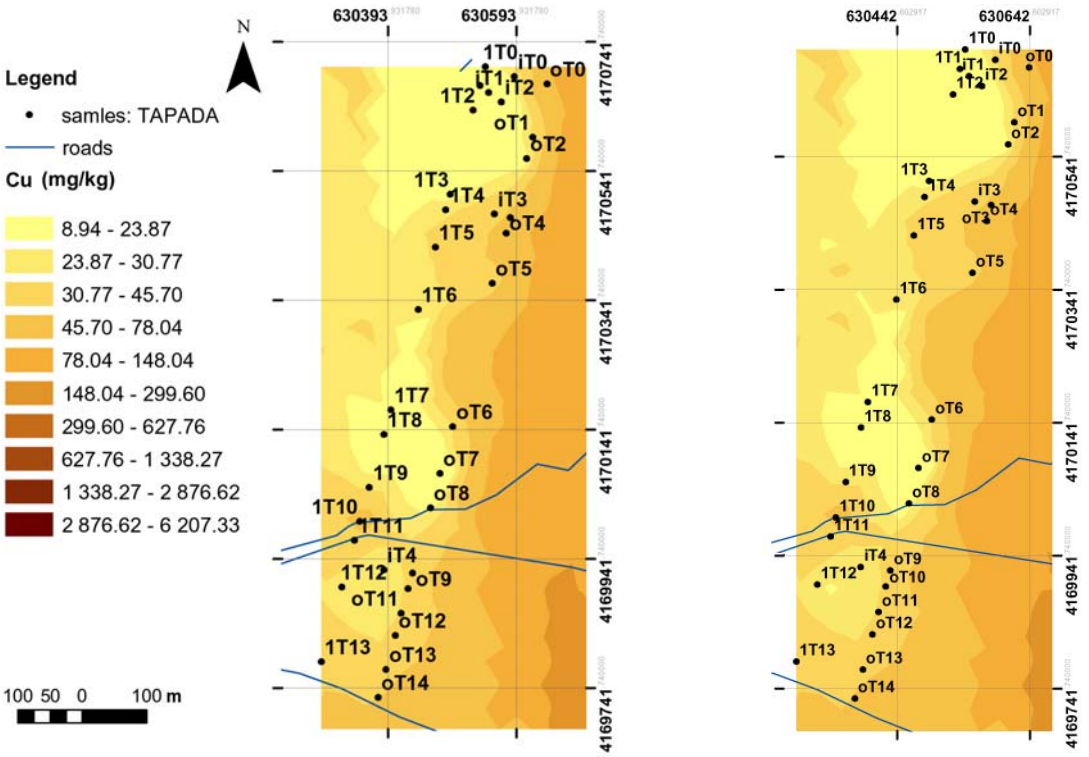

Figure A.8.5.2 - Cu map (Tapada) estimated by kriging (left) and cokriging (right)

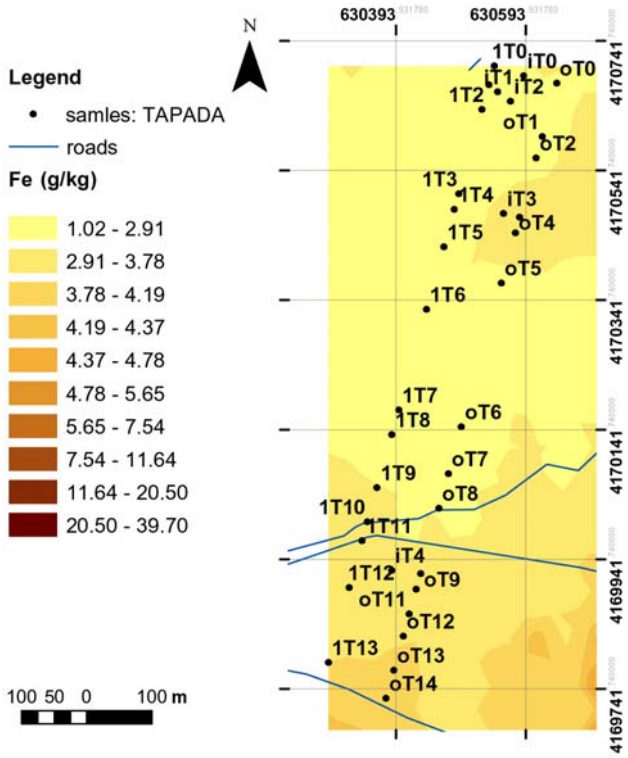

Figure A.8.5.3 - Fe map (Tapada) estimated by kriging

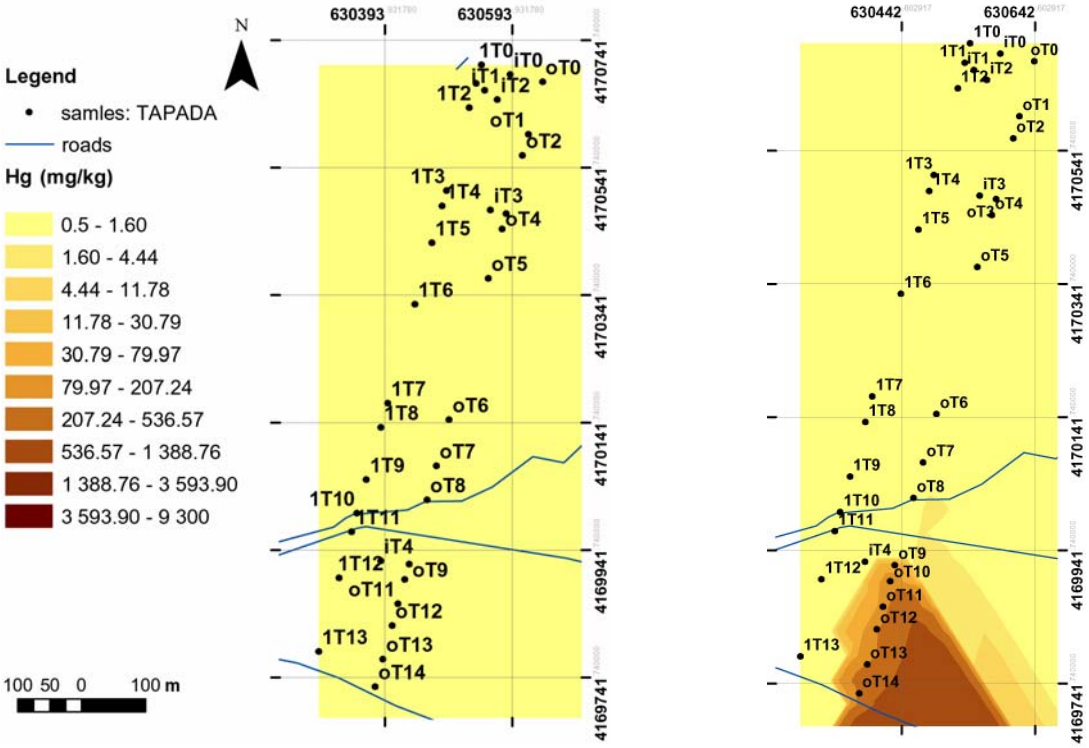

Figure A.8.5.4 - Hg map (Tapada) estimated by kriging (left) and cokriging (right)

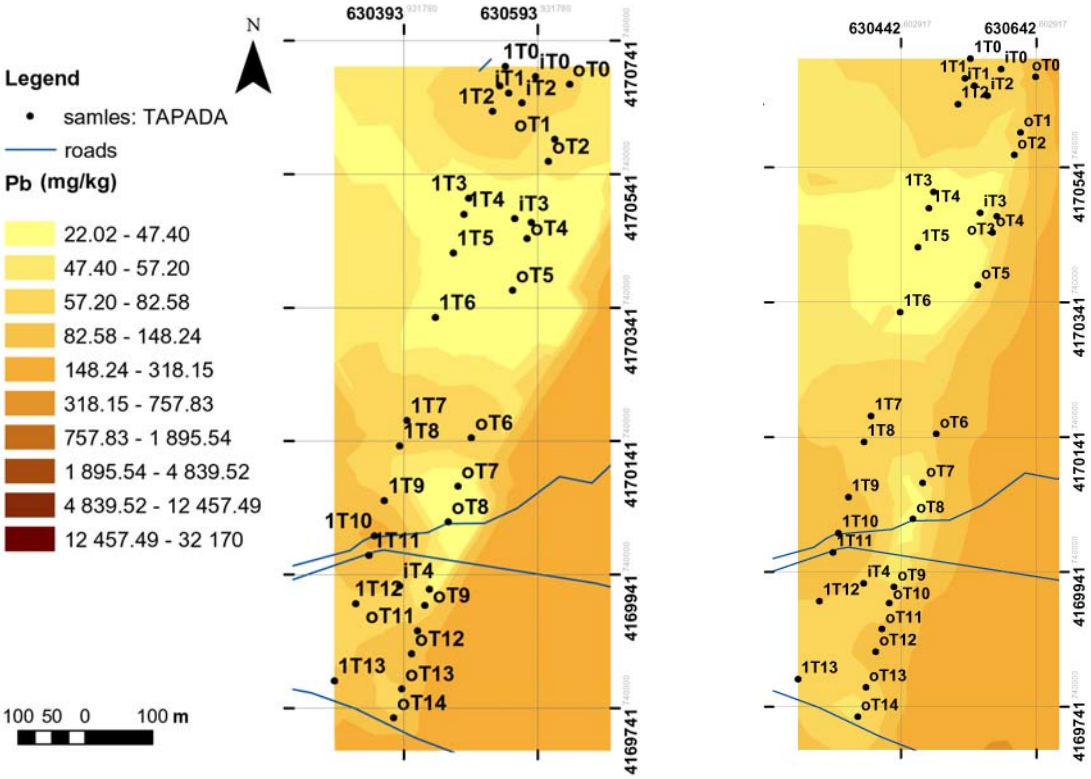

Figure A.8.5.5 - Pb map (Tapada) estimated by kriging (left) and cokriging (right)

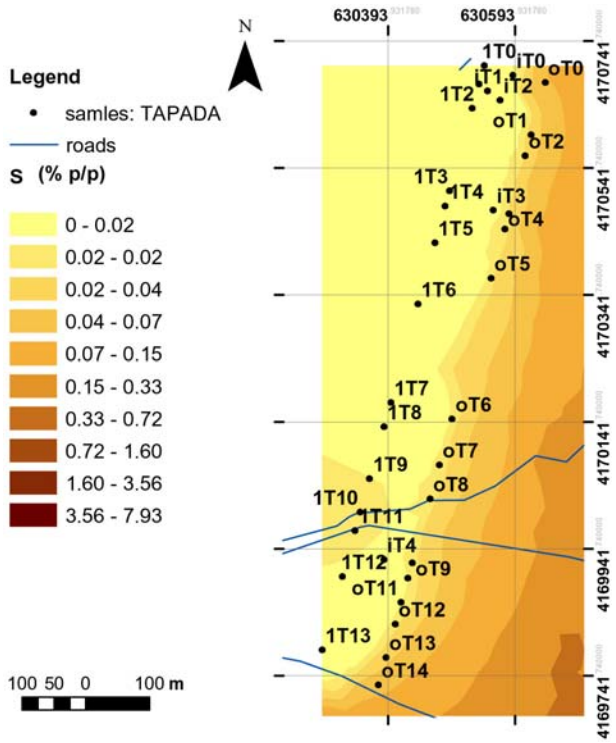

Figure A.8.5.6 - S map (Tapada) estimated by kriging

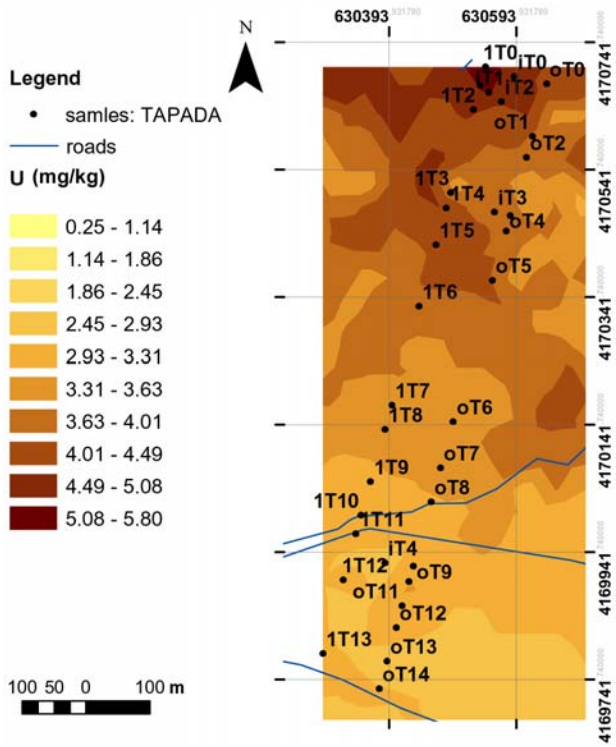

Figure A.8.5.7 - U map (Tapada) estimated by kriging

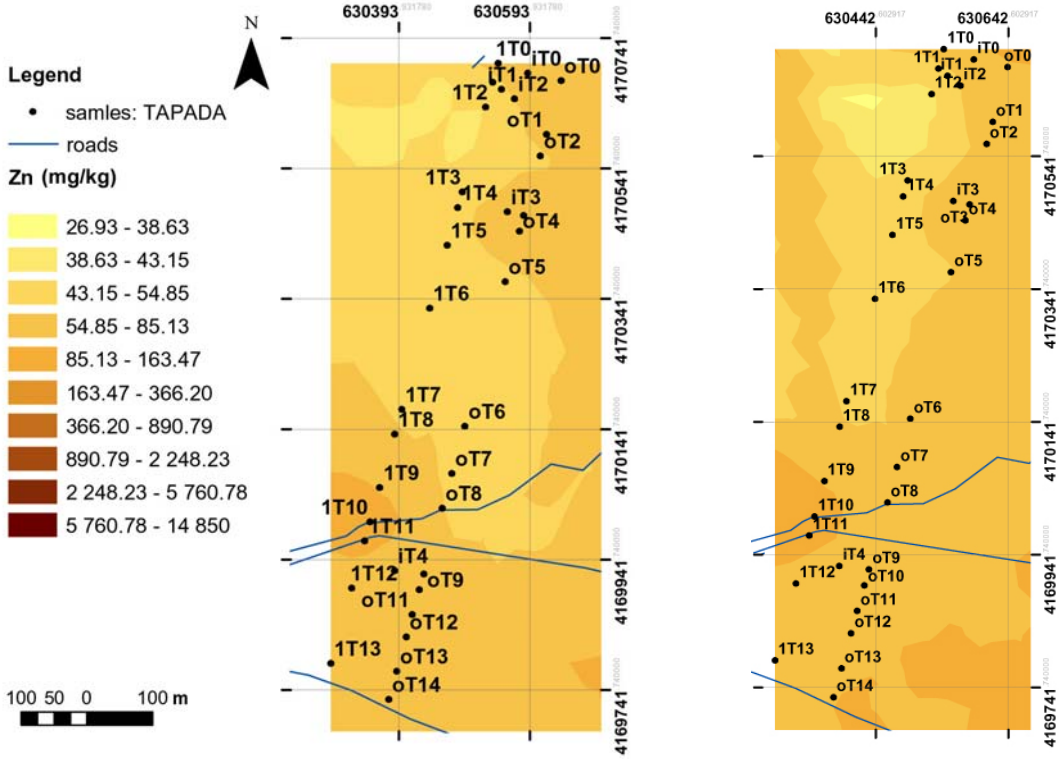

Figure A.8.5.8 - Zn map (Tapada) estimated by kriging (left) and cokriging (right)

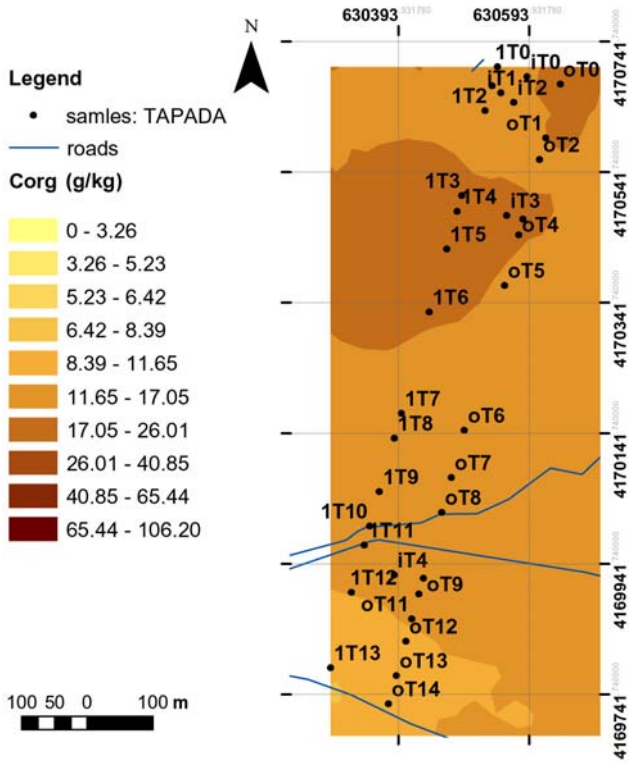

Figure A.8.5.9 - Corg map (Tapada) estimated by kriging

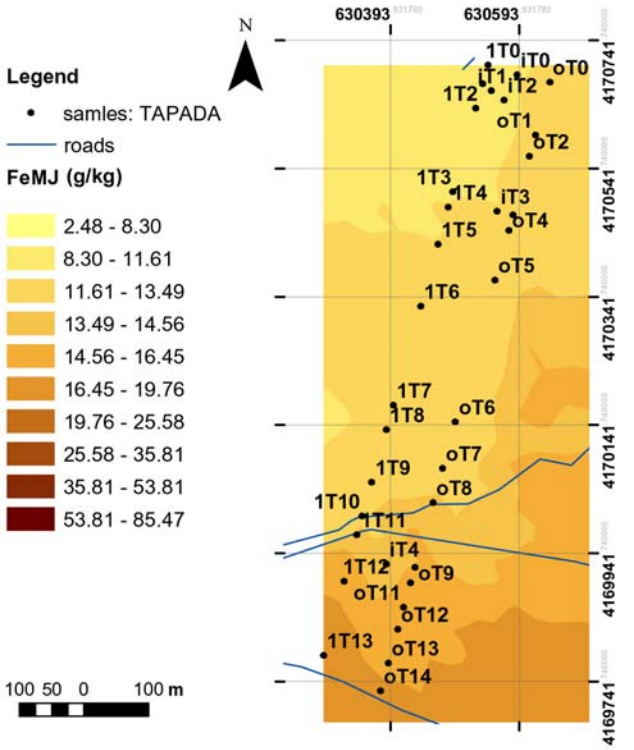

Figure A.8.5.10 - Fe*MJ* map (Tapada) estimated by kriging

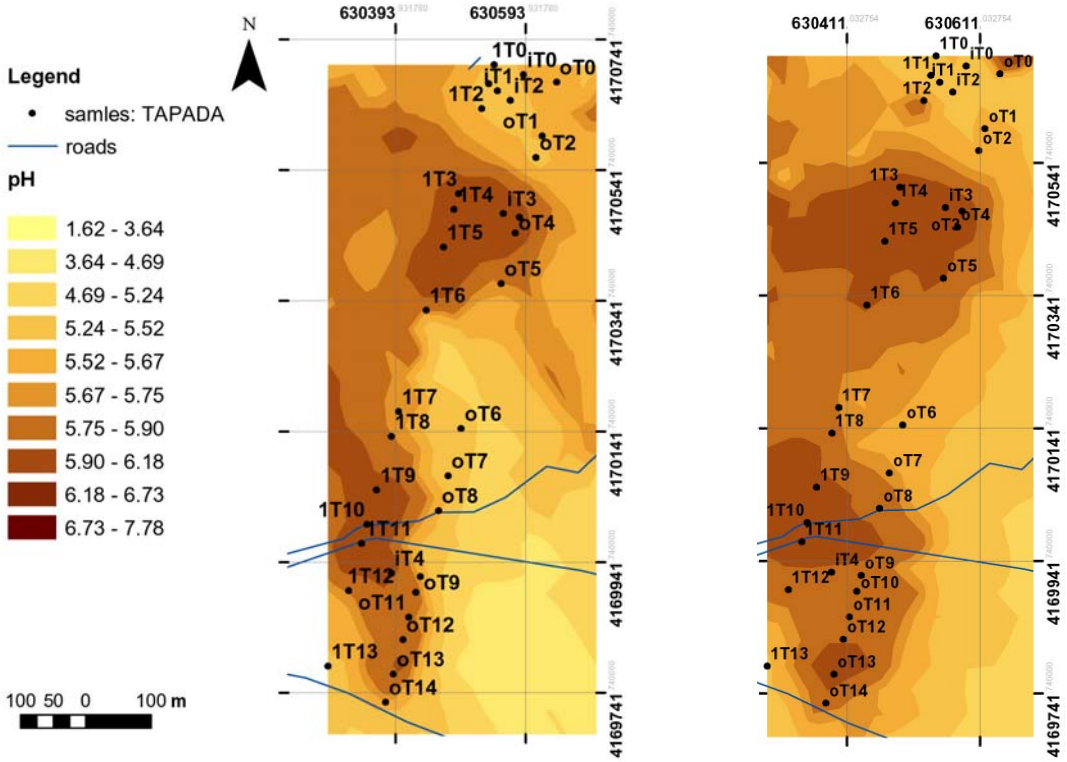

Figure A.8.5.11 - pH map (Tapada) estimated by kriging (left) and cokriging (right)

A.8.6 - ESTIMATED MAPS IN ACHADA SUB-AREA

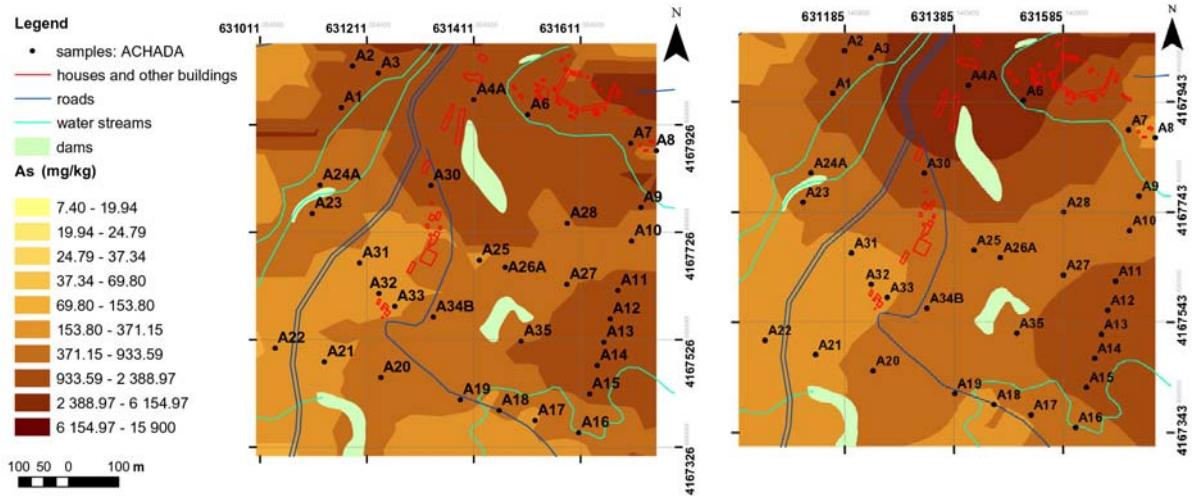

Figure A.8.6.1 - As map (Achada) estimated by kriging (left) and cokriging (right)

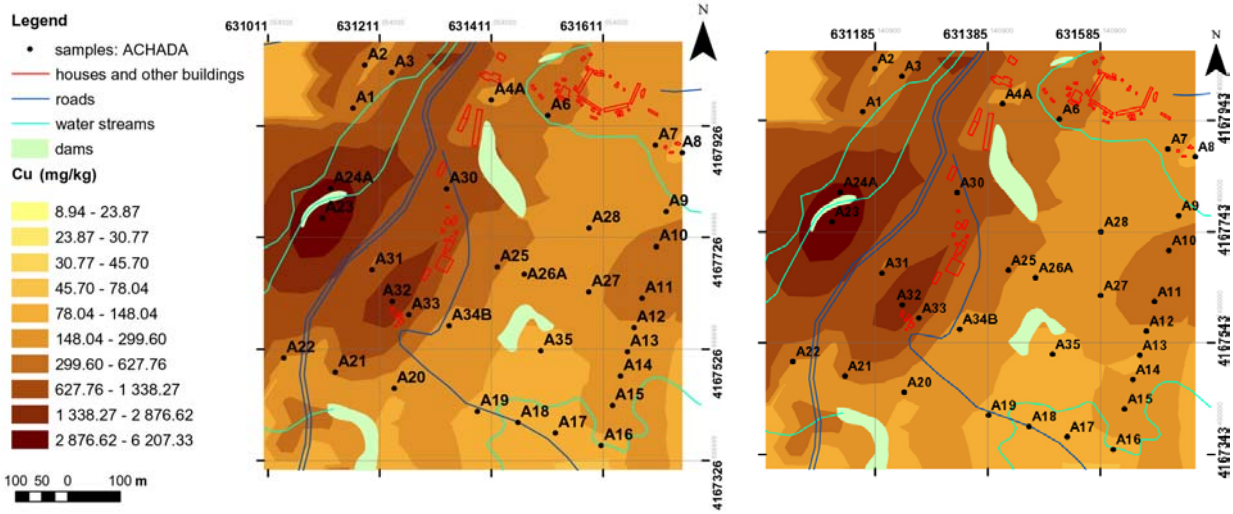

Figure A.8.6.2 - Cu map (Achada) estimated by kriging (left) and cokriging (right)

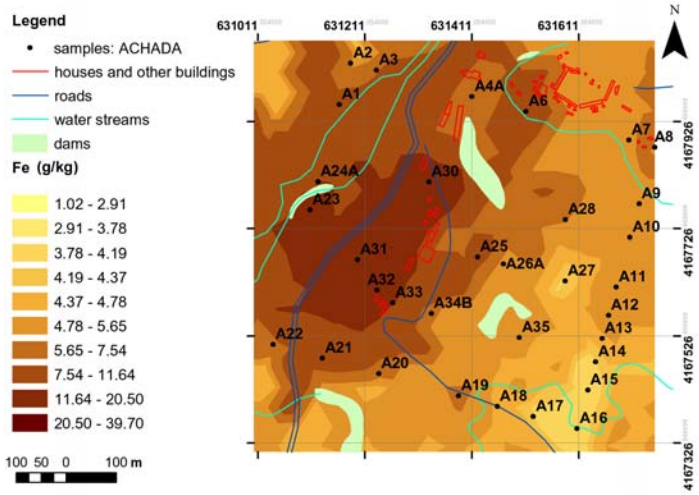

Figure A.8.6.3 - Fe map (Achada) estimated by kriging

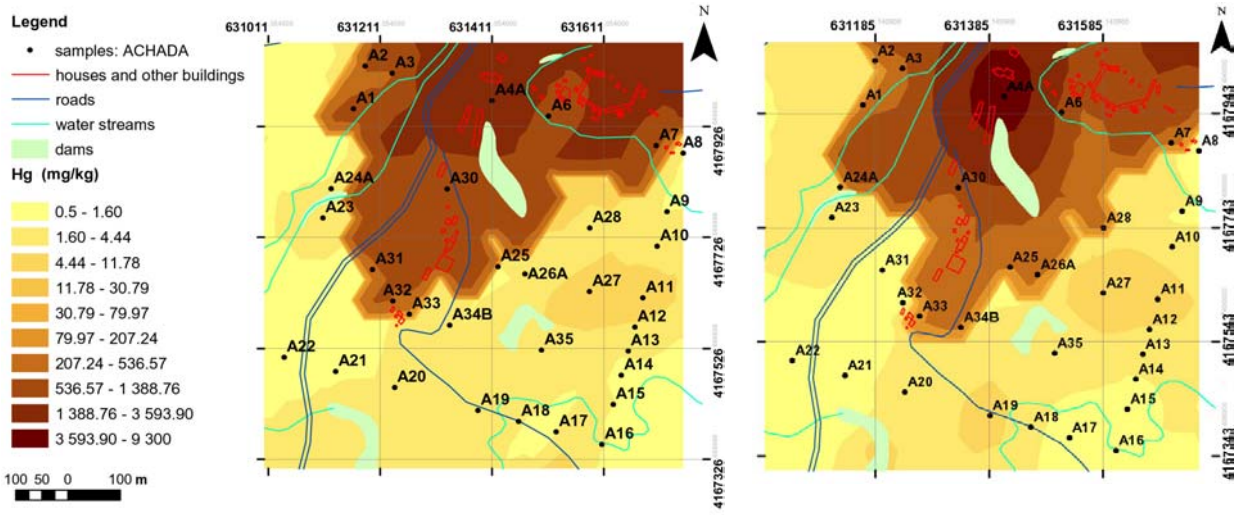

Figure A.8.6.4 - Hg map (Achada) estimated by kriging (left) and cokriging (right)

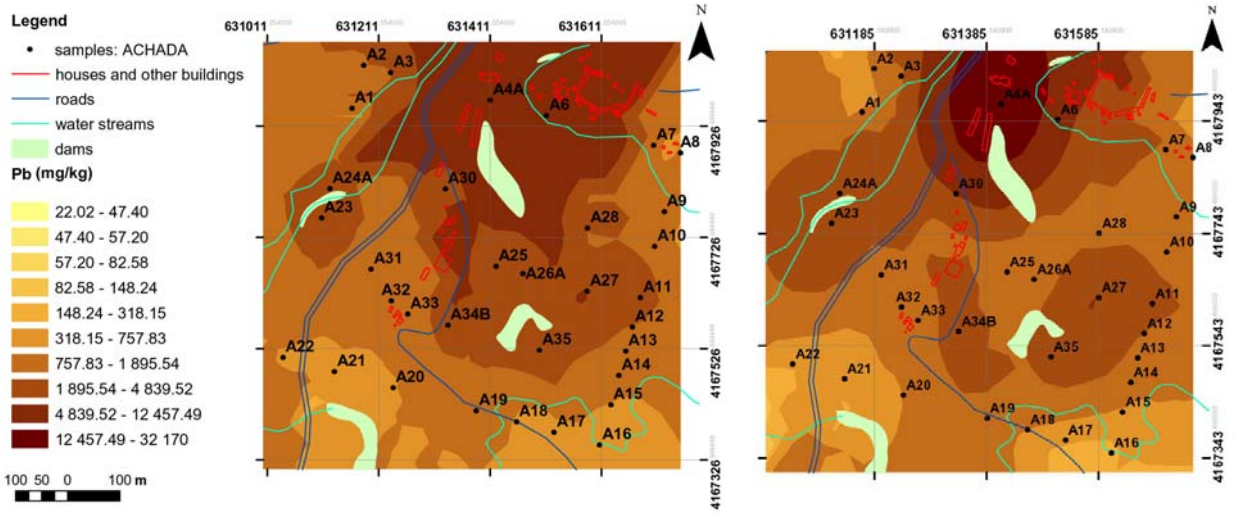

Figure A.8.6.5 - Pb map (Achada) estimated by kriging (left) and cokriging (right)

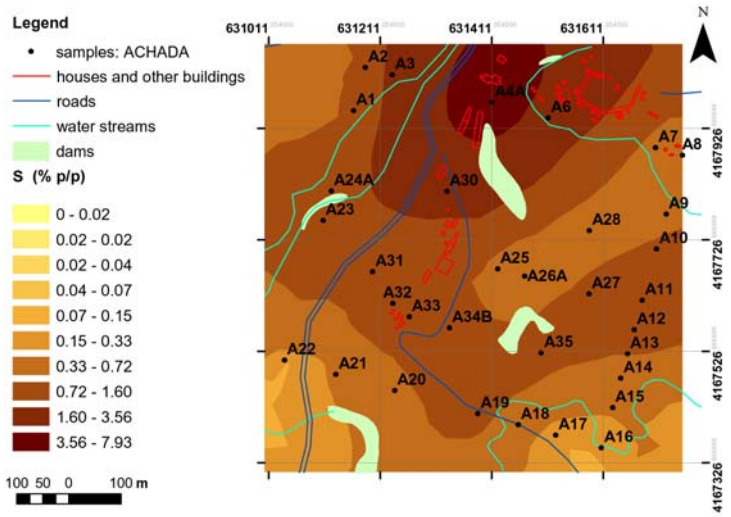

Figure A.8.6.6 - S map (Achada) estimated by kriging

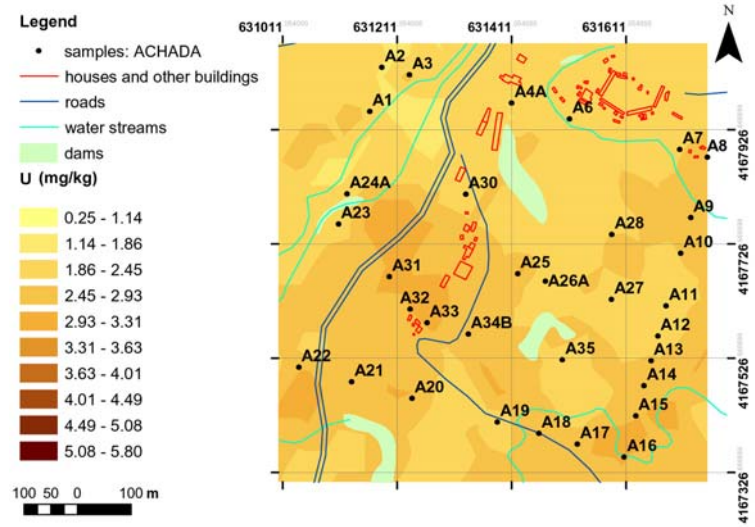

Figure A.8.6.7 - U map (Achada) estimated by kriging

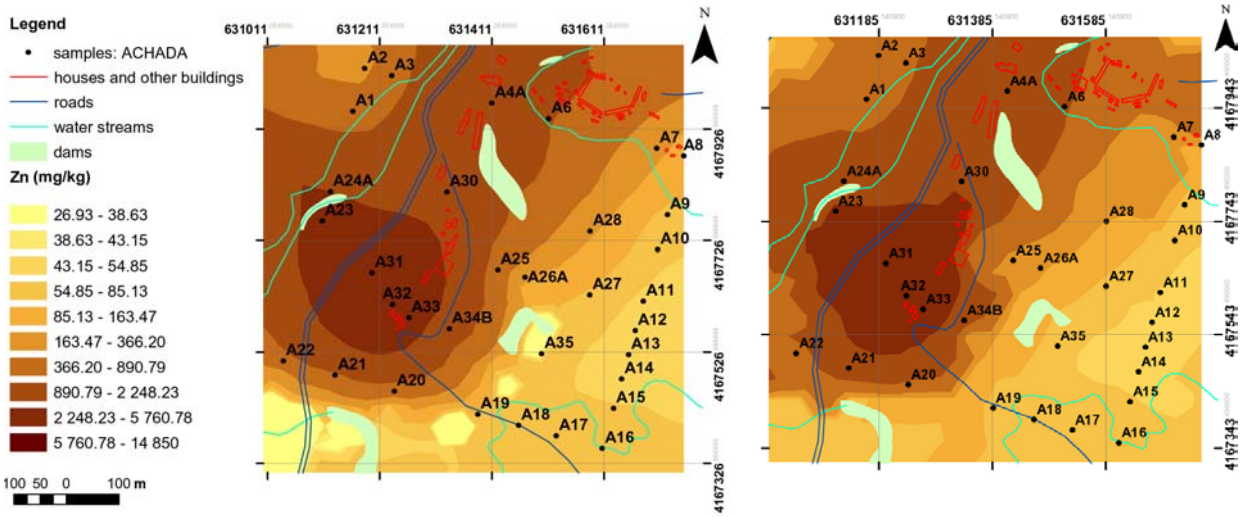

Figure A.8.6.8 - Zn map (Achada) estimated by kriging (left) and cokriging (right)

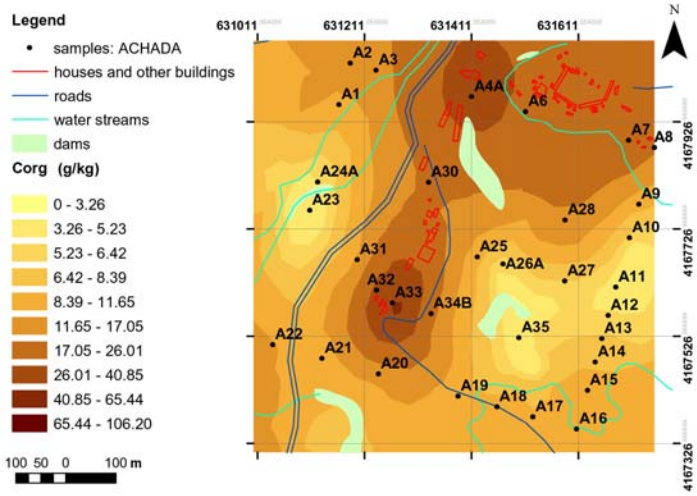

Figure A.8.6.9 - Corg map (Achada) estimated by kriging

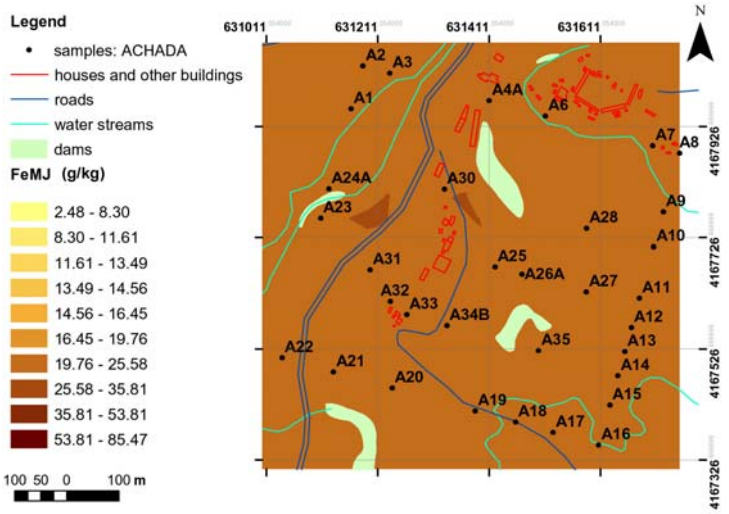

Figure A.8.6.10 - Fe*MJ* map (Achada) estimated by kriging

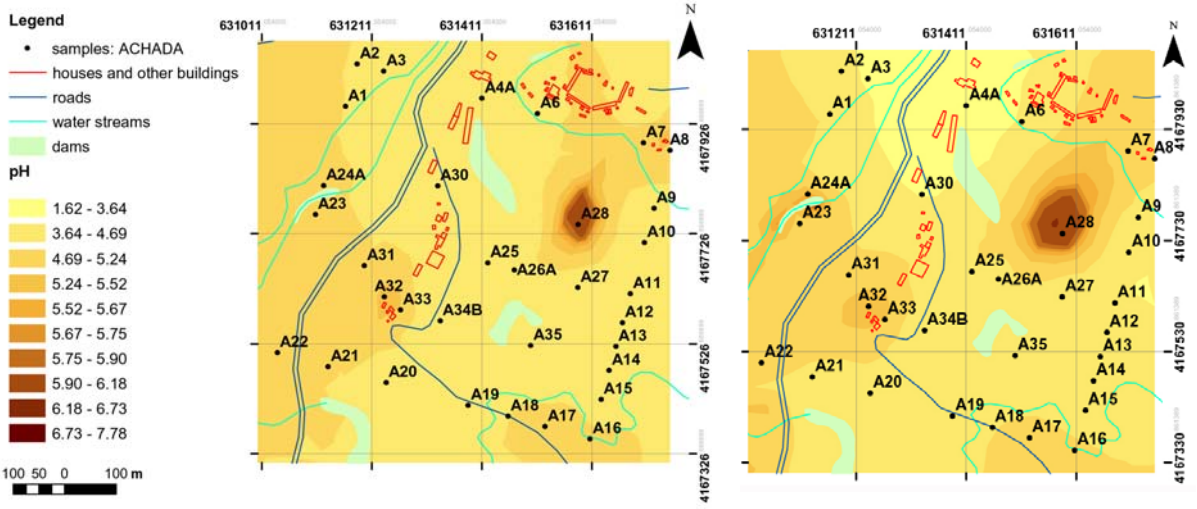

Figure A.8.6.11 - pH map (Achada) estimated by kriging (left) and cokriging (right)

A.8.7 - ESTIMATED MAPS IN TELHEIRO SUB-AREA

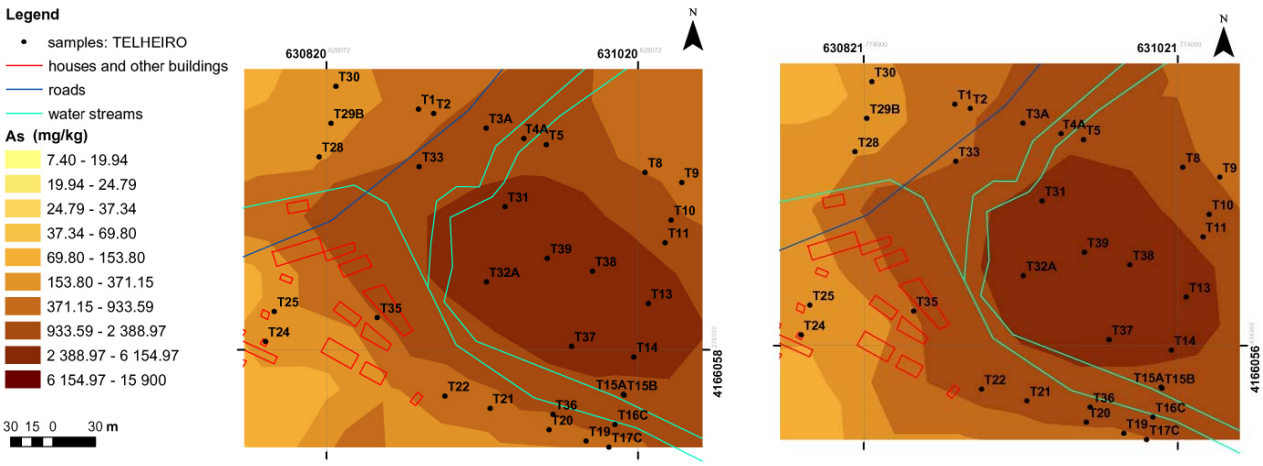

Figure A.8.7.1 - As map (Telheiro) estimated by kriging (left) and cokriging (right)

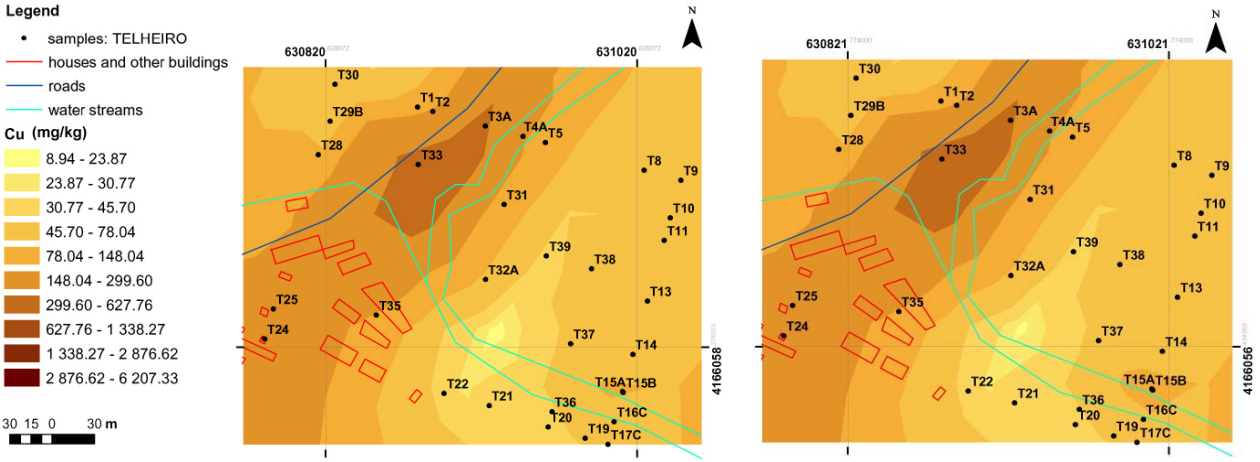

Figure A.8.7.2 - Cu map (Telheiro) estimated by kriging (left) and cokriging (right)

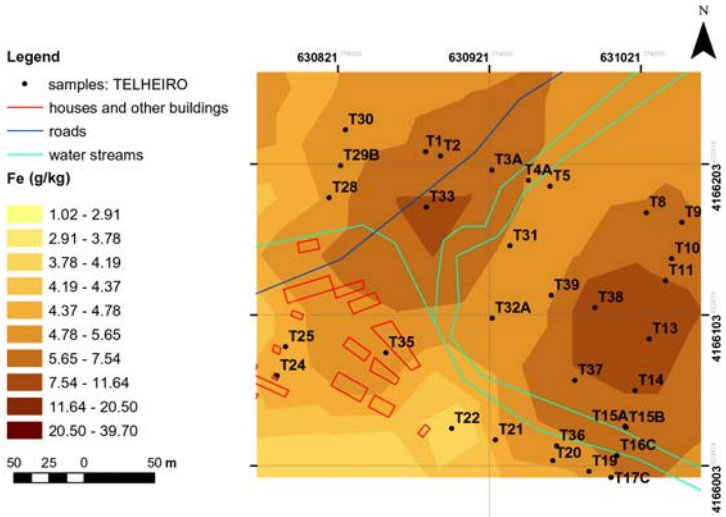

Figure A.8.7.3 - Fe map (Telheiro) estimated by kriging

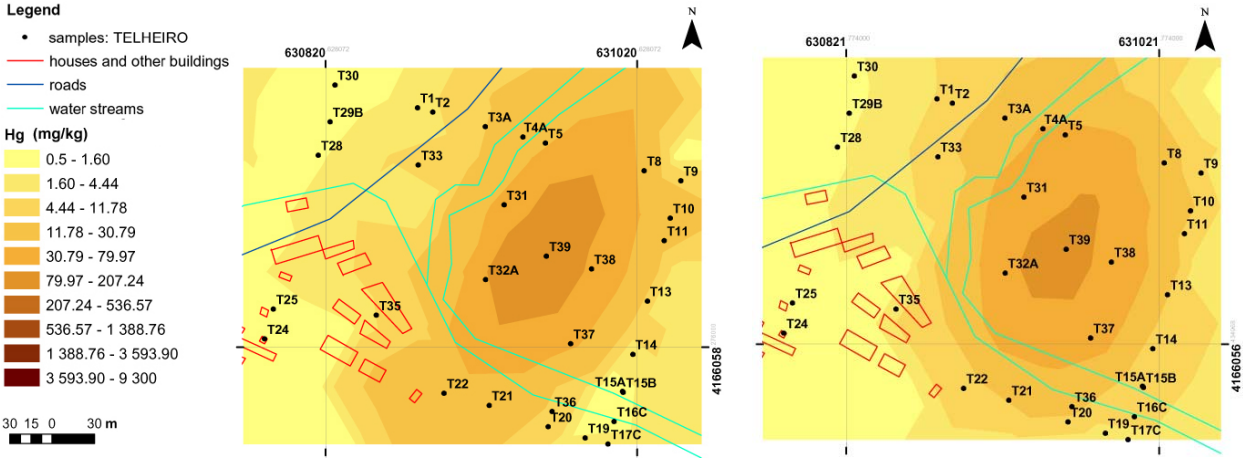

Figure A.8.7.4 - Hg map (Telheiro) estimated by kriging (left) and cokriging (right)

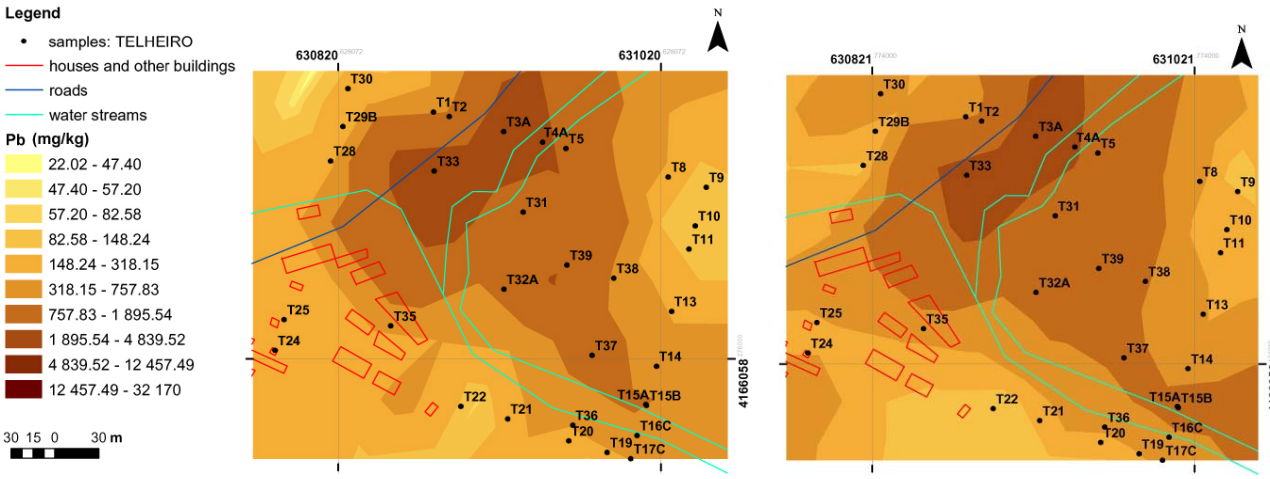

Figure A.8.7.5 - Pb map (Telheiro) estimated by kriging (left) and cokriging (right)

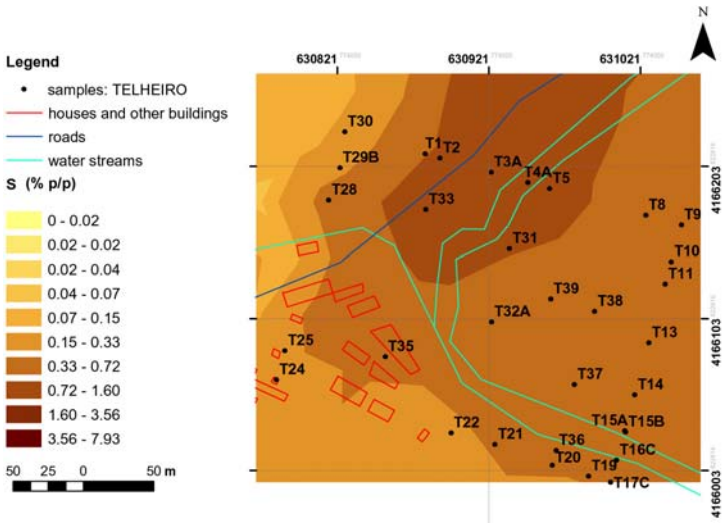

Figure A.8.7.6 - S map (Telheiro) estimated by kriging

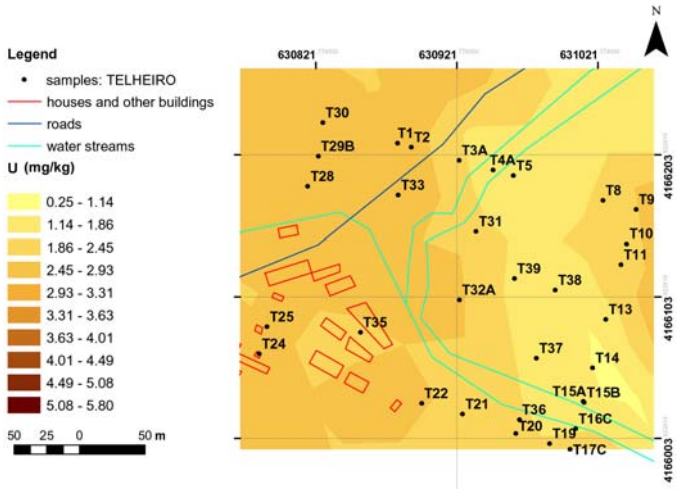

Figure A.8.7.7 - U map (Telheiro) estimated by kriging

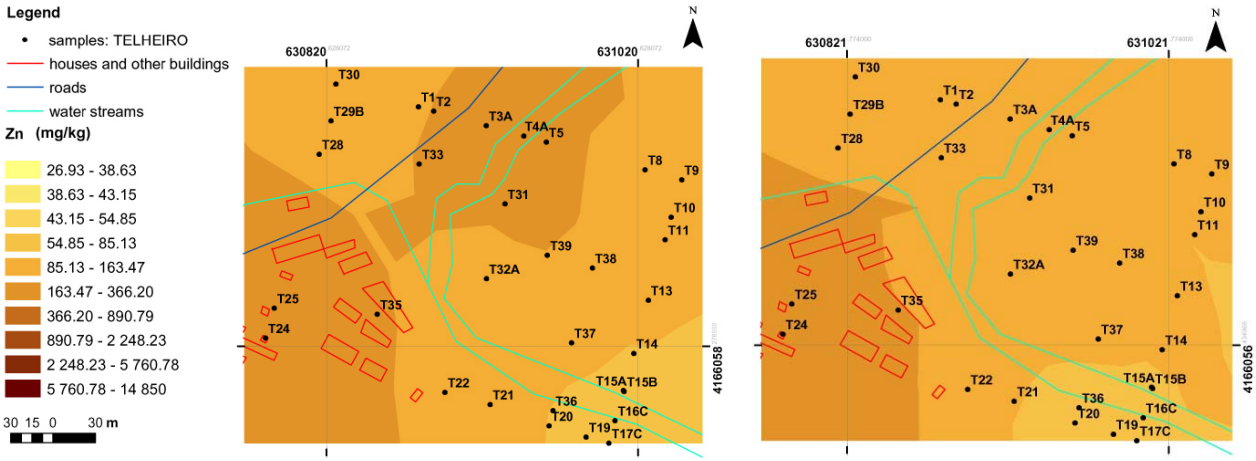

Figure A.8.7.8 - Zn map (Telheiro) estimated by kriging (left) and cokriging (right)

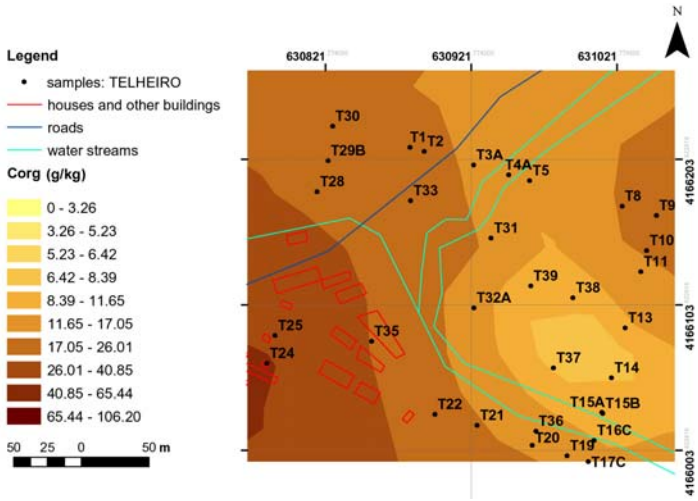

Figure A.8.7.9 - Corg map (Telheiro) estimated by kriging

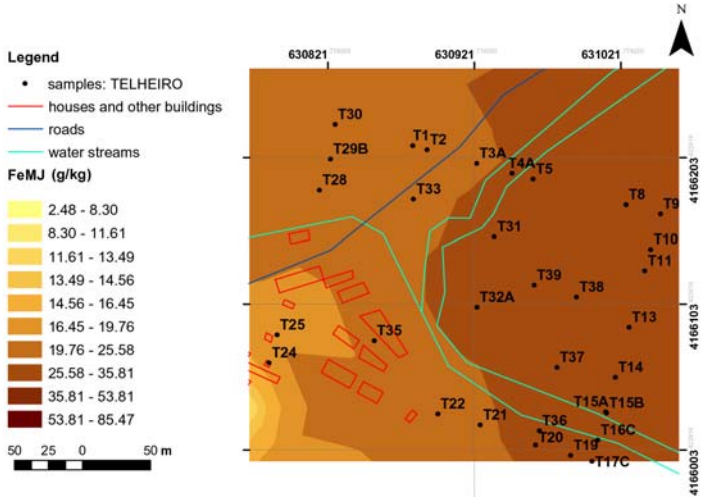

Figure A.8.7.10 - Fe*MJ* map (Telheiro) estimated by kriging

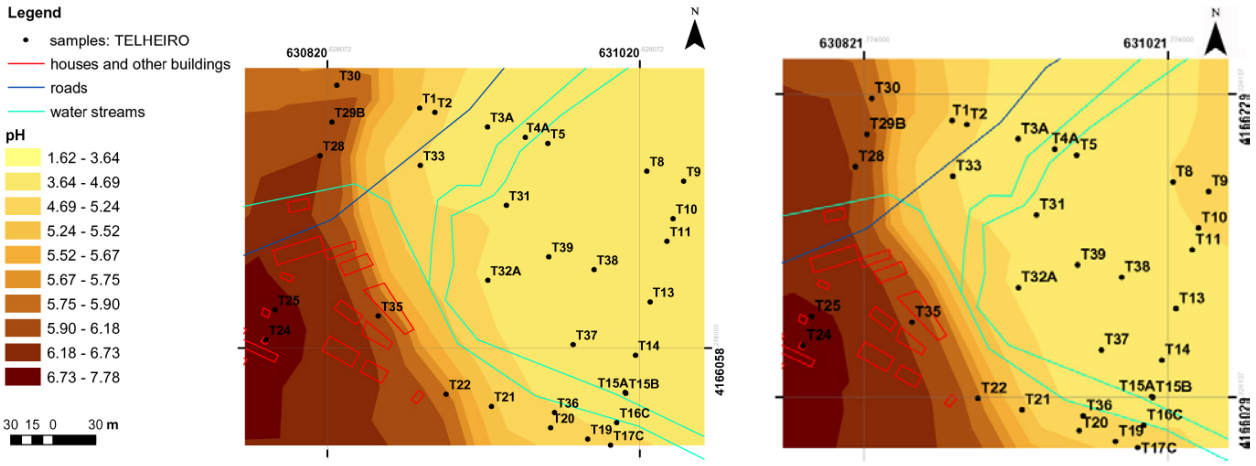

Figure A.8.7.11 - pH map (Telheiro) estimated by kriging (left) and cokriging (right)